UNIVERSIDAD EUROPEA DE MADRID

ESCUELA DE ARQUITECTURA, INGENIERÍA Y DISEÑO

DEGREE IN AEROSPACE ENGINEERING

FINAL PROJECT REPORT

HIGH ACCURACY NUMERICAL SIMULATIONS OF FULLY-COUPLED FLUID STRUCTURE INTERACTION ON AN AIRCRAFT WING FOR AEROELASTIC APPLICATIONS

DANIEL DE LA PEÑA JIMÉNEZ

YEAR 2021-2022

TITLE: HIGH ACCURACY NUMERICAL SIMULATIONS OF FULLY-COUPLED FLUID STRUCTURE INTERACTION ON AN AIRCRAFT WING FOR AEROELASTIC APPLICATIONS

AUTHOR: DANIEL DE LA PEÑA JIMÉNEZ

SUPERVISOR: JOSE OMAR MARTINEZ LUCCI

DEGREE OR COURSE: AEROSPACE ENGINEERING (4^{th})

DATE: 2021-2022

ACKNOELEDGEMENTS

I want to express my deepest gratitude for my supervisor Dr. Martínez Lucci, for his dedication and willingness to help and guide me through this Final Year Project. His knowledge, counsel and expertise were crucial factors to finish this project and he was an overall excellent professor throughout my academic experience. I want to thank Lab Technician Jose Antonio Caballero for his support during the experimental set up.

Also, I want to thank my ERAU & UEM colleagues, especially my closest friends who accompanied me throughout the last four years of completing my degree for their true friendship.

I would also like to thank my family for their love and unconditional support, which have sustained and encouraged me during the elaboration of this Final Year Project.

To UEM faculty and all my teachers, I have to leave a word of appreciation for developing my technical knowledge, my analytical thinking, my proactivity and all my abilities as an engineer and as a person.

PUBLICATIONS RELATED TO THIS FINAL YEAR PROJECT

De la Peña Jiménez D., Golubev V. 2022 "Numerical Studies of Viscous Limit-Cycle Oscillations in Modified Glauert Airfoil". *2022 AIAA Aviation Forum*, organized by the American Institute of Aeronautics and Astronautics. (June-July, 2022)

De la Peña Jiménez D., Vega Coso A. 2021 Presented paper on "Flutter and aerodynamic work per cycle analysis on an aircraft wing". *4th annual Student Research Symposium*, organized by the Office of Undergraduate Research of Embry-Riddle Aeronautical University (Nov. 2021).

De la Peña Jiménez D., Vega Coso A. 2021 Presented paper on "Flutter and aerodynamic work per cycle analysis on an aircraft wing". *National Conference on Undergraduate Research*, organized by the American Council on Undergraduate Research. (April, 2022)

De la Peña Jiménez D., Golubev V. 2023 "Fluid Structure Interaction on Controlled Viscous Limit-Cycle Oscillations in Modified Glauert Airfoil" to the *2023 AIAA SciTech,* organized by the American Institute of Aeronautics and Astronautics. (December, 2023)

ABSTRACT

The present Final Year Project aims to study the aeroelastic behaviour of a 3D aircraft wing by Fluid-Structure Interaction. Aeroelasticity is a physical phenomenon resulting from the interaction of aerodynamic, elastic and inertial forces.

Flutter, is an unstable self-excited vibration in which the structure extracts energy from the air stream and often results in catastrophic structural failure. These coupling occurs when the aerodynamic forces associated with motion in two modes of vibration cause the modes to couple in an unfavourable manner. ANSYS Fluid-Structure Interaction Framework, FSIF, was designed to discretise both fluid and structural domains. FSI Methods are validated with one way and two-way coupling methods. Reynolds Averaged Navier-Stokes equation and Turbulence Transport equations governing the flow were integrated in the FSI solver. The results are presented for an RV-10 wing structure denoted as reference case. K-P Method was defined to stablish critical flutter speed and flutter limits. Simulations were run for steady and transient models by applying SST K-omega turbulence model into ANSYS FSIF. Furthermore, numerical results have been post-processed in order to obtain the phase difference and classical coupling motion. Those results indicate unstable flow for the selected Critical Flutter Speed. Comparison between literature review on rectangular wings and numerical results shows accurate results. Moreover, experimental pressure distributions of an oscillating wing tested at European University Wind Tunnel facility are analysed aiming to provide accurate results. Despite the simplifications implemented in both the fluid and structural solvers, this framework proves to be useful to predict the aeroelastic performance of a wing in the early stages of aircraft design.

Keywords: Aeroelasticity, Finite element method, Fluid-structure interaction, Flutter.

RESUMEN

El presente Trabajo de Fin de Grado tiene como objetivo estudiar el comportamiento aeroelástico de un modelo tridimensional del ala de un avión mediante interacción fluido-estructura. La aeroelasticidad es un fenómeno físico resultante de la interacción de fuerzas aerodinámicas, elásticas e inerciales.

La inestabilidad aeroelástica por flameo es una vibración autoexcitada inestable en la que la estructura extrae energía de la corriente de aire y, a menudo, provoca una fallo estructural. Este acoplamiento ocurre cuando las fuerzas aerodinámicas asociadas con el movimiento en dos modos de vibración hacen que dichos modos se acoplen de manera desfavorable y amplifiquen el movimiento. La Interfaz Fluido-Estrcutura fue diseñada en ANSYS con el fin de discretizar tanto el dominios del fluido, como el dominio estructural. Los métodos de acoplamiento son validados de forma unidireccional y bidireccional. Los resultados aeroelasticos son presentados para una estructura de ala de un avión ultraligero Deportivo. Para dicho caso, se utilizó el método K-P para establecer la velocidad crítica de inestabilidad aeroelástica por flameo y sus límites. Distintas simulaciones numéricas para modelos estacionarios y transitorios fueron obtenidos aplicando el modelo de turbulencia SST K-omega. Además, los resultados numéricos se han procesado posteriormente para obtener la diferencia de fase y el movimiento de acoplamiento clásico, característico en muchos de estos aviones. Los resultados obtenidos indican un flujo inestable para la velocidad crítica de flameo analizada. Estos resultados muestran grandes similitudes con los estudados en distintos proyectos de investigación. Finalmente, se analizan las distribuciones de presión de un ala oscilante cuyo ensayo se realizó en las instalaciones del Túnel de Viento de la Universidad Europea. A pesar de las simplificaciones implementadas en la interfaz numérica, este marco demuestra ser útil para predecir el rendimiento aeroelástico de un ala en las primeras etapas del diseño de aeronaves.

Palabras Clave: Aeroelasticidad, Método de Elementos Finitos, Interación Fluido-Estructura, Inestabilidad aeroelástica por flameo.

TABLE OF CONTENTS

LIST OF TABLES

LIST OF FIGURES

NOMENCLATURE

α	Angle of attack
Δ	Variation
μ	Molecular viscosity coeffcient, doublet strength
π	Mathematical constant
ρ	Density
σ	Source strength or volumetric rate
Γ	Stress tensor
ω	Natural frequency
Φ	Velocity potential
Δ	Differential operator
∂	Partial derivative
AR	Wing aspect ratio
C_l	Lift coefficient
C_m	Moment coefficient
C_p	Pressure coefficient
E	Young's modulus

G Shear modulus

M Structural Mass matrix

K Structural Stiffness matrix

p Pressure

t Time

T Temperature

V Fluid velocity vector with components (u; v; w)

GLOSSARY

FSI	Fluid-Structure Interaction
CFD	Computational Fluid-Dynamics
CAE	Computer-Assisted Engineering
CAD	Computer-Assisted Design
DOF	Degrees of Freedom
FSIF	Fluid-Structure Interface Framework
NACA	Family of airfoils by National Advisory Comitte for Aeronautics
MATLAB	Matrix Laboratory software
ALE	Arbitrary Lagrangian-Eulerian
NSE	Navier-Stokes Equations

CHAPTER 1

"Start by doing what's necessary;
then do what's possible; and
suddenly you are doing the
impossible"

Francis of Assisi

Contents

1. INTRODUCTION

The current study is motivated by the need to develop an accurate, robust prediction tool for analysis of Fluid-Structure Interaction (FSI) on an aircraft wing subjected to high-aerodynamic forces and the associate nonlinear-aeroelastic response. A fully-coupled FSI model is analysed by the implementation of structural and unsteady aerodynamics as a unique aeroelastic system that could lead to a premature transition to flutter and/or LCO of the structure. According to [1], flutter, an unstable self-excited vibration in which the structure extracts energy from the air stream, is analysed as dynamic instability which may eventually result in stall or buffeting conditions or classical bending and torsion coupling actions. These coupling occurs when the aerodynamic forces associated with motion cause the modes to couple in an unfavourable manner.

The scope of the present Final Year Project aims to provide insight of aeroelastic phenomenon by a coupled numerical analysis, in which the nonlinear equations of motion for the wing structure are solved simultaneously with a set of governing Navier-Stokes equations, resulting in a coupled dynamic system in which the fluid and structure components are treated as a unique system. High-order operators are used in the numerical simulation to provide accurate solutions to this aeroelastic problem.

These coupling occurs when the aerodynamic forces associated with motion in two modes of vibration cause the modes to couple in an unfavourable manner. ANSYS Fluid-Structure Interaction Framework, FSIF, was designed to discretise both fluid and structural domains. FSI Methods are validated with one way and two-way coupling methods. Reynolds Averaged Navier-Stokes equation and Turbulence Transport equations governing the flow were integrated in the FSI solver. Steady and transient models will be analysed by applying different turbulence models for 1DOF and 2DOF scenarios involving pitching and plunging. Furthermore, numerical results will be post-processed in order to obtain the phase difference exerted by the fluid onto the wing airfoil.

Once the analytical and numerical models are set up, experimental data comparison will be achieved. As future engineer, one of the motivations that led me to choose this topic is to tighten studies to research about dynamic aeroelasticity problems and its solution applied on aviation. Therefore, this proposed study will provide a professional research study through analytical, numerical and experimental arguments in order to ensure a high-professional research ability on an aeronautic phenomenon.

The roots of this Final Year Project main interest can be traced back in time 75 years ago, when wooden structures were manufactured for the first family of aircrafts within the old wood and iron warehouses of the Fernández Palacios, at San Jacinto Street, Triana, Sevilla. Inside these walls, preliminary details were applied to the first aircraft prototype designed and built in the Andalusian capital. Without hesitation, it was the Hispano-Suiza HS.42, a two-seater for training and transition of mixed construction and retractable gear, similar to the T-6 Texan or Harvard.

What amazed me is that the wing, especially, was very particular, given that its structure, built entirely of wood, was box-shaped, with the rear spar being especially complex as it had a double inflection: 6º positive dihedral and 8º progressive slack, conserving mechanical characteristics of an end to end. The central part of the wing was flat, but the outer sections, trapezoidal in plan, had a slight sag on the

leading edge and much more pronounced on the trailing edge. The only concessions to metal were the moving surfaces: camber (flaps) and warping ailerons, made of welded steel tube and covered in dural and fabric.

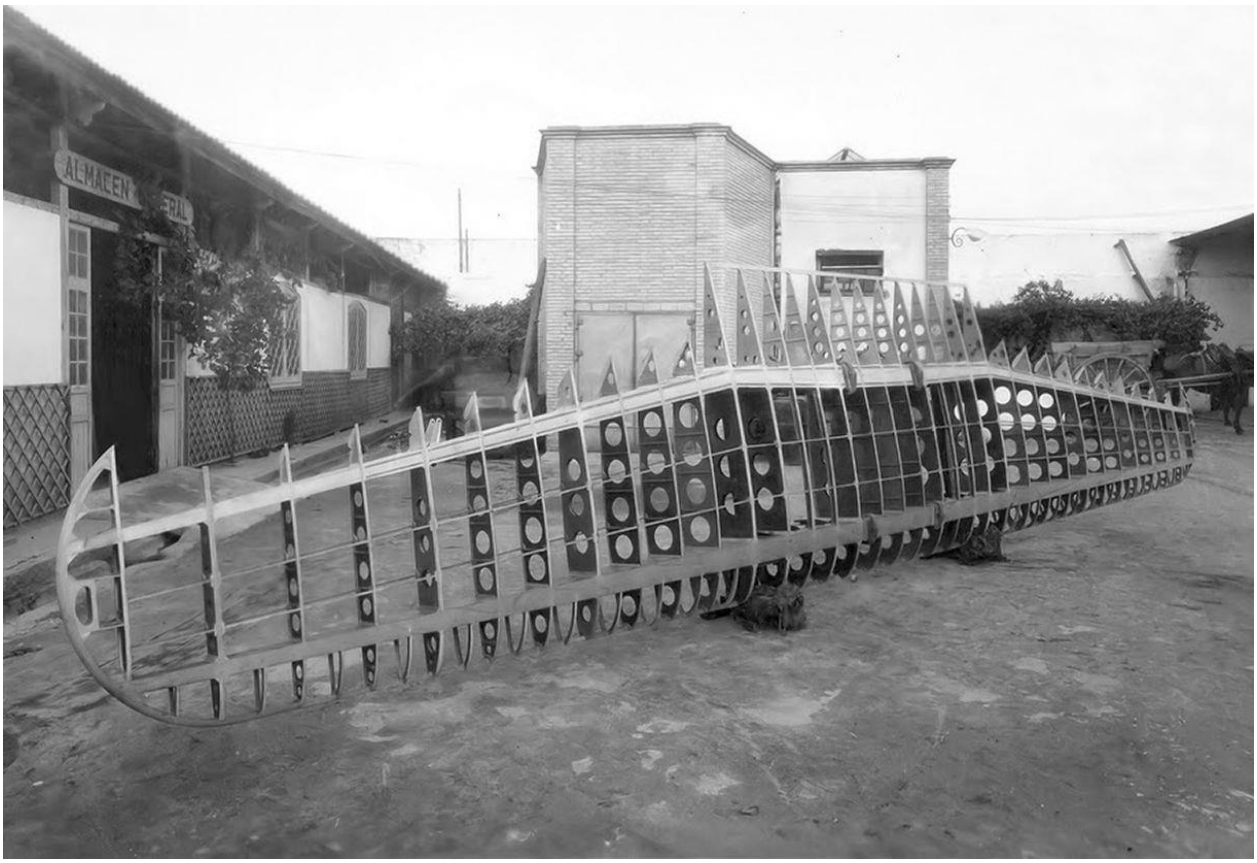

FIGURE 1. Fernández Palacios manufacturing center. San Jacinto street, Triana, Sevilla. First Hispano-Suiza HS.42 prototype. Ref[38].

The images allow us to appreciate not only the complexity of the design, but also the rusticity of the facilities. That is the reason why I asked myself: how is possible to overcome aerodynamic forces if you have a wooden structure? How is possible the fluid-structure behaviour on those first aircraft models? However, aviation has evolved, as well as its procedures, manufacturing techniques and aeronautic solutions. Currently, technological developments allow us to implement computational aeroelasticity programs. The behaviour between the structural components and the loads, have been always of special interest. Throughout the years, several studies have constituted a remarkable base towards reliable progress developing robust investigations on unsteady response on aircraft structures. Moreover, flutter stability studies have been of special interest along next generation aircraft models. In that sense, this final year project aims to answer the previous questions.

1.1. MOTIVATION

A challenging problem which arises in Aeroelasticity domain is to provide insight into high-accuracy fluid-structure interaction by the numerical and experimental analysis of a fully-coupled model on an aircraft wing, with unsteady pressure field. This topic highlights the Final Year Project problem statement on the research field based on ensuring a robust prediction tool for analysis of aeroelastic nonlinearities responses that may result in a premature transition to flutter and/or LCO.

Last, but not least, the reason that triggered this Final Year Project was my Study Abroad Experience at Embry Riddle Aeronautical university, what I discovered aeroelasticity field through numerical and experimental research projects.

1.2. FLUID-STRUCTURE INTERACTION

When a fluid moves around a solid body, it ejects several forces on it. If the solid is deformable, it will adopt a stationary deformation or it will continue to deform itself over time, generally in an oscillatory manner.

The Fluid-Structure Interaction comprises an important field of research in order to evaluate and predict structural response to different phenomenon that are present in our daily live, e.g., in nature, along the interaction of the wind with a tree birds, fish and insects locomotive system within a fluid; in engineering fields, slender bridges behaviour over gust, piping structures over a dynamic pressure gradient; and last, but not least, the aerospace sector, with main focus on flutter instability on aircraft wings, turbomachinery blades or wind turbines. Therefore, the relevance of FSI models is find on basic events. And thus, its importance. [18]

These approaches have been influential in the aeronautical field because of the importance of structural response over aerodynamic loads on flight dynamics. Recent theoretical developments have revealed that Fluid-Structure Interaction (FSI) models allow aeroelastic phenomenon to be predicted by a coupled numerical analysis. A number of works have shown that this problem can be overcome by simultaneously solving the nonlinear equations of motion for the wing structure with a set of governing Navier-Stokes equations, resulting in a coupled dynamic system in which the fluid and structure components are treated as a unique system.

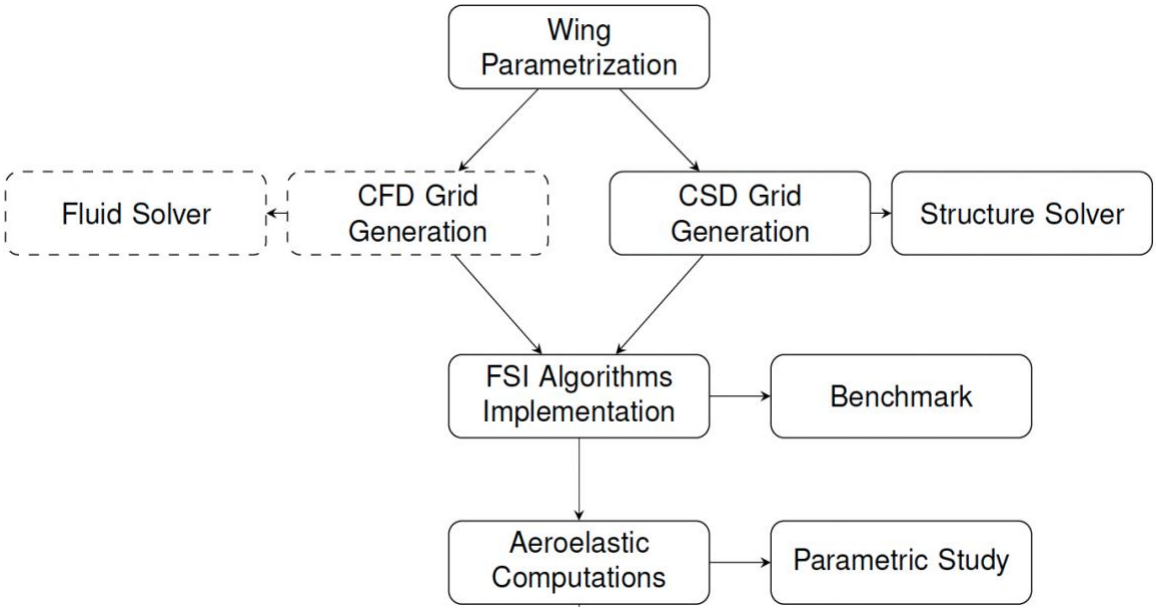

FIGURE 2. Final Year Project flowchart according to Fluid-Structure Interface Algorithm

1.3. OBJECTIVES

The objective of this Final Year Project is to establish two and three-dimensional CFD model of an aircraft wing to evaluate aeroelastic response based on elastic, inertial and aerodynamic performance. A RV-10 aircraft wing model is used as a reference aeroelastic system and numbers of objectives were set as follow:

- To design a Fluid-Structure Interface able to predict flutter instability and aeroelastic response. The purpose of this three-dimensional analysis is to compare the results with analytical results and validate its numerical accuracy by means of a fully-coupled solver.
- To establish the flow behaviour around the three-dimensional RV-10 wing model and predict the flutter velocity by conducting flow simulations using ANSYS®.
- To represent flutter dynamic motion and obtain the amplitude, frequency and angle of attack variation along the average time.
- To study the dependence (sensitivity) of aircraft wing geometric/design parameters on aeroelastic phenomenon using ANSYS® Workbench 14.5 by integrating a fully coupled staggered Fluid-Structure Interaction (FSI).

1.4. METHODOLOGY

There are grounds for believing that a Development Plan is an essential tool along this TFG to organize and track the objectives in a specific period of time. In order to achieve those objectives, a Fishbone diagram, which is a problem-solving technique used in Project Management designed to explore and visually depict the causes of a problem, will be presented to evaluate project phases. Those phases involved in this Graduation Project have been sorted into four main categories in order to identify cause and effect model: Analytical Model, Numerical Analysis, Experimental Set Up and Wind Tunnel Analysis. The actions involved in every phase are defined below each section, with arrows pointing towards the effect or consequence, which is the horizontal arrow in the middle of the diagram, which corresponds to the time duration of the Graduation Project. The fishbone diagram for this development plan is provided in Figure 2.

The whole schedule is provided in Figure 1, where a Gantt diagram provides objectives relation with time under each phase with the achieved level and actual status of every action. Office hours with Dr. Martínez Lucci will be held on Thursdays, 16:30h., via videoconferencing and face-to-face when needed. Wind Tunnel lab testing will be schedule with José Antonio Caballero Montes, UEM lab technician, in order to define experimental set-up requirements and lab facilities. Once every phase is completed, the final Graduation Project will be check with different professors and professionals before submitting it to the Campus.

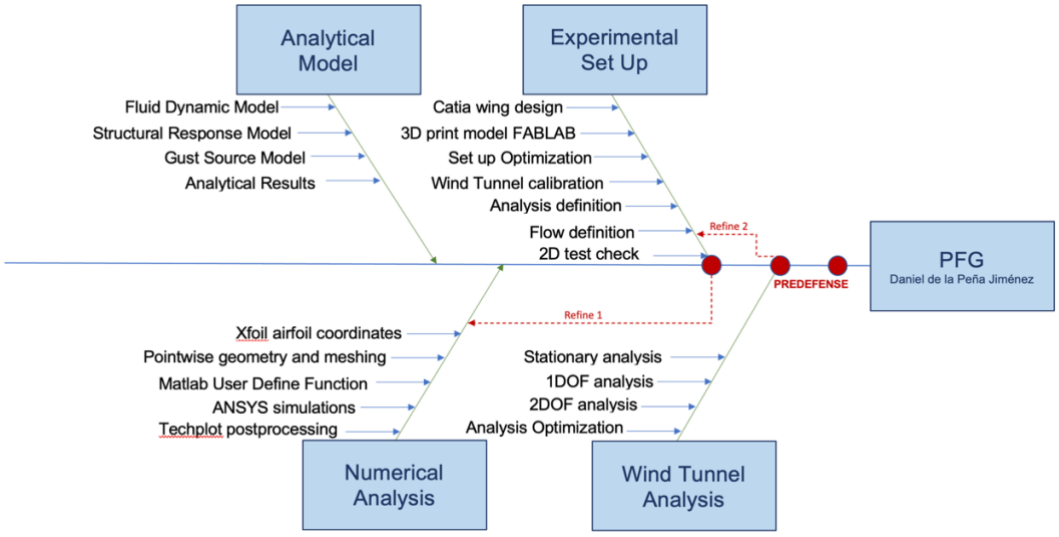

FIGURE 3. Fishbone Diagram Graduation Project.

GRADUATION PROJECT

DANIEL DE LA PEÑA JIMÉNEZ

HIGH-ACCURARY NUMERICAL AND EXPERIMENTAL ANALYSIS OF CONTROLLED VISCOUS LIMIT-CYCLE OSCILLATIONS IN A MICRO AIR VEHICLE MODEL

Project Start: Wed, 12/1/2021

Display Week: 1

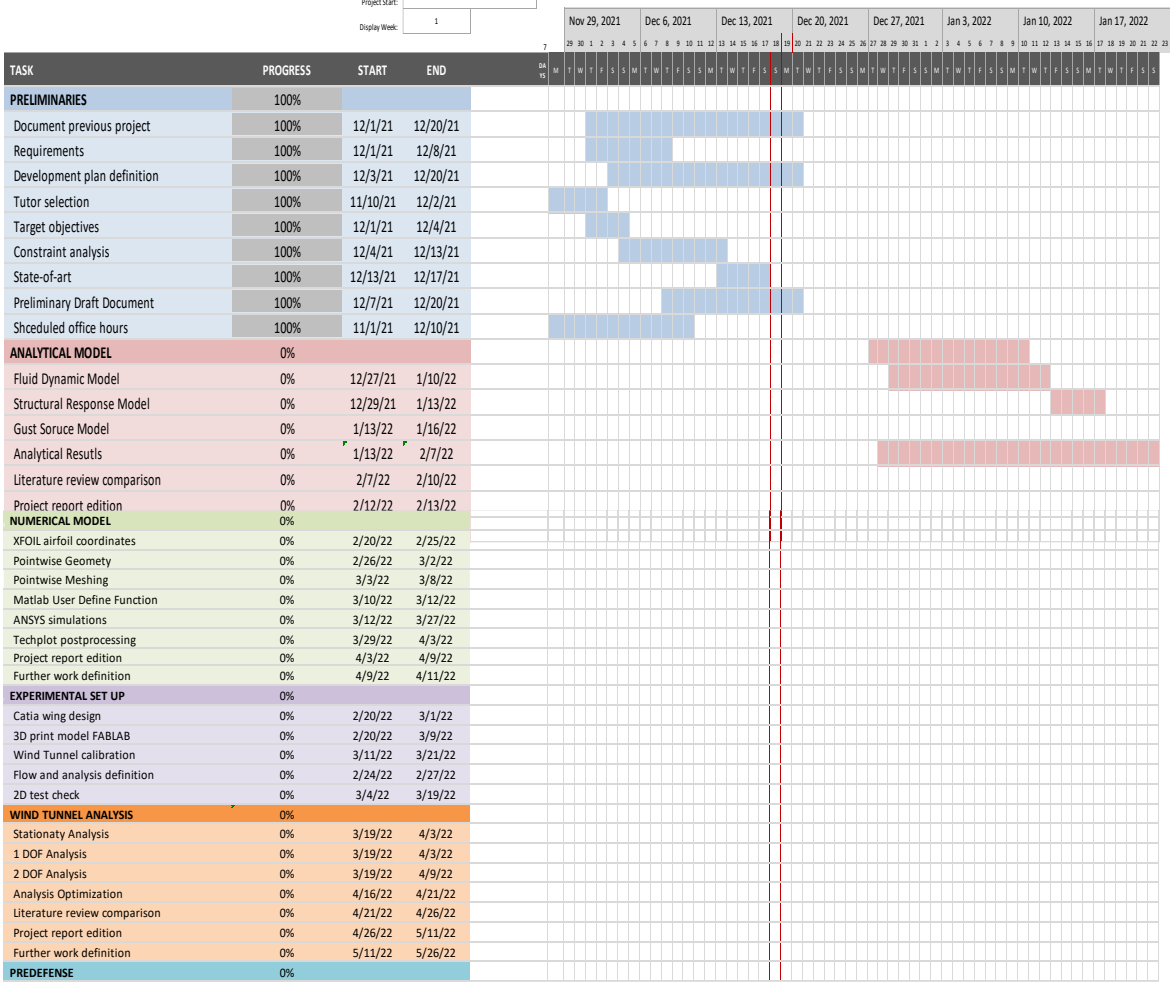

TASK	PROGRESS	START	END
PRELIMINARIES	100%		
Document previous project	100%	12/1/21	12/20/21
Requirements	100%	12/1/21	12/8/21
Development plan definition	100%	12/3/21	12/20/21
Tutor selection	100%	11/10/21	12/2/21
Target objectives	100%	12/1/21	12/4/21
Constraint analysis	100%	12/4/21	12/13/21
State-of-art	100%	12/13/21	12/17/21
Preliminary Draft Document	100%	12/7/21	12/20/21
Shceduled office hours	100%	11/1/21	12/10/21
ANALYTICAL MODEL	0%		
Fluid Dynamic Model	0%	12/27/21	1/10/22
Structural Response Model	0%	12/29/21	1/13/22
Gust Soruce Model	0%	1/13/22	1/16/22
Analytical Resutls	0%	1/13/22	2/7/22
Literature review comparison	0%	2/7/22	2/10/22
Project report edition	0%	2/12/22	2/13/22
NUMERICAL MODEL	0%		
XFOIL airfoil coordinates	0%	2/20/22	2/25/22
Pointwise Geomety	0%	2/26/22	3/2/22
Pointwise Meshing	0%	3/3/22	3/8/22
Matlab User Define Function	0%	3/10/22	3/12/22
ANSYS simulations	0%	3/12/22	3/27/22
Techplot postprocessing	0%	3/29/22	4/3/22
Project report edition	0%	4/3/22	4/9/22
Further work definition	0%	4/9/22	4/11/22
EXPERIMENTAL SET UP	0%		
Catia wing design	0%	2/20/22	3/1/22
3D print model FABLAB	0%	2/20/22	3/9/22
Wind Tunnel calibration	0%	3/11/22	3/21/22
Flow and analysis definition	0%	2/24/22	2/27/22
2D test check	0%	3/4/22	3/19/22
WIND TUNNEL ANALYSIS	0%		
Stationaty Analysis	0%	3/19/22	4/3/22
1 DOF Analysis	0%	3/19/22	4/3/22
2 DOF Analysis	0%	3/19/22	4/9/22
Analysis Optimization	0%	4/16/22	4/21/22
Literature review comparison	0%	4/21/22	4/26/22
Project report edition	0%	4/26/22	5/11/22
Further work definition	0%	5/11/22	5/26/22
PREDEFENSE	0%		

FIGURE 4. Final year project Gannt chart

CHAPTER 2

"Try not to become
a man of success, but rather try to
become a man of value."

Albert Einstein

Contents

2. AEROELASTICITY FUNDAMENTALS

In the past several decades, aeroelasticity have played an important role in aviation. The roots of aeroelastic problems in Aviation can be traced back to Wright brother's era, where structural failures were the result of excessive wing twist coupled with low torsional stiffness. Kehoe [40] reported the first aeroelastic instability as violent oscillations on the horizontal tail plain on Handley Page 0/400 bomber in 1916 during the I War World. The field has been gradually broadened by the development of analytical and numerical methods to analyze aeroelastic forces by aerospace engineers as Earl Dowell, Josef Panovsky and Robert Kielb. In previous publications at Embry-Riddle Aeronautical University [1], Aeroelasticity is defined as a combination of physical phenomena related with the iteration between inertia, elastic and aerodynamic forces. A challenging problem which arises in this domain is the impact on stability and control, static and dynamic aeroelasticity and structural vibrations. In that manner, **Collar diagram** provides a useful tool which allows to relate inertial, elastic and aerodynamic forces:

COLLAR DIAGRAM

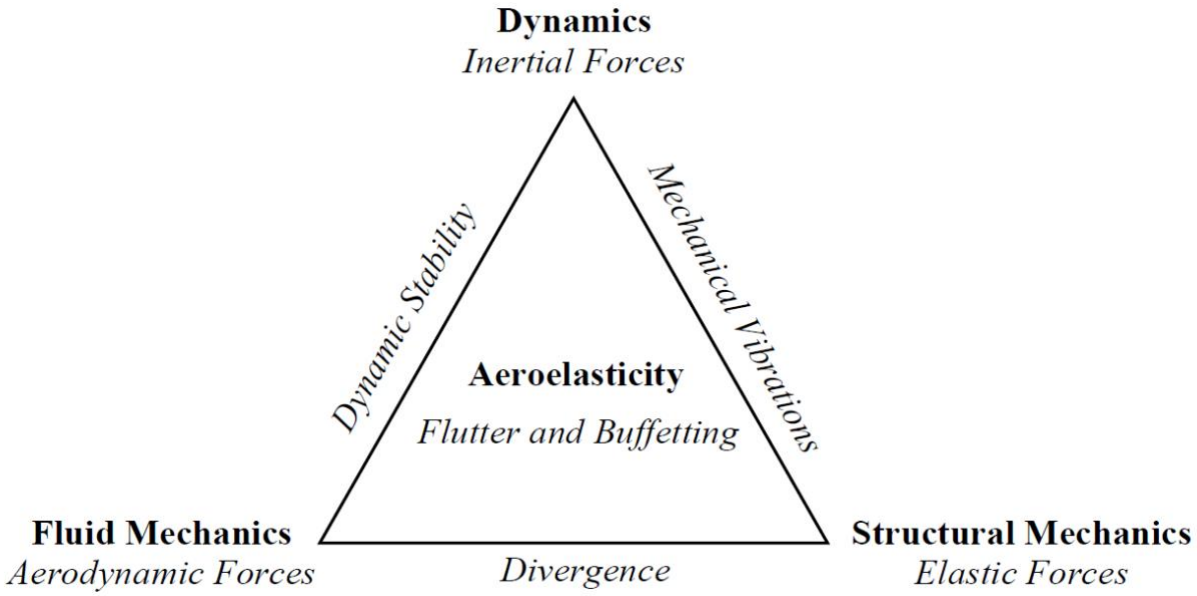

FIGURE 5. Collar Aeroelasticity Diagram. Ref [41]

A comprehensive description can be found by the interaction of different forces into four categories: classical vibration, regarding inertial and elastic forces interaction; stability and control, where aerodynamic are combined with inertial forces; static aeroelasticity, which deals with the interaction of aerodynamic and elastic forces; and finally, dynamic aeroelasticity, which corresponds to the interaction of inertial, elastic and aerodynamic forces. In aviation, both static and dynamic aeroelasticity, are a major cause of concern since unsteady aerodynamic forces and torsional divergence need to be certified according to airworthiness requirements by regulatory authorities such as FAA (14 CFR 25.629) and EASA (CS 25.629).

Firstly, in order to provide an accurate approach to Fluid-Structure Interaction (FSI) analysis, static aeroelasticity is evaluated as constitutes the first engineering design criteria that every design must fulfil to prevent aircraft wing from divergence, which may eventually result in structural catastrophe.

Secondly, dynamic aeroelasticity must also be taken into study. This aeroelastic phenomena differs from static aeroelasticity, since vibration is also involved. The main aeroelastic phenomena of interest

are flutter, forced response and non-synchronous vibrations (NSV). Flutter is a dynamic instability which may be produced by stall of buffeting conditions, or by classical bending and torsion coupling actions. Forced response is defined as a response to external aerodynamic excitation loading that may be coupled with the natural frequencies leading to resonance on aircraft wings, HTP and VTP due to atmospheric turbulence or gust. Non-Synchronous Vibrations are aerodynamic instabilities produced by vortex shedding that interacts with the natural frequencies. These vortex induced vibrations are aerodynamic disturbances occurring near the stability limit.

2.1. STATIC AEROELASTICITY

According to [8]**,** the interaction of aerodynamic and elastic forces on a vibration-free system is defined as static aeroelasticity. Aircraft wings are subject to aerodynamic loads. As the wing is flexible, steady aerodynamic loads cause structure deformation. Consequently, as the angle of attack incidence varies, a redistribution of aerodynamic loads occurs. Assuming that the center of twist is behind the aerodynamic center, the moment generated by the pressure distribution gradually increases due to a change on the angle of attack, and hence, on lift.

A. TORSIONAL DIVERGENCE

Therefore, static aeroelasticity is constitutes the first engineering design criteria that every design must fulfil in order to prevent structural system from in torsional divergence on the aircraft wing, which may result in catastrophic failure. The torsional moment due to aerodynamic forces achieves stable equilibrium when it balances the torsional rigidity of the aircraft wing. Hence, the diverge speed is reached when the stream speed surpasses this critical limit. The principal model representing 2D static aeroelasticity is the rotation of the plate (and consequent twisting of the spring) as under the influence of airspeed. Megson stated that if the spring is stiff or airspeed is slow, the rotation would be rather small; however, for flexible springs or high flow velocities the rotation may twist the spring beyond its ultimate strength and lead to structural failure[8]. The following diagram constitutes a physical simplification of an aircraft wing for mathematical modelling.

The airspeed at which the elastic twist increases rapidly to the point of failure is called the **'divergence airspeed'**, U_D. In the following section, analytical solution to static aeroelasticity will be analyzed on reduced model.

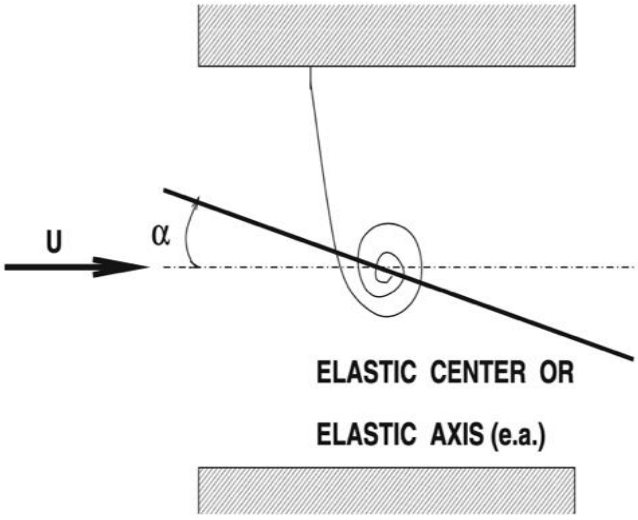

FIGURE 6. Aeroelastic simplification of an airfoil**.** Ref [10]

In order to determine U_D, equation of momentum equilibrium is applied. Ref [8] states that "the sum of **aerodynamic** and **elastic moments** at which the resulting force at any point on the airfoil is zero". By considering lift is acting at the aerodynamic center, the elastic moment can be mathematically simplified and represented as a spring with a linear-twist movement.

The momentum due to aerodynamic force and elastic moment is:

$$\sum M_y = 0; \;\; K_\alpha(\alpha - \alpha_0) \; - \; Le = 0 \tag{2.1}$$

Where:

$\boldsymbol{M_y}$ is the moment about elastic axis or center.

$\boldsymbol{L}$ is the lift, net vertical force positive up.

$\boldsymbol{e}$ is the distance from aerodynamic center to elastic axis, positive aft.

$\boldsymbol{K_\alpha}$ is the elastic spring constant with units of moment (torque) per angle of twist.

$\boldsymbol{\alpha}$ is the angle of attack.

Based on lift equation, lift with velocity relationship are related with the angle of attack as:

$$L = q_\infty S C_L'(\alpha - \alpha_0) \tag{2.2}$$

$$C_L = C_L'(\alpha - \alpha_0) + C_L'_0 \tag{2.3}$$

For a flat plate subject to incompressible flow, we can assume that $\partial CL/\partial\alpha = 2\pi$. For small angle of attack, C_{L0} can be neglected.

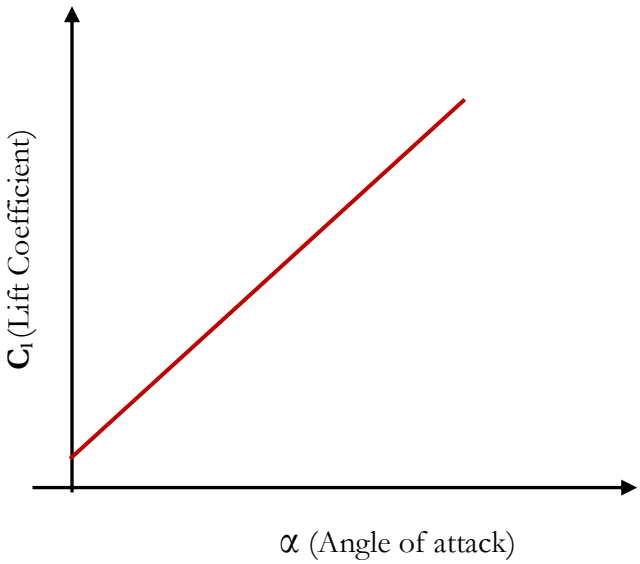

$$\left.\frac{\partial C_L}{\partial \alpha}\right| = 2\pi$$

$$C_{L_0} = 0$$

So, finally, the equilibrium momentum equation for static aeroelasticity is:

$$K_\alpha(\alpha - \alpha_0) - \frac{1}{2}\rho U_\infty{}^2 S\, e \cdot \left(\frac{\partial C_L}{\partial \alpha}\right)\alpha = 0 \tag{2.4}$$

Solving for dimensionless parameters, we obtain:

$$\frac{\alpha_{eq}}{\alpha_0} = \frac{1}{1 - \beta^2} \tag{2.5}$$

Where β^2 can be defined by:

$$\beta^2 = \frac{1}{2}\rho U_\infty{}^2 \frac{S\, e}{K_\alpha}\left(\frac{\partial C_L}{\partial \alpha}\right) \tag{2.6}$$

Thus, under those static aeroelasticity circumstances two different phenomena may occur assuming linear stiffness and lift coefficient characteristic:

- Torsional divergence.
- Control surface reversal over the aircraft wings.

Therefore, if elastic center lies behind the aerodynamic center, divergence may occur as the distance from aerodynamic center to elastic axis is greater than cero.

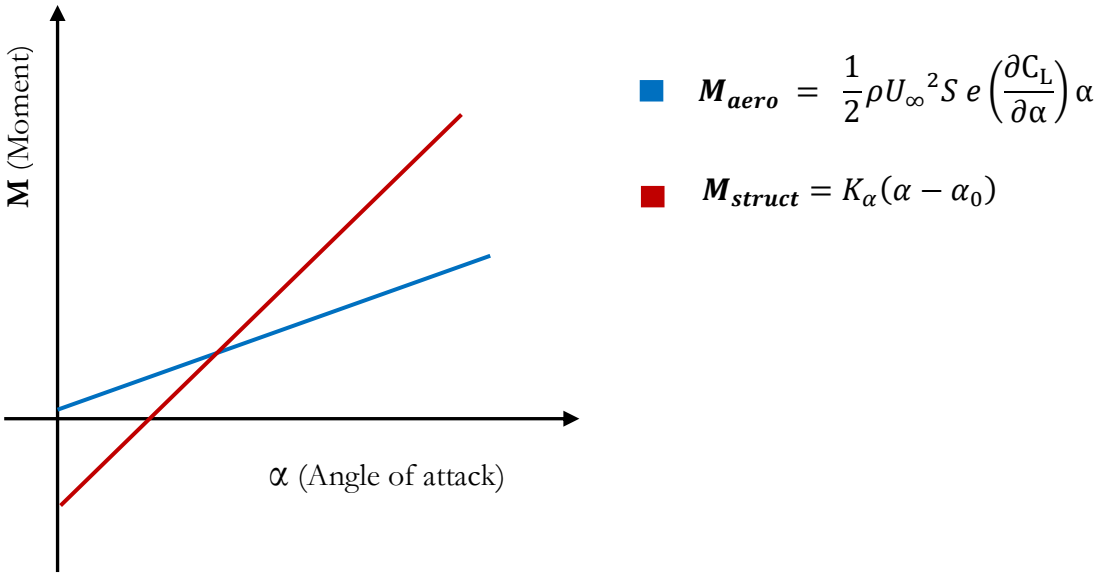

Finally, the critical divergence speed must be designed to avoid torsional divergence as function of the aeroelastic and structural moments for different angles of attack as followed:

$$K_\alpha(\alpha - \alpha_0) - \frac{1}{2}\rho U_\infty{}^2 S\, e \cdot \left(\frac{\partial C_L}{\partial \alpha}\right)\alpha = 0 \tag{2.7}$$

$$U_\infty = \sqrt{\frac{2\, K_\alpha(\alpha - \alpha_0)}{\rho S\, e \left(\frac{\partial C_L}{\partial \alpha}\right)\alpha}} \tag{2.8}$$

The airspeed at which the elastic twist increases rapidly to the point of failure is called the **'divergence airspeed'**, U_D. Therefore, as aerospace engineer, different solutions are proposed to solve real engineering problems. In order to increase the divergence speed limit, two design solutions are presented: redesign wing by stiffening the structure or decreasing

the distance between the flexural and aerodynamic centers. According to [12], the latter approach introduces weight and cost penalty, so this solution is neglected.

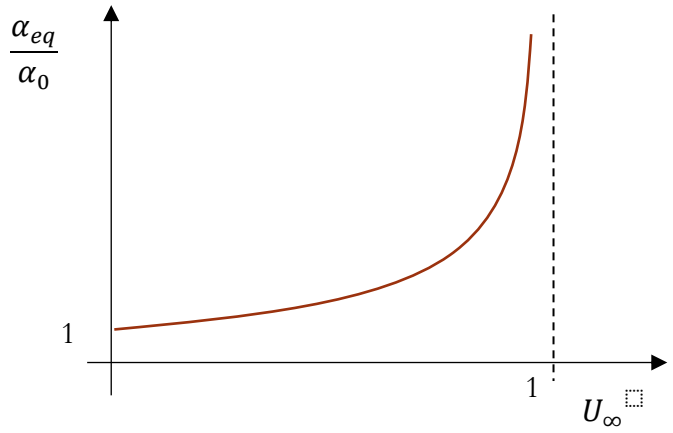

2.2. DYNAMIC AEROELASTICITY

Dynamic aeroelasticity concerns the interaction of inertial forces, unsteady aerodynamics and elastic response [9]. Flutter, Non-Synchronous Vibrations (NSV) and Forced Response are potential sources of dynamic aeroelastic failure. Forced response is defined as a response to external aerodynamic excitation loading that may be coupled with the natural frequencies leading to resonance on aircraft wings, HTP and VTP due to atmospheric turbulence or gust. Non-Synchronous Vibrations are aerodynamic instabilities produced by vortex shedding that interacts with the natural frequencies. These vortices induced vibrations are aerodynamic disturbances occurring near the stability limit.

A. FLUTTER

The main dynamic aeroelasticity phenomena of interest in this Final Year Project is flutter, a self-excited dynamic instability. It is considered one of the most difficult oscillatory phenomena to predict in which the aerodynamic forces modify the natural mode-shapes and frequency, resulting in vibrations with increasing amplitude. Depending on whether the force is lagging or leading the displacement, the incoming flow absorbs or feeds in energy from the aircraft wing, and the motion is damped or amplified, respectively. coupled bending-torsion motion or stall or buffeting conditions. Hence, it is important to evaluate the critical airspeed limit for properly structural and aeroelastic design.

Flutter occurs at the critical flutter speed, which is the lowest airspeed at which a given structure oscillates with sustained simple harmonic motion [7]. No perturbations or unsteadiness characteristics coming from the upstream flow are necessary to initiate this mode coalescence phenomena. Flutter instability is due to the phase between the aerodynamic forces acting on the aircraft wing and the structural displacements. The main reason that triggers purely structural natural modes to couple in an unfavorable manner due to the interaction of aerodynamic forces, depends on the mass ratio (the ratio of the aircraft wing mass to the mass of the surrounding fluid).

Flutter is categorized into at least five different areas, each with its own characteristic modes of motion: classical flutter, -wing bending & torsion-; control surface flutter, -surface rotation and wing bending-; empennage flutter, -fuselage torsion and tail torsion-; stall flutter, -wing torsion-; and finally, body freedom flutter, -wing bending and fuselage pitch-. In the following section, the fundamental equations of motion of a linear aerodynamic system will be presented, as described in Hodges and Pierce [2].

If the resonant oscillation occurs in the tailplane as a consequence of the airflow coming from the wing wake, *buffeting* dynamic phenomena occurs when aerodynamic strikes the natural frequency of the HTP structure. A proper tail positioning with a clean aerodynamic design will avoid this phenomenon to take place.

B. NON-SYNCHRONOUS VIBRATIONS

Non-Synchronous Vibrations (NSV) are aerodynamic instabilities produced by vortex shedding, resulting in Vortex Induced Vibrations. Aerodynamic disturbances occurs near the stability limit and boundary layer detachment leads to the development of notable fluid-structure interaction in which the wing oscillates. In this scenario, the limits of unsteady effects by pulsating flow is estimated by the Strouhal number. It is defined as the ratio of the characteristic time, -time for fluid particles to be transported through the wing chord-; and residence time, -time scale of the unsteadiness pulsating flow-. Belvis defined The Strouhal number (St) as the ratio of the product of the predominant frequency of vortex shedding and the cross-wind dimension of the body to the free stream velocity[44].

The Strouhal number can be expressed as:

$$St = \frac{2\pi f c}{U_\infty}$$

Where:

f is the vortex shedding frequency, Hz.

c is the chord of the airfoil, m.

U_∞ is free stream velocity, m/s.

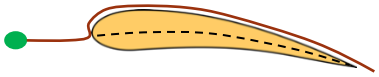

$$t_{residence} = \frac{c}{U_\infty}$$

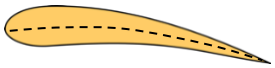

$$t_{charact.} = 2\pi f$$

Residence time is the time that particles invest on traveling through the airfoil section. Characteristic time is related with the vibration of the airfoil.

C. FORCE RESPONSE

Force response aeroelastic phenomenon occurs as a response to external aerodynamic nature excitation loading due to atmospheric turbulence or gust on aircraft wing, HTP and VTP. In this case, the excitation load frequency is coupled with the natural vibration frequency. For this given situation in which the external excitation frequency coincides with the natural vibration frequency, **resonance** will appear. Main potential source for external response on aircraft wing and control surfaces is the **gust**.

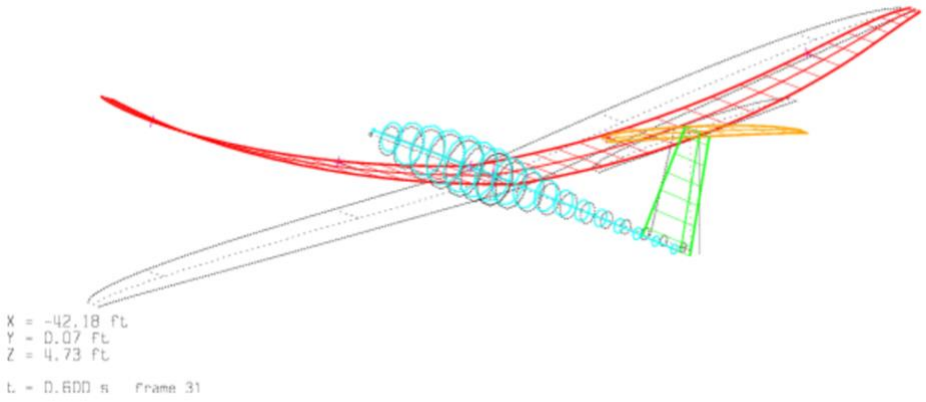

FIGURE 7. FEA model of an aircraft subject to gust. Ref [27]

2.3. INSTABILITY

According to [8], "the most dramatic physical phenomenon in the field of aeroelasticity is flutter, a dynamic instability which often leads to catastrophic structural failure". In this case, it is convenient to define instability to avoid confusion between resonance & instability. Instability is a growing motion with two distinguish features: on the one hand, it is self-excited, -caused by the motion itself, as no forced is applied onto the system-. On the other hand, it grows exponentially, leading to a linear failure due to an increased-on amplitude:

- Linear System: Destructive failure as instability grows exponentially due to the fact that stresses are higher than those of the design envelope as amplitude is high. Small oscillations appear compared with the characteristic length.

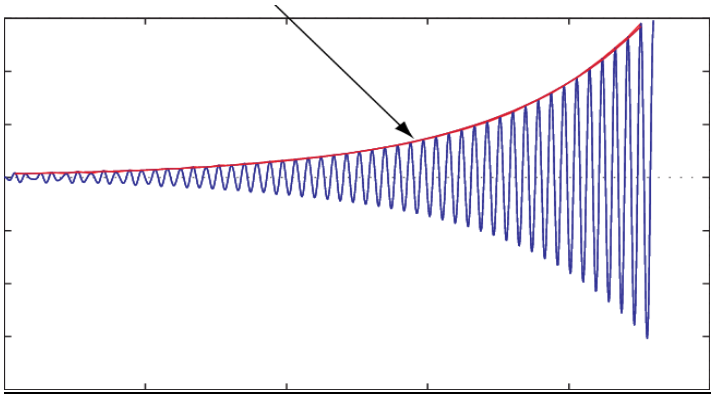

FIGURE 8. Instability linear system. Ref [1]

- Non-Linear System: Motion grows exponentially at the beginning. As nonlinearities become significant, Limit-Cycle Oscillations of large amplitude that promotes excessive vibrations & fatigue appear.

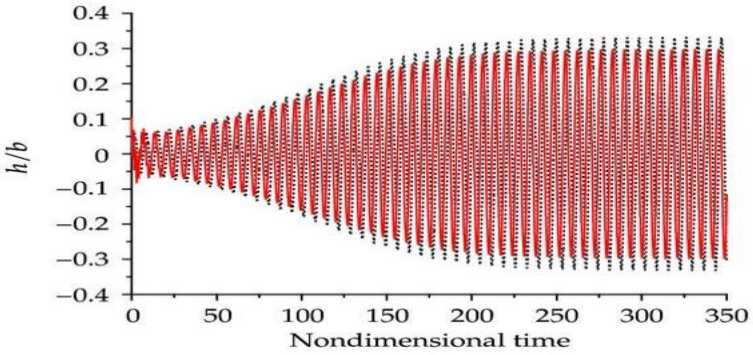

FIGURE 9. Instability non-linear system. Ref [1]

Finally, it can be concluded that resonance requires external excitation and can only grow linearly. In that case, natural frequencies cannot coincide with the external excitation frequency as it is a self-induced vibration.

2.4. VIBRATIONS

According to [2], vibrations are oscillations of a mechanical or structural system about an equilibrium position. Vibrations are classified by its nature as free vibrations and forced vibrations. If the vibrations are initiated by an initial energy present in the system and no other source is present, the resulting vibrations are called free vibrations. If the vibrations are caused by an external force or motion, the vibrations are called forced vibrations. If the external input is periodic, the vibrations are harmonic. Furthermore, essential data to describe vibration motion is needed, regarding the number of degrees of freedom necessary for their modelling and the boundary conditions used in the modelling. Vibrations of systems that have a finite number of degrees of freedom are called discrete systems. In this Final Year Project, the main focus will be on two degree of freedom self-induced vibration as a simplification of an aircraft wing.

A. AEROELASTIC MODEL OF AN AIRCRAFT WING

Free vibrations can be defined as a system which no external force is causing the motion, and that the motion is primarily the result of initial conditions, such as an initial displacement of the mass element of the system from an equilibrium position and/or an initial velocity.

In this one degree of freedom case, the **aircraft wing** will be represented as a mass attached to a spring, being the last one a **physical model** simplification for storing kinetic energy that the wing may absorb. In order to provide a real approximation to the physical model, it is assumed that there is a force acting on the mass in a direction opposite to the motion. This force is also proportional to the motion, -the faster an object moves, the higher the friction-. So, **damping force** of viscous nature is introduced. By applying equation of motion, representing the free vibration 1DOF damped spring-mass system,

we can obtain the differential equation for damped motion of an aircraft wing simplification expressed as:

$$m\ddot{x} + c\dot{x} + kx = 0$$

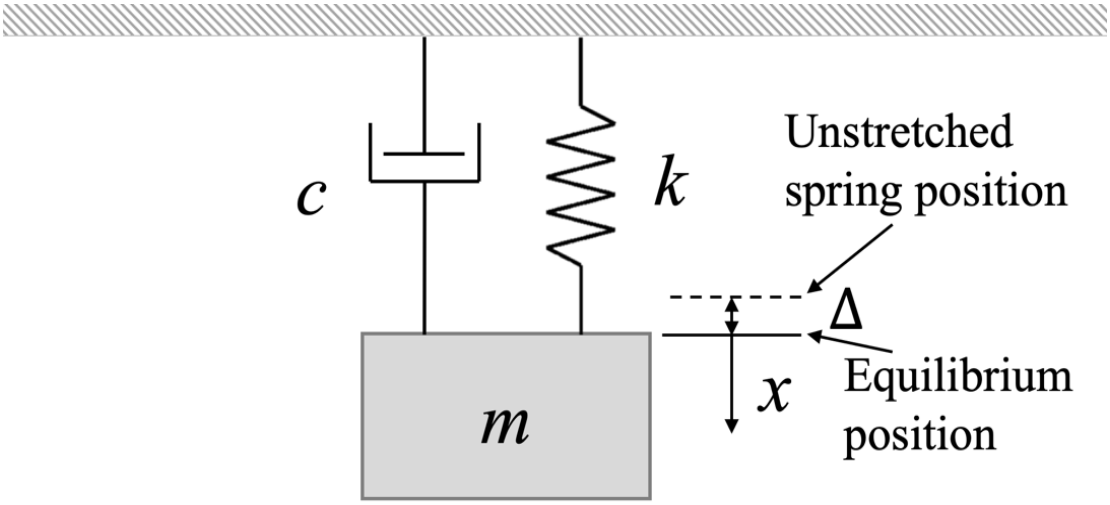

FIGURE 10. Free vibration damped spring–mass system. Ref [2]

Where **m** and **k** are the mass and stiffness matrices, respectively; **c**, is the damping force, and **x** is the *n*-dimensional column vector of generalized coordinates. To solve the differential equation, we first need to solve the characteristic equation:

$$m\lambda^2 + c\lambda + k = 0 \rightarrow Assuming\ exponential\ form: x(t) = Ce^{\lambda t}$$

$$\lambda = \frac{-c \pm \sqrt{c^2 - 4mk}}{2m}$$

Therefore, the behavior of the system exclusively depends on the factor inside the square root. The critical damping coefficient c_{cr} is defined as:

$$c_{cr}{}^2 - 4mk = 0\ ; \quad c_{cr} = 2\sqrt{mk} = 2m\omega$$

For calculus convenience, it may express this equation in terms of:

$$\ddot{x} + \frac{c}{m}\dot{x} + \frac{k}{m}x = 0$$

Thus, damping ratio and the undamped natural frequency can be defined:

$$\zeta = \frac{c}{2\sqrt{mk}} = \frac{c}{c_{cr}} \; ; \qquad \omega_n = \sqrt{\frac{k}{m}}$$

The following equation is obtain by rearranging terms:

$$\lambda \; = \; - \; \zeta\omega_n \; \pm \; \omega_n\sqrt{\zeta^2 - 1}$$

Therefore, different scenarios will eventually take place as a function of the damping ratio.

i) $\zeta > 1$ (Overdamped motion, the roots of the characteristic equation are two real values)

ii) $\zeta = 1$ (Critically damped, the roots of the characteristic equation are two real & similar values)

iii) $0 < \zeta < 1$ (Underdamped motion, the roots of the characteristic equation are complex conjugates)

iv) $\zeta < 0$ (Flutter response, self-excitation instability)

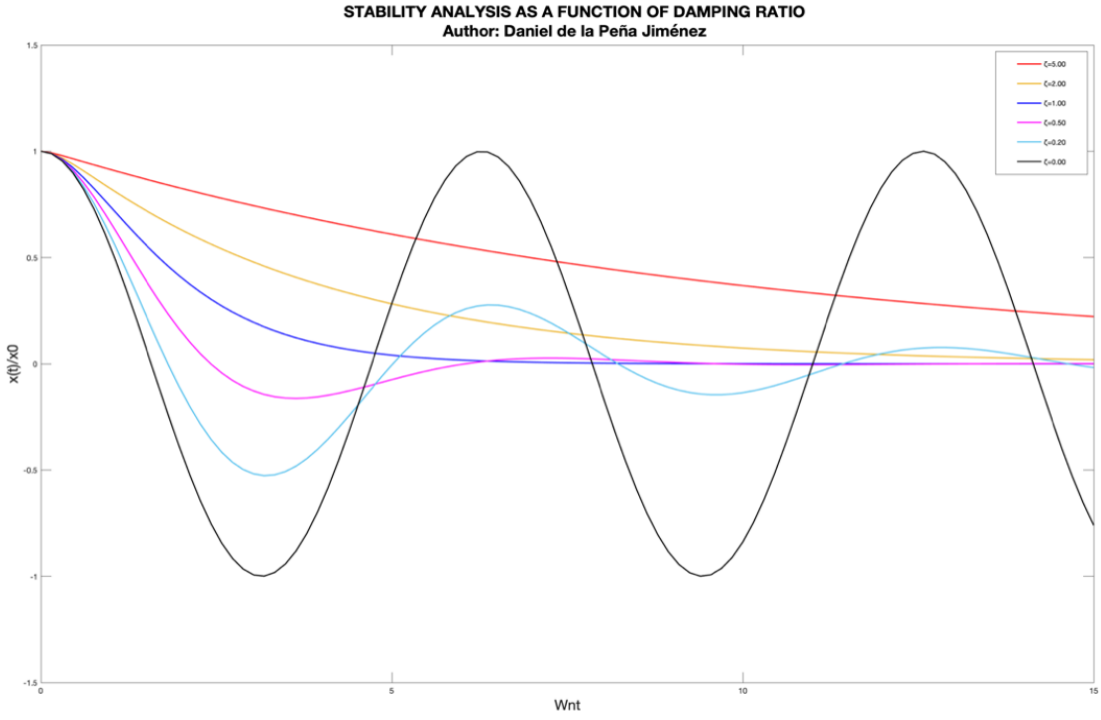

FIGURE 11. Stability analysis as a function of damping ratio.

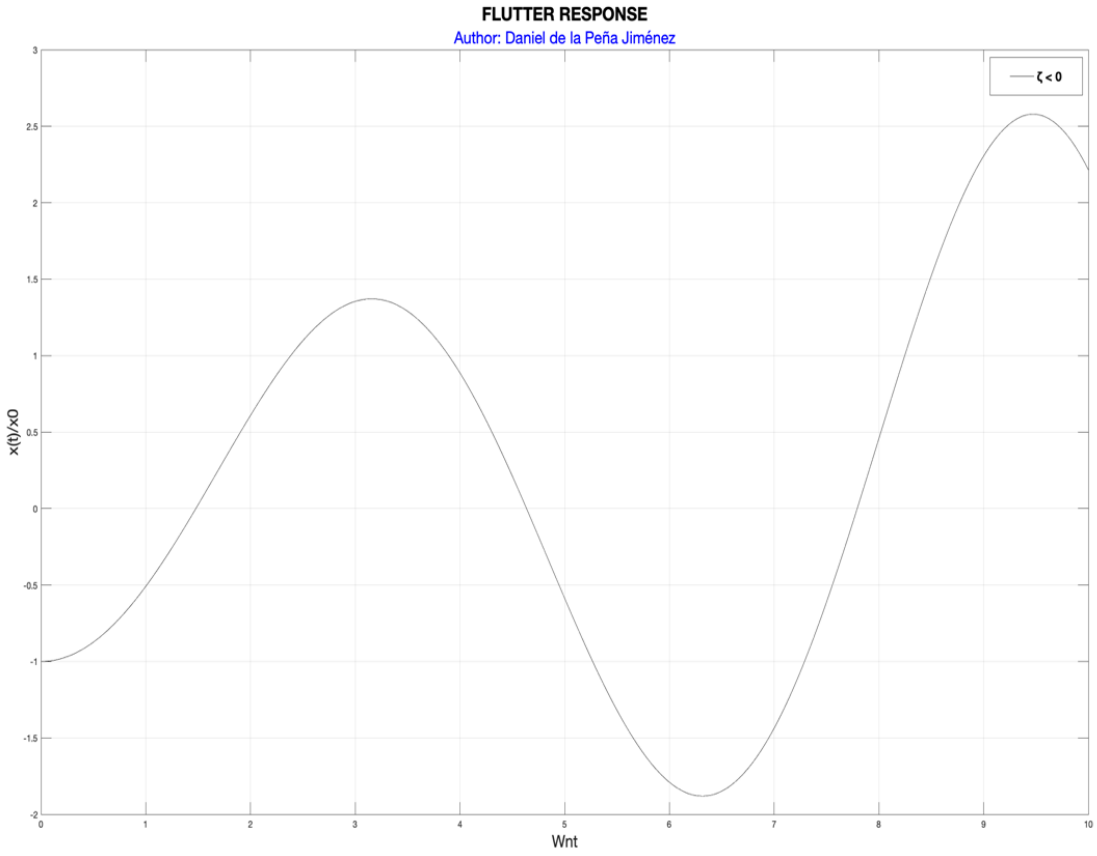

FIGURE 12. Flutter response as a function of damping ratio.

CHAPTER 3

""A ship in harbor is safe,
but that is not what ships are built for."

William G.T. Shedd

Contents

3. FLUID-SOLID INTERFACE MODELS

There are grounds for believing that aircraft structures can be considered engineering masterpieces in modern world. Aircraft structures are typified by arrangements of thin, load-bearing skins, frames and stiffeners, fabricated from lightweight, high strength materials of which aluminum alloys are the most widely used examples. Therefore, an aircraft is basically an assembly of shell structures ranging from the single cell closed section fuselage to multicellular wings and tail surfaces each subjected to bending, shear, torsional and axial loads. Mesgson, in his Masterpiece "Aircraft Structures for Engineering Students", assumes that those complex structural elements may be idealized into simpler "mechanical models" which behave, -under given loading conditions-, in the same, or very nearly the same, way as the actual structure[6]. These different models of the same structure are required to simulate actual behavior under different systems of loading.

3.1. FLUID-MECHANICS GOVERNING EQUATIONS

Computational Fluid Dynamics involves the analysis of a moving fluid into a media. In this Final Year Project, Navier-Stokes equations are solved at the Fluid-Structure Interface domain under dynamic mesh boundary conditions. Assumptions are made for continuity equation, regarding **Conservation of Mass**; **Conservation of Momentum**, in which the momentum Equation is solved by applying Newton's Second Law; and finally, **Conservation of Energy**, stated in the first law of Thermodynamics.

The law of **conservation of mass** establishes that the mass of a closed mass-energy system, the mass is constant through time since it is not created, neither destroyed. Hence, the mass quantity is conserved at steady state condition.

$$\frac{\partial \rho}{\partial t} + \ (\nabla \cdot \rho v) = 0 \tag{3.1.1}$$

$$\frac{\partial \rho}{\partial t} + \ \frac{\partial}{\partial x}(\rho v_x) + \frac{\partial}{\partial y}\left(\rho v_y\right) + \frac{\partial}{\partial z}(\rho v_z) = 0 \tag{3.1.2}$$

CONTINUITY EQUATION. Navier-Stokes equation for Mass Conservation.

The **conservation of momentum** law states that, if an object in motion collides with an isolated object in an isolated system, the sum of the both momentum before the collision of the objects is equal to the sum of the both momentum after the collision. Simply, it means that the second object gains the penalty in momentum of the first object as a consequence of the collision.

$$\rho \frac{Dv}{Dt} = -\nabla \mathrm{p} + \rho g + \ \mu \nabla^2 v \tag{3.1.3}$$

$$\rho\left(\frac{\partial v_x}{\partial t} + \ v_x \frac{\partial v_x}{\partial x} + v_y \frac{\partial v_x}{\partial y} + v_z \frac{\partial v_x}{\partial z}\right) \ = \ - \frac{\partial p}{\partial x} \ + \rho g_x \ + \ \mu\left[\frac{\partial^2 v_x}{\partial x^2} + \frac{\partial^2 v_x}{\partial y^2} + \frac{\partial^2 v_x}{\partial z^2}\right] \nabla^2 v \tag{3.1.4}$$

MOMENTUM EQUATION. Navier-Stokes Equation for Momentum Conservation.

Conservation of Energy, which is the first law of Thermodynamic as learnt from previous courses on "Thermodynamic & Propulsion", states that there is an increment on energy balance in the system if work and heat are added to the system itself.

$$dE_t = dQ + dW \tag{3.1.5}$$

$$\rho\left[\frac{\partial h}{\partial t} + \nabla\cdot(h\vec{v})\right] = -\frac{\partial p}{\partial t} + \nabla\cdot(k\nabla T) + \emptyset \tag{3.1.6}$$

ENERGY EQUATION. Navier-Stokes Equation for Energy Conservation.

Where, dQ is the heat added to the system, dW is the work done on the system and dEt is the increment in the total energy of the system. This equation simply studies the local variation of the convective term, pressure gradient, heat flux and source term with respect local time.

Due to the complexity of Fluid-Mechanics equations, involving several unknowns for each integrer, numerical methods are needed to predict flow field behavior. Therefore, Computational Fluid Dynamics (CFD) are implemented to obtain an approximated solution to that system of equations. Once, the disclaimer of fluid-mechanics complexity equations have been broaden, the next step is to select the most accurate mathematical model with an adequate approximation level to the physical problem. In our case, potential flow will be assumed in order to apply panel method in every node of the fluid domain. No compressibility effects will be taken into account. Figure 13 provides a closer view to the different computational models in which complexity, time cost and accuracy of the approximations needs to be considered for every case.

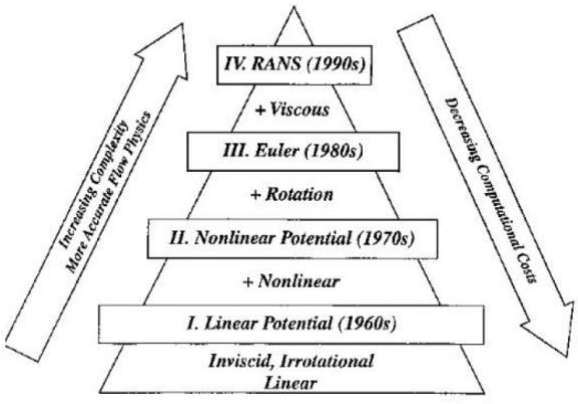

FIGURE 13. Levels Of Approximation for Fluid Flow. Ref[45].

3.2. STRUCTURAL MODEL

To provide an accurate structural analysis of an aircraft wing, a cantilever beam was chosen as a mathematical simplification of an aircraft wing model. Hence, the analysis presented in this report is therefore approximate and the degree of accuracy obtained depends on the number of simplifying assumptions made. Numerical and analytical results show a relative error on calculations. Therefore, we should consider some factors that may result in solution variations such as warping restraint, structural and loading discontinuities and shear lag. Those implications significantly affect the analysis.

Consider the following illustration regarding classical linear elastic beam theory to implement the driving "force" variables in terms of beam curvatures, etc., and on substituting into the equation of motion. This will serve as a reference to understand its derivation process:

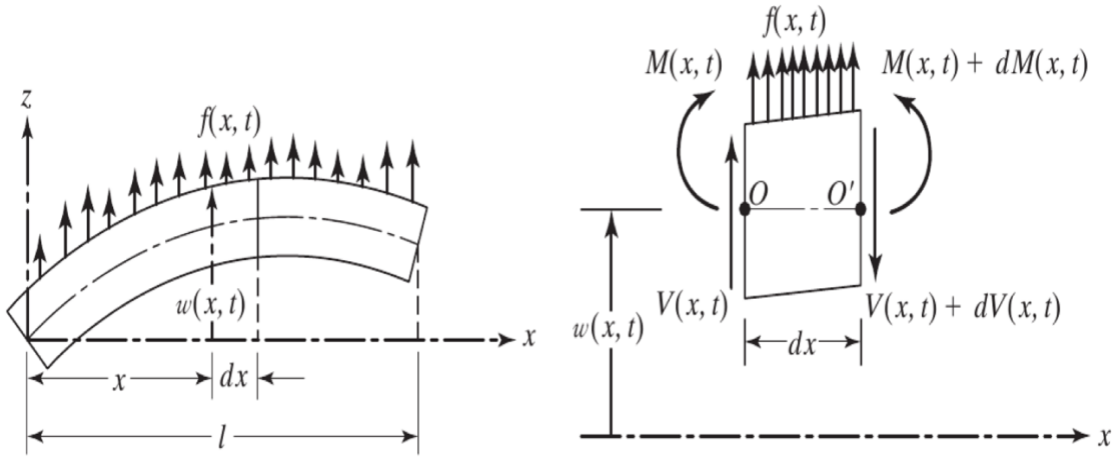

FIGURE 14. Bending of a beam overcoming a flexural moment and load analysis. Ref [8]

Introducing equilibrium equations of motion for an infinitesimal beam segment undergoing a motion in absence of distributed loads (P = 0), the net y direction force applied to an infinitesimal beam slice between "x" and "x + dx":

$$\sum F_y = V(x + dx, t) - V(x, t) \cong dx\left(\frac{\partial V(x, t)}{\partial x}\right)$$

Where V (x, t) is the shear force in the beam at position x and time t. Applying Newton second law and classical linear elastic beam theory to implement the driving "force" variables in terms of beam curvatures, etc., and on substituting into the equation of motion, we obtain:

$$-(V + dV) + f(x,t)dx + V = \rho A(x)dx\frac{\partial w^2}{\partial x^2}(x,t)$$

In order to relate the bending moment with the equation of motion, we can substitute the Euler-Bernoulli equation in the previous formula:

$$\frac{d^2}{dx^2}\left\{EI(x)\frac{d^2Y(x)}{dx^2}\right\} = \omega^2 m(x)Y(x)$$

Where E, is the modulus of rigidity; I, is the moment of inertia of the beam cross section; ω, is the natural frequency; and m, is the mass of the cantilever beam($\varrho A_{(x)}$). An important assumption regarding cantilever beam properties, **inertia is considered constant along the cantilever beam.**

$$\frac{d^4Y(x)}{dx^4} = \beta^4 Y(x)$$

$$\beta = \frac{\omega^2 m}{EI}$$

For uniform beam, we obtain the 4th order ordinary differential equation for Y as function of x, including 4 arbitrary constants of integration as a function of:

$$\mathrm{Y}(x) = C_1\mathrm{sen}\beta x + C_2\mathrm{cos}\beta x + C_3\mathrm{senh}\beta x + C_4\mathrm{cosh}\beta x$$

Applying boundary conditions at the beam ends x = 0 and x = L to evaluate the constants:

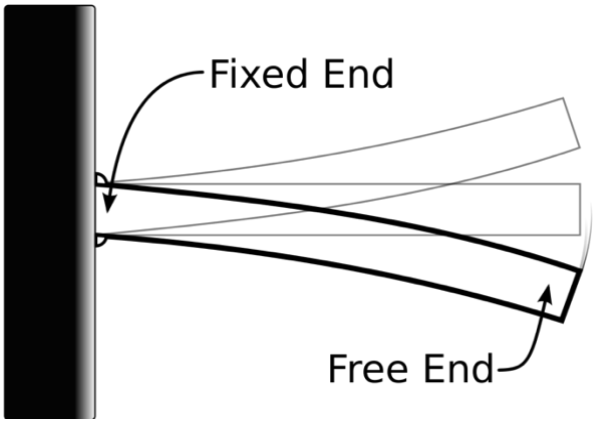

$Y(0) = 0$ (Fixed end)

$\left.\frac{dY}{dx}\right|_{x=0} = 0$ (Neutral axis)

$\left.\frac{d^2Y}{dx^2}\right|_{x=L} = 0$ (Bending moment)

$\left.\frac{d^3Y}{d^3x}\right|_{x=L} = 0$ (Kinematic const.)

FIGURE 15. Boundary conditions of a cantilever beam

3.3. STRUCTURAL IDEALIZATION OF AN AIRCRAFT WING

According to [6], wing sections consist of thin skins stiffened by combinations of stringers, spar webs, and caps and ribs. The multicellular wing sections are frequently subjected to bending, torsional and shear loads. The large number stringers that are close to each other allows the following assumption: the skin between adjacent stringers is effective carrying constant shear flow; booms are effective carrying direct stress. In order to idealize an aircraft wing, direct stress distribution in the panel must be assumed in order to reduce it to a simplified representation. As direct stress varies linearly, and the idealized panels must be similar, we can equate moments and obtain:

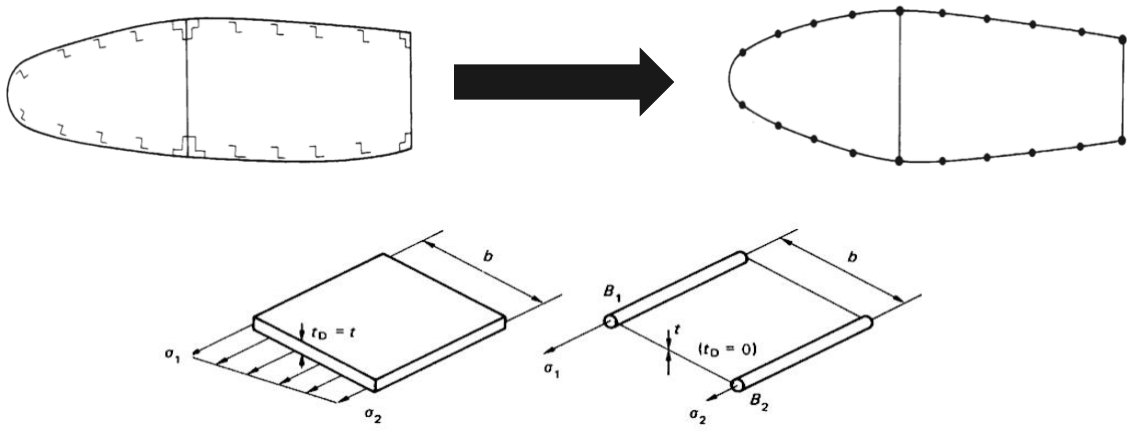

FIGURE 16. Structural Idealization of Booms And Direct Stresses. Ref[6]

$$\sigma_2 t_D \frac{b^2}{2} + \frac{1}{2}(\sigma_1 - \sigma_2) t_D b \frac{2}{3} b = \sigma_1 B_1 b$$

$$B_1 = \frac{t_D b}{6}\left(2 + \frac{\sigma_2}{\sigma_1}\right)$$

$$B_2 = \frac{t_D b}{6}\left(2 + \frac{\sigma_1}{\sigma_2}\right)$$

A. BENDING MOMENT & DIRECT STRESS

Analyzing the direct stress distribution produced by pure bending under the assumptions in which the plane cross-section of the beam remains plane and normal to the longitudinal fibers of the beam after bending, we can obtain that:

$$\sigma_z = -\frac{M}{I} y$$

The direct stresses are formed by a group of direct stresses concentrated at the centroid of the booms when the beam cross-section is completely idealized. Therefore, booms carry direct stresses and panels undergo shear stresses.

B. SHEAR

As we have seen, direct stress σ_z is produced by bending moments or by the bending action of shear loads. In this case, the shear stresses are due to shear and/or torsion of a closed section beam or shear of an open section beam.

$$\frac{\partial q}{\partial s} + t\frac{\partial \sigma_z}{\partial z} = 0$$

Therefore, we can integrate the equation with the respective implications regarding idealized structure in order to obtain the shear flow distribution in a close beam:

$$q_s = \left(\frac{S_x I_{xx} - S_y I_{xy}}{I_{xx} I_{yy} - {I_{xy}}^2}\right)\left(\int_0^s t_D x \, ds + \sum_{r=1}^{n} B_r x_r\right) - \left(\frac{S_y I_{yy} - S_x I_{xy}}{I_{xx} I_{yy} - {I_{xy}}^2}\right)\left(\int_0^s t_D y \, ds + \sum_{r=1}^{n} B_r y_r\right) + q_{s,0}$$

C. DISPLACEMENTS

Deflections on an aircraft wing are mainly introduced by bending and shear interaction over the wing surface.

(i) BENDING

Deflections due to bending, can be related with the increment in total complementary energy due to the application of a virtual unit load:

$$\Delta M = \int_L \left(\int_A \sigma_z \, \epsilon_z \, dA\right) dz$$

Where $\sigma_{z,1}$ is the direct bending stress along the beam cross-section:

$$\sigma_z = \left(\frac{M_y I_{xx} - M_x I_{xy}}{I_{xx} I_{yy} - {I_{xy}}^2}\right) x + \left(\frac{M_x I_{yy} - M_y I_{xy}}{I_{xx} I_{yy} - {I_{xy}}^2}\right) y$$

And ϵ_z is the strain produced by the virtual load that can be expressed as:

$$\epsilon_z = \frac{1}{E}\left[\left(\frac{M_y I_{xx} - M_x I_{xy}}{I_{xx} I_{yy} - {I_{xy}}^2}\right)x + \left(\frac{M_x I_{yy} - M_y I_{xy}}{I_{xx} I_{yy} - {I_{xy}}^2}\right)y\right]$$

Therefore, we can express the following displacement equation for a symmetric airfoil as:

$$\Delta M = \frac{1}{E}\int_L \left(\frac{M_{y,1} M_{y,0}}{I_{yy}} + \frac{M_{x,1} M_{x,0}}{I_{xx}}\right) dz$$

(ii) BENDING

Deflections due to shear, can be related with the increment in total complementary energy due to the application of a virtual unit load:

$$\Delta S = \int_L \left(\int_{sect} \frac{q_0 q_1}{Gt}\, ds\right) dz$$

Where the shear stresses correspond to:

$$q_0 = \left(\frac{S_{x,0} I_{xx} - S_{y,0} I_{xy}}{I_{xx} I_{yy} - {I_{xy}}^2}\right)\left(\int_0^s t_D x\, ds + \sum_{r=1}^{n} B_r x_r\right) - \left(\frac{S_{y,0} I_{yy} - S_{x,0} I_{xy}}{I_{xx} I_{yy} - {I_{xy}}^2}\right)\left(\int_0^s t_D y\, ds + \sum_{r=1}^{n} B_r y_r\right)$$

$$q_1 = \left(\frac{S_{x,1} I_{xx} - S_{y,1} I_{xy}}{I_{xx} I_{yy} - {I_{xy}}^2}\right)\left(\int_0^s t_D x\, ds + \sum_{r=1}^{n} B_r x_r\right) - \left(\frac{S_{y,1} I_{yy} - S_{x,1} I_{xy}}{I_{xx} I_{yy} - {I_{xy}}^2}\right)\left(\int_0^s t_D y\, ds + \sum_{r=1}^{n} B_r y_r\right)$$

3.4. UNSTEADY AERODYMIC MODEL

The current Final Year Project develops and implements a Fluid-Structure Interface to evaluate and study aeroelastic response within the framework of the viscous flow solver. The monolithic and staggered solvers acquire the capability to conduct fully coupled nonlinear aeroelastic, aerodynamic and inertial analyses of structure's unsteady responses. In the FSI model, the equations governing the fluid motion are essentially coupled: fluid and structure are treated as a single dynamic system.

A. FLUTTER

The general form of a rigid airfoil's 2-DOF motion may be derived by using Lagrange's equations and considering the total energy of motion for the wing section's center of mass. This approach leads to a set of nonlinear equations of motion for the airfoil plunging and pitching amplitudes *y=h(t)* and *a(t)*, respectively. These two flexible supports restrict the motions of the airfoil with the exception in the two modes of translation and rotation. For the case of zero damping, the equations of motion of the airfoil subjected a uniform flow can be written as:

$$M_s\ddot{v} + K_s v = \begin{bmatrix} -Lift \\ Moment \end{bmatrix}$$

where *v*(t)=[*h(t), a(t)*] is the displacement vector, and Lift, L(t), and Moment, M(t), are the lift and pitching moment about the rotation axis, correspondingly.

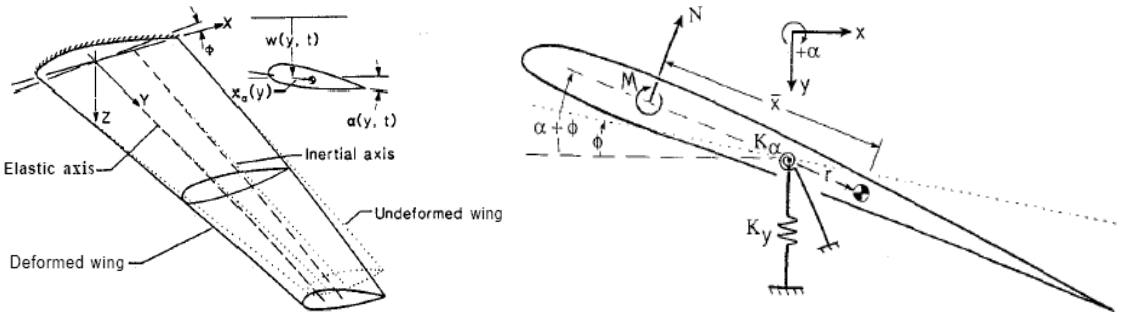

FIGURE 17. Binary Flutter Model Aeroelastic Phenomena. Ref [9]

The structural wing section properties include the linear mass matrix $\boldsymbol{M_s}$ and the stiffness matrix $\boldsymbol{K_s}$, given by the following equation, which assumes no damping:

$$\begin{bmatrix} m & mx_\alpha b \\ mx_\alpha b & I_g + m(x_\alpha b)^2 \end{bmatrix} \begin{Bmatrix} \ddot{h} \\ \ddot{\alpha} \end{Bmatrix} + \begin{bmatrix} k_\alpha & 0 \\ 0 & k_\alpha \end{bmatrix} \begin{Bmatrix} h \\ \alpha \end{Bmatrix} = \begin{bmatrix} -L \\ Lec + M_{ac} \end{bmatrix}$$

Where m denotes the total mass of the wing section, I_g is the mass moment of inertia, $mx_\alpha b$ is the static moment. Theodorsen's unsteady aerodynamic model was implemented to analyze pitching and torsion motions of the airfoil in the frequency domain by assuming small amplitudes 5% chord. In the analysis performed, the flow is assumed to be inviscid and incompressible with no flow separation.

By imposing an harmonic function to the motions in both torsion and bending modes:

$$\begin{Bmatrix} h \\ \alpha \end{Bmatrix} = \begin{Bmatrix} \hat{h} \\ \hat{\alpha} \end{Bmatrix} e^{i\omega t}$$

The aerodynamic loading can be represented as the expression:

$$F_{aero} = \begin{bmatrix} -L \\ Lec + M_{ac} \end{bmatrix} = \frac{1}{2}\rho {U_\infty}^2 Q_f \begin{Bmatrix} h \\ \alpha \end{Bmatrix}$$

To validate the aeroelastic response module, it is assumed no structural damping effect into the equation of motion. Hence, and to investigate the airfoil response near the flutter boundary, V-g method will be implemented. In V-g analysis, the structural damping of all the modes of vibration is assumed to have one unknown value, g.

$$M\ddot{h} + Mx_\alpha \ddot{\alpha} + K_h \left[(g_h + g)\frac{\dot{h}}{\omega} + h \right] = -Le^{i\omega t}$$

$$I_\alpha \ddot{\alpha} + Mx_\alpha \ddot{h} + K_\alpha \left[(g_\alpha + g)\frac{\dot{\alpha}}{\omega} + \alpha \right] = M_a e^{i\omega t}$$

V-g method is based on the balance of energy between the flow and the motion of the structure corresponding to flutter boundary for a linear aeroelastic system. The analysis is conducted in frequency domain where harmonic motions in pitching and plunging are imposed to the dynamic response of the structure to represent the state of the aeroelastic system in the stability boundary.

Subsequently the equations of motion will lead to the solution of the eigenvalues problem. To perform this analytical analysis, the corresponding mass, inertial and geometric parameters will correspond to the numerical design for validation purposes. These results will be compared in the following sections.

Table 1. Properties of aeroelastic model.

Structural Parameters	Value
$\boldsymbol{Mass, m_T}$	200 kg
$\boldsymbol{Spring\ constant, k_h}$	2800 N/m
$\boldsymbol{Mass\ moment\ of\ Inertia, I_\alpha}$	40,4 $kg \cdot m$
$\boldsymbol{Spring\ constant\ pitch, k_{\alpha\ 1}}$	23.3 N/m
$\boldsymbol{Wing\ chord}$	4.8 m

In Figure 17, the results for two modes (roots of the flutter determinant) of the simple wing model with 2 degrees of freedom are shown in the form of frequency versus velocity and damping versus velocity curves. In the bottom plot, the velocity at which the upper curve passes through g=0 corresponds to the flutter velocity of the model if the (conservative) assumption of zero structural damping is made. One is then able to determine the flutter frequency of the model using the upper plot and picking off the frequency value of the unstable mode at the flutter velocity value. The slope of the damping versus velocity curve as it passes through the flutter velocity can be thought of as a qualitative measure of how violently the oscillations would occur during accelerated flight.

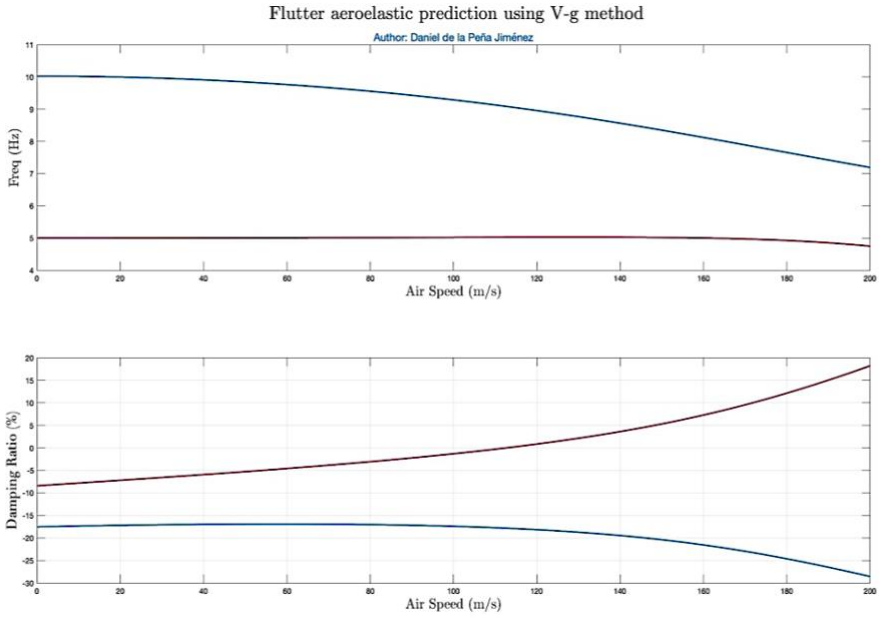

FIGURE 18. P-K method for critical flutter speed velocity validation.

CHAPTER 4

"It is the time you have wasted
for your rose that makes your rose so important."

Antoine De Saint-Exupéry

Contents

4. FLUID - SOLID SOLVER

In Chapter 2, aeroelastic fundamentals were introduced in order to define and differentiate static and dynamic aeroelasticity models, as well as its impact on aero-structural parameters. In Chapter 3, the Navier-Stokes governing equations for the fluid domain were analysed regarding computational need for the simulation of fluid dynamics problems. In the current Chapter, coupling and interaction between Fluid and Structural domain are stated as monolithic or staggered Fluid-Structure Interaction (FSI). Moreover, intuitive alternatives to achieve higher numerical accuracy by reducing computational time is proposed at the end of the section.

4.1. FLUID-STRUCTURE COUPLING METHODS

According to [46], FSI solvers are classified in two different categories: strongly-coupled, -or monolithic-; and partitioned-coupled, -or staggered-. Aeroelastic phenomenon can be predicted

by means of a coupled numerical analysis, in which the nonlinear equations of motion for the wing structure are solved simultaneously with a set of governing Navier-Stokes equations, resulting in a coupled dynamic system. The fluid and structure components are treated as a unique entity throughout the iterations.

High-order operators are used in the numerical simulation to provide accurate solutions to this aeroelastic problem. In a monolithic model, the equations of fluid, structure and movement of the grid are solved simultaneously. This approach increases the accuracy of the solution but can be very difficult to perform academic projects. This model is "computationally challenging, mathematically suboptimal and software-wise unmanageable when nonlinearities are present either in the fluid or structural equations"[47].

Alternatively, the fluid and structural equations can be solved by a staggered procedure, which consists in the successive decoupled integrations of the structure and the fluid fields. Hence, each field is frozen during the time integration of the other field, which brings many advantages, such as the possibility of using one way or two ways schemes and procedures for both separate fields. The main drawback is the fact that this method is not always stable and mesh-convergence anomalies may arise. In this Final Year Project, only staggered procedures will be considered, which are a high-mathematical challenge but a simple way to predict aircraft aeroelastic behaviour. Several aeroelastic tests will be performed on a 3D wing using different coupling procedures presented in the current section for comparison.

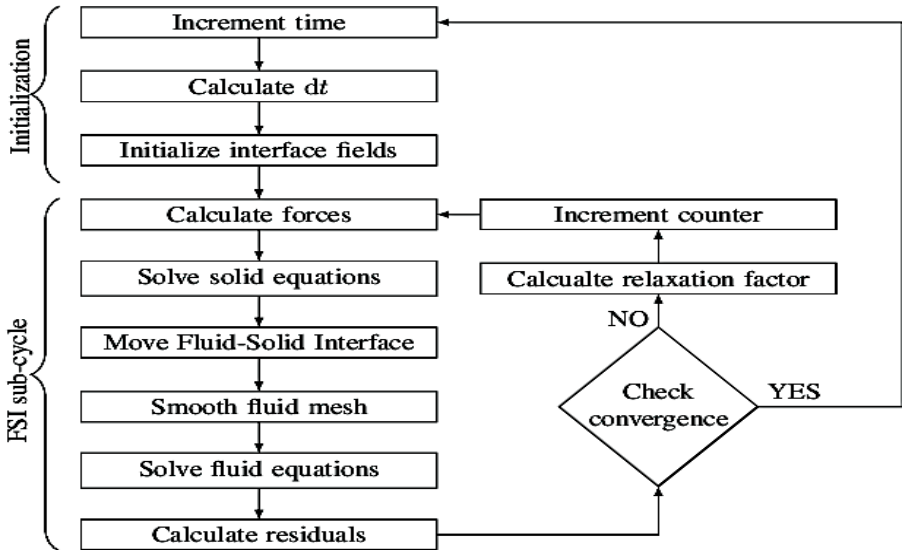

FIGURE 19. Coupled Fluid-Structure Flow Diagram.

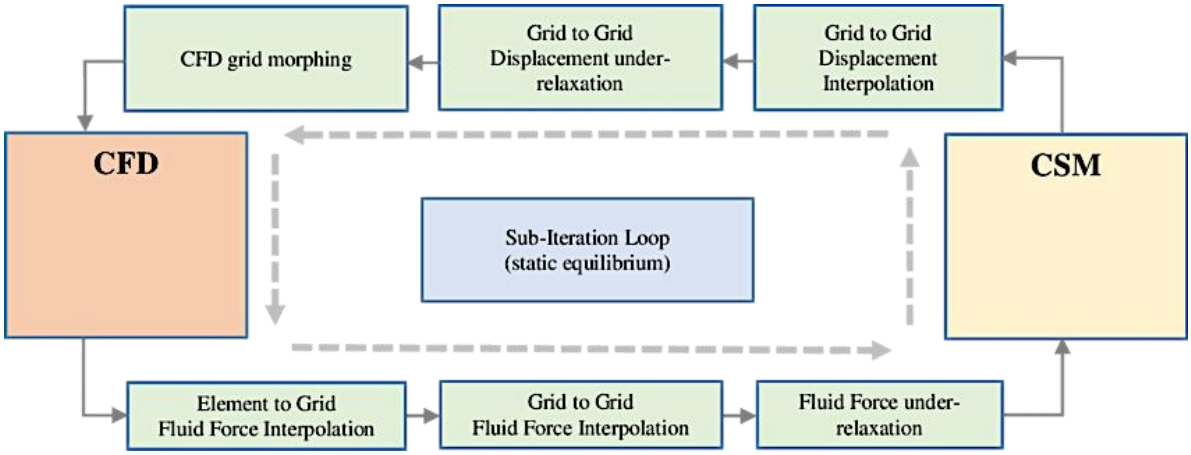

FIGURE 20. Coupled Fluid-Structure flow diagram.

Throughout the iterations, the presence of different forces as a consequence of a difference in pressure over the wall boundaries leads to a deformation and displacement in the vicinity of the structural model. Hence, if those displacements whose nature is given by fluid pressure are computed, we can update mesh by deforming the vicinity of the fluid-structural boundary. Both the fluid and solid constitutes a 2 DoF spring-mass system under forced response. The main principal algorithm of an staggered model is defined as follows:

- For every time-step, fluid pressures action over the wing walls are mapped, computed and shared within structural grid, at which the aerodynamic force is obtained for every node. Then, boundary conditions are updated to continue the FSI interaction.

- This pressure and aerodynamic force induce a displacement on the wing, which is integrated, solved and shared with the fluid solver for every-time step. This time-integrated method is widely used for aeroelastic phenomena, but also for industrial processes involving FSI solvers.

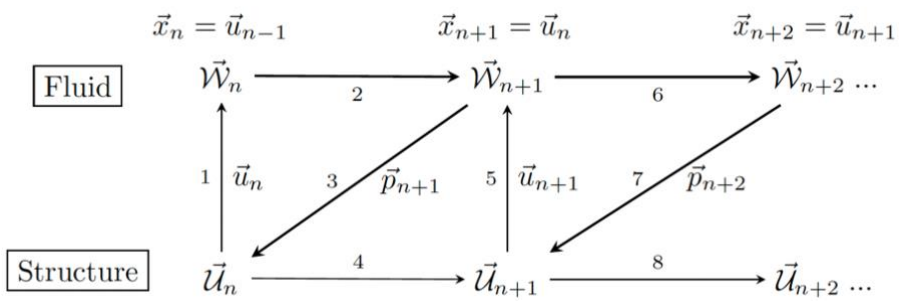

FIGURE 21. Sequential Staggered FSI Algorithm

A. STAGGERED ALGORITHYM

The sequential staggered algorithm will firstly discretize fluid and solid domain in time and different time step size. Once the Fluid and Structural equations are set according to the model specification, the following time, $n + 1$, will implement the following algorithm:

- Define an explicit grid node predecessor of the structural interface displacement at the new time level.
- Compute the fluid velocity and mesh displacement at n+1condition.
- Solve the fluid equations on the deforming domain to get Vn+1 and boundary conditions.
- Solve the structural field to get Vn+1 under consideration of the fluid boundary traction n+1.
- Proceed to the next time step.

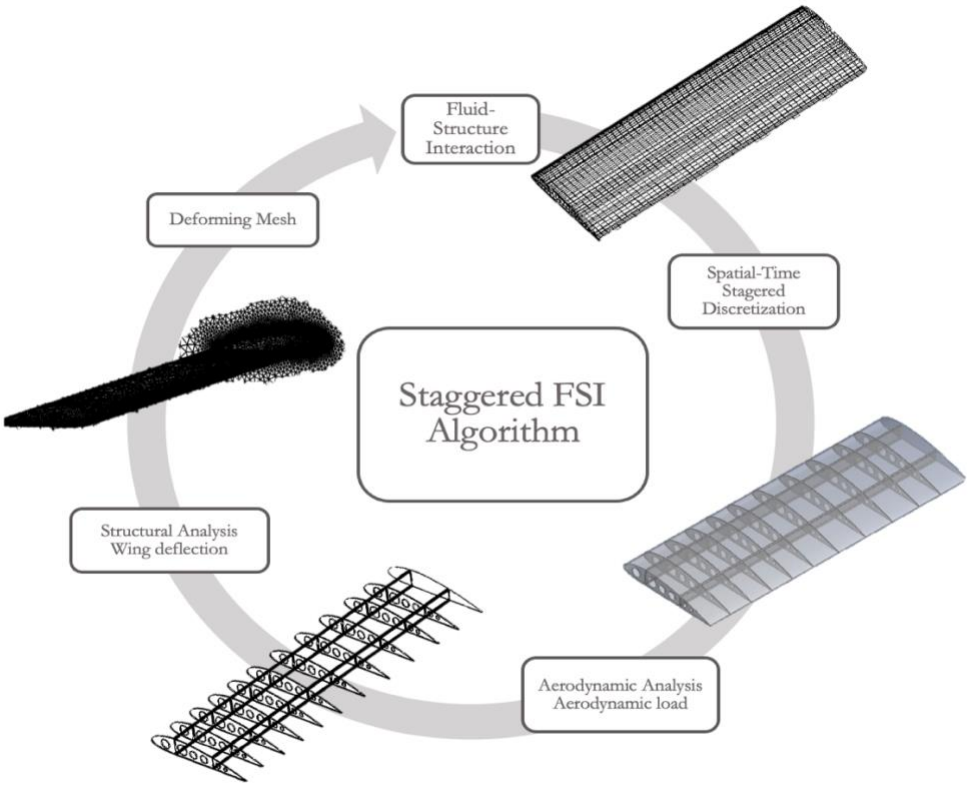

FIGURE 22. Final Year Project Flowchart for computational Aeroelastic study of an Aircraft Wing.

CHAPTER 5

"The journey of a thousand miles
must begin with a single step."

Lao Tzu

Contents

5. COMPUTATIONAL FSI DOMAIN

5.1. AIRFOIL SELECTION

Firstly, aircraft wing airfoils selection will be discussed by means of **Airfoil Selection Decision Matrix**. In order to provide an accurate airfoil geometry design, different airfoil geometries and families were analysed using XFLR5 to evaluate and optimize the lift distribution at cruise condition. A light-sport airplane, RV-10, was selected a reference for Mach values: the lift coefficient at cruise is about 0.30, and the required cruise Mach number is 0.25.

Hence, a set of airfoils collected from different aircraft database models were used in this decision matrix. **Table 2** includes information regarding the initial selection phase, the year it was developed, the thickness to chord ratio and Mach divergence.

The baseline selected was NACA2412 airfoil as they are able to sustain laminar-incompressible flow as far aft as 50% of the chord with a low AoA. The analysed value of the lift coefficient at cruise configuration is close to the required Cl and rival aircrafts lift coefficient's values. The root airfoil selected has 15% thickness, and the tip airfoil is 12%. The root is thicker due to higher bending moment and the space needed for internal rib structure. Hence, the optimization was performed at Mach 0.25 at 7.000 ft. The result shows the lift coefficients distribution, and the airfoil designed Cl is picked from the result at the designated locations.

TABLE 2. Airfoils selection decision matrix.

ID	Parameter	Airfoil 1	Airfoil 2	Airfoil 3	Airfoil 4	Airfoil 5	Airfoil 6	Airfoil 7	Score						
1	R_e for stall	$2.31x10^6$							Airfoils are scored by entering different grades being 1 the best characteristics.						
2	R_e for best ROC	$6.88x10^6$													
3	R_e for cruise	$8x10^6$													
4	Target C_{Lmax}	2.2													
5	C_L for best ROC, $C_{L\,ROCmax}$	0.7													
6	C_L for best target cruise, C_{LC}	0.27 - 0.31													
7	Name	SHM-01	RONCZ	66-210	65415	23015	NLF(1)-0115	2412	1	2	3	4	5	6	7
8	Thickness ratio	0.15	0.15	0.15	0.15	0.15	0.15	0.15	1	1	1	1	1	1	1
9	Sensitive to surface quality?	**Y**/N	**Y**/N	Y/**N**	**Y**/N	Y/**N**	**Y**/N	Y/**N**			1		1		1
10	R_e for data below	6.2E+06	6.2E+06	6.2E+06	6.2E+06	6.2E+06	6.2E+06	6.2E+06							
11	C_l for AOA = 0º	0.27	0.12	0.30	0.21	0.10	0.28	0.20						1	1
12	AOA for C_l = 0	-2.6º	-1.0º	-2.3º	-3.00	-1.00	-1.30	-1.40							
13	C_{lmax}	1.48	1.35	1.10	1.45	1.65	1.40	1.70							1
14	AOA of C_{lmax}	16.8º	15º	10.5º	15º	18º	14º	20º							1
15	Stall characteristics (A, B, C)	B	A	C	A	C	B	C		1		1			
16	C_{dmin}	0.0044	0.00843	0.0056	0.00529	0.00607	0.00454	0.00542	1						
17	C_l of C_{dmin}	0.3	0.26	0.19	0.29	0.31	0.30	0.32	1					1	
18	$(C_l/C_d)_{max}$	120	-	110	140.00	150.00	100.00	125.00					1		
19	C_l of $(C_l/C_d)_{max}$	0.63	0.84	0.37	0.56	0.45	0.47	0.60			1				
20	Cruise C_m	-0.008	-0.02	-0.01	-0.07	-0.01	-0.06	-0.05	1						
21	Drag bucket start at C_l	0.1	0.2	0.2	0.2	0.0	0.2	0							
22	Drag bucket ends at C_l	0.5	0.6	0.7	0.7	0.3	0.5	0.4							
23	Is $C_{L\,ROCmax}$ inside drag bucket?	Y/**N**	Y/**N**	**Y**/N	**Y**/N	Y/**N**	**Y**/N	Y/**N**			1	1		1	
24	Is $C_{L\,CRUISE}$ inside drag bucket?	**Y**/N	**Y**/N	Y/**N**	**Y**/N	Y/**N**	Y/**N**	**Y**/N	1	1		1			1
								Sum:	5	3	4	4	3	4	6

Several conclusions can be obtained from the Decision Matrix. NACA2412 airfoil constitutes the selected airfoil according to the given parameters to be optimized in XFLR5. Aerodynamic performance and similar aircraft models were also compared to the selected airfoil, leading to accurate decision. Similarities with NLF(1)-0115 and SHM-01 airfoil as a result of high aerodynamic performance are compared to NACA2412. It is observed that XFLR5 highly provides explicit performance parameters and results for Natural Laminar Flow airfoils family. This fact is due to software limitations. Real case must be analysed. The lack of unsteadiness

scenarios and mathematical model assumptions lead to non-reliable results regarding RONCZ airfoil. It can be easily observed by observing the graphs obtained. High stall characteristics characterized this airfoil. Results are shown in Figure X through Figure X.

The actual analysis does not include flaps feature. Further analyses on flaps system will be presented as future work for Master Thesis achievements.

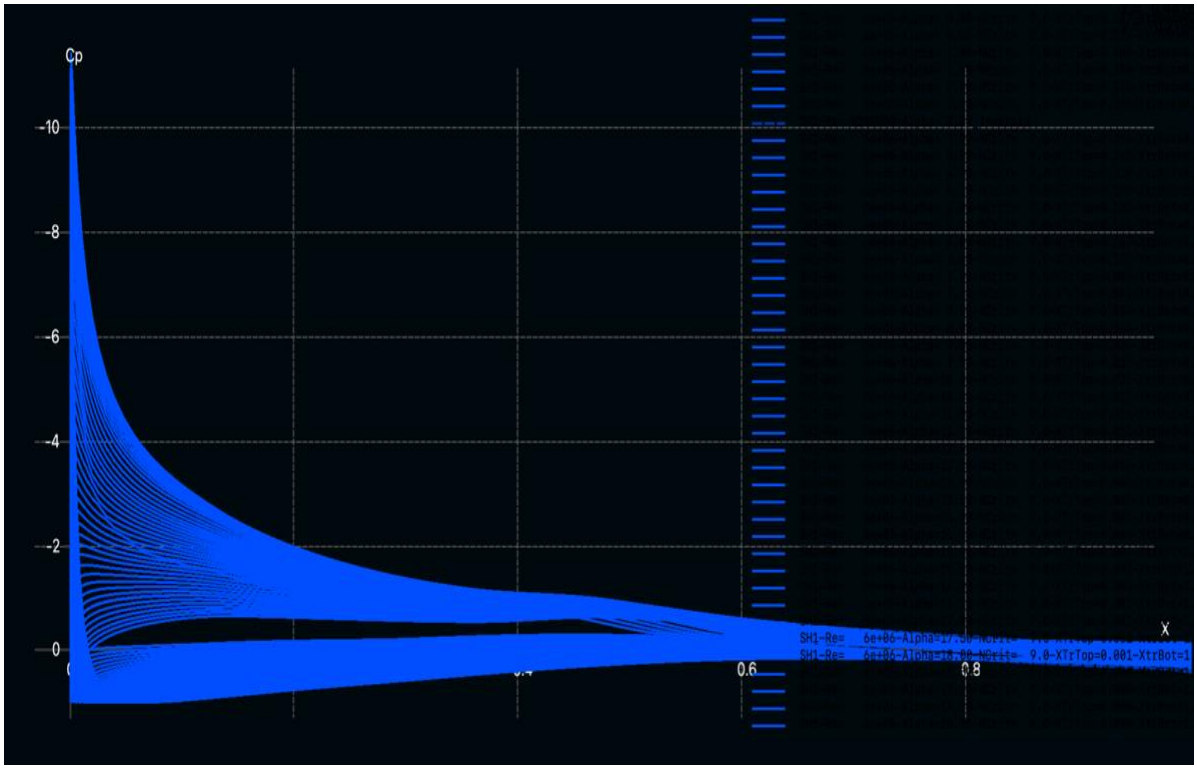

FIGURE 23. Pressure distribution for different Angles of Attack XFLR5.

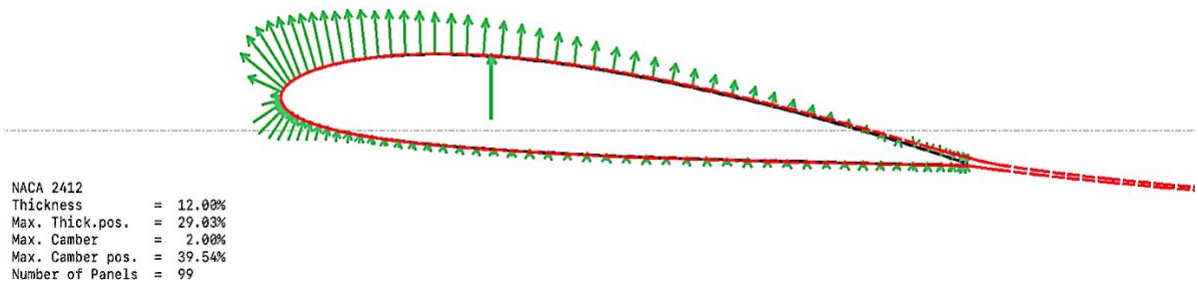

FIGURE 24. NACA2412 airfoil boundary layer and pressure distribution at 5º AoA.

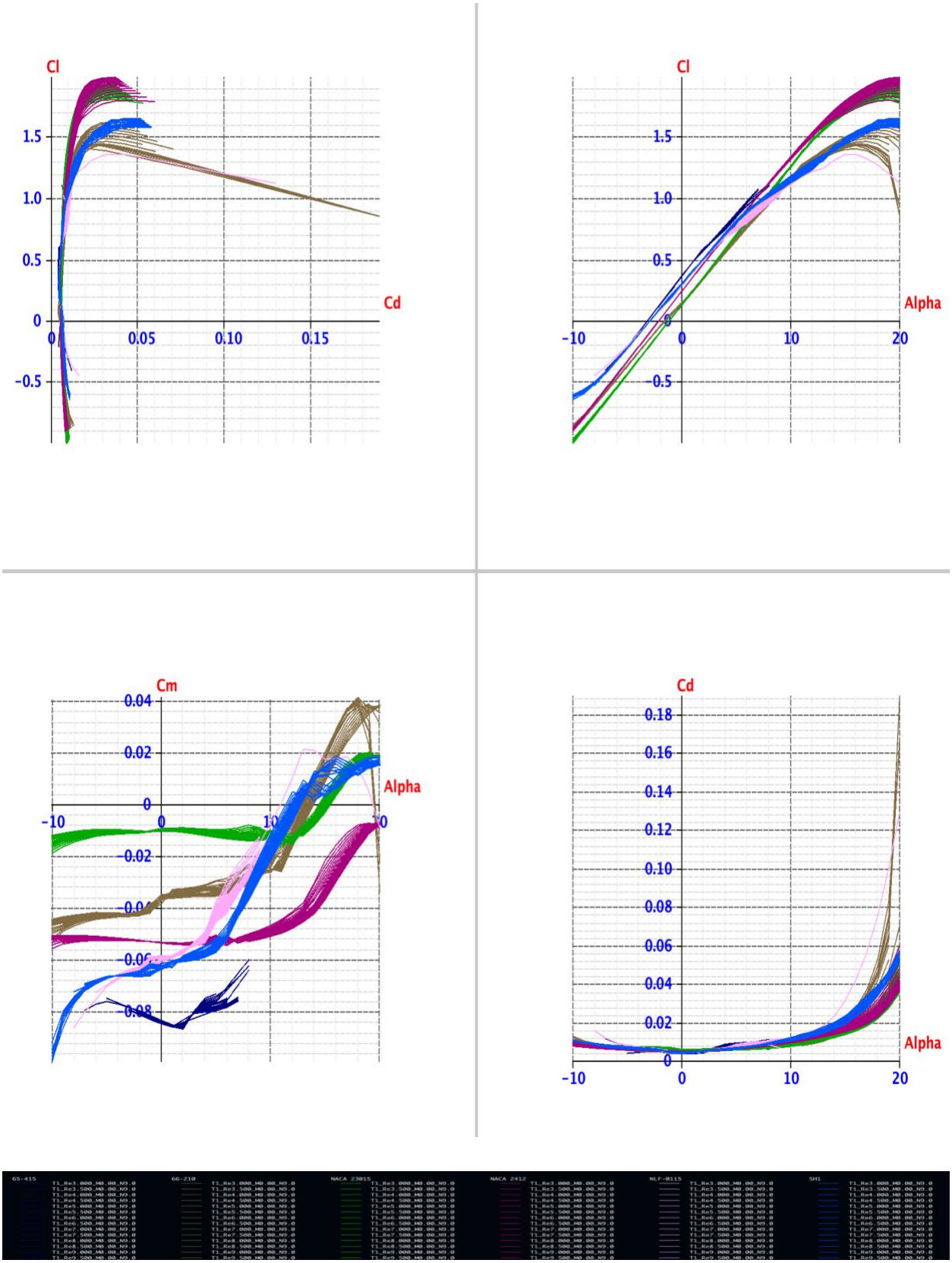

FIGURE 25. Batch analysis for Reynolds Number range between 2e6 and 10e6.

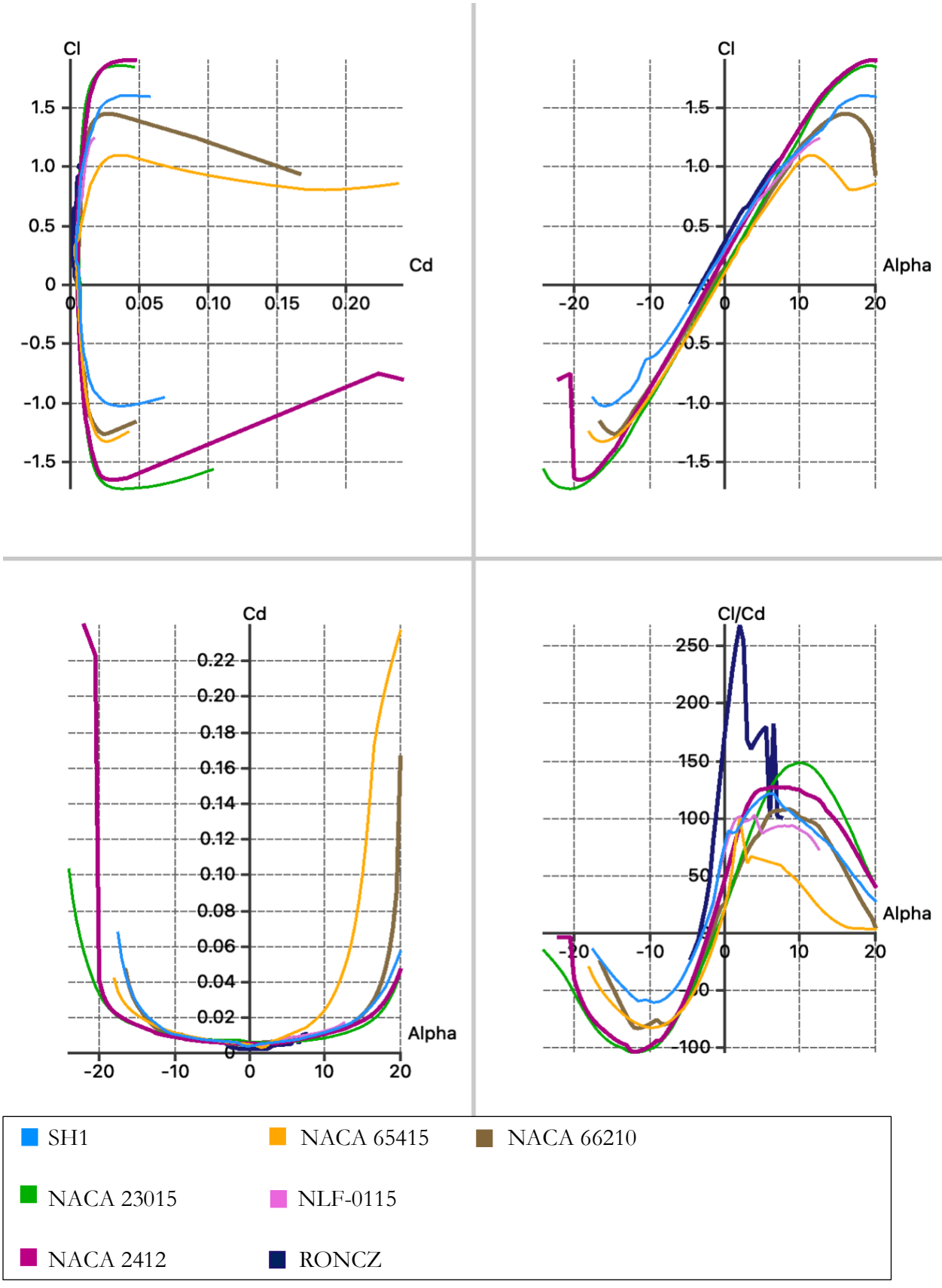

FIGURE 26. Batch analysis for Reynolds Number 8e6.

5.2. WING GEOMETRY

Vans' RV-10 wing, a single engine four-seat light-sport airplane, with aspect ratio of 6.85 was studied as seen in Figure X. The cross section of the wing was NACA2412 airfoil in the stream-wise direction. This NACA2412 airfoil is a cambered airfoil with a maximum thickness 12% at 30% chord and maximum camber 2% at 40% chord. The constant chord of the wing is 1.40 m and the span is 9.8 m. The properties of the light sport aircraft wing are given in Table 1. The geometrical design of the wing was performed using CATIA Computer -Aided Design to ensure the accuracy of the constructed model. The RV-10 wing was modelled at a 4º angle and ribs distribution according to its original model. Only wing surface was design.

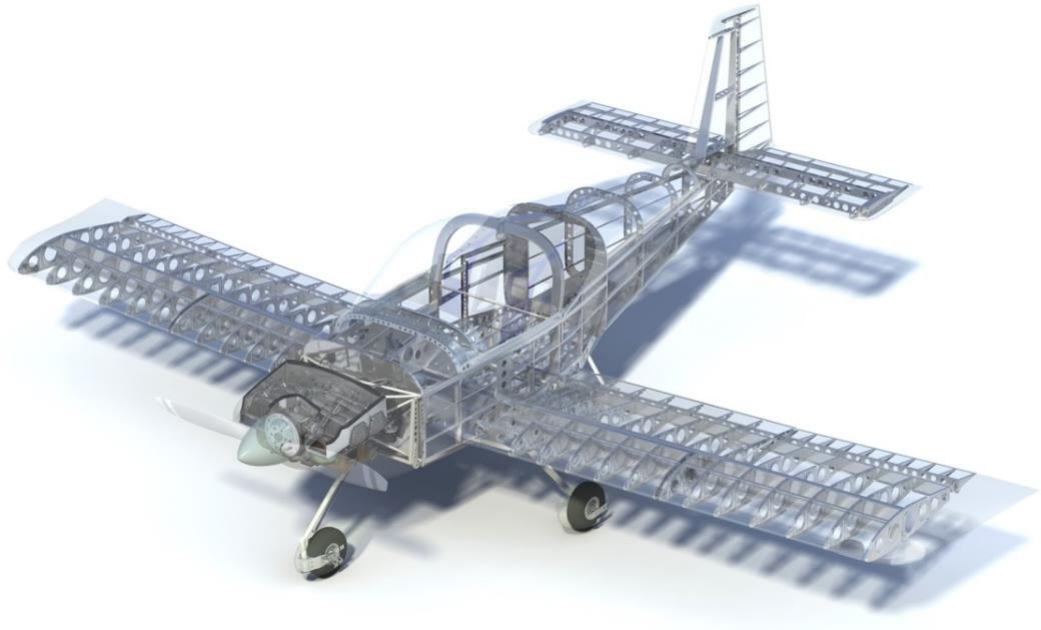

TABLE 3. R-10 wing geometric parameters.

Description	Symbol	Value	Units
Wing area	S_W =	13.45	m^2
Wing Aspect Ratio	AR_W =	7	
Wing Taper Ratio	λ_W =	1	
Airfoil thickness ratio	t/c =	0.10	
Wing sweep at 25% MAC	Λ =	0	º
Average chord	C_{AVG} =	1.40	m
Mean Geometric Chord	C_{MGC} =	4.80	m
Wing span	b_W =	9.60	m
Location of MGC LE	Y_{ref} =	2.45	m

The aircraft wing was modelled using CATIA software. Once the geometry was imported to ANSYS DesignModeler, fluid domain was created by means of fluid enclosure. Boolean subtract operation was needed to define solid and fluid domain. The upper and lower wing surfaces belong to Fluid-Solid Interface, as well as the tip chord surface, where the fluid and solid equations are simultaneously solved to prevent aeroelastic phenomenon.

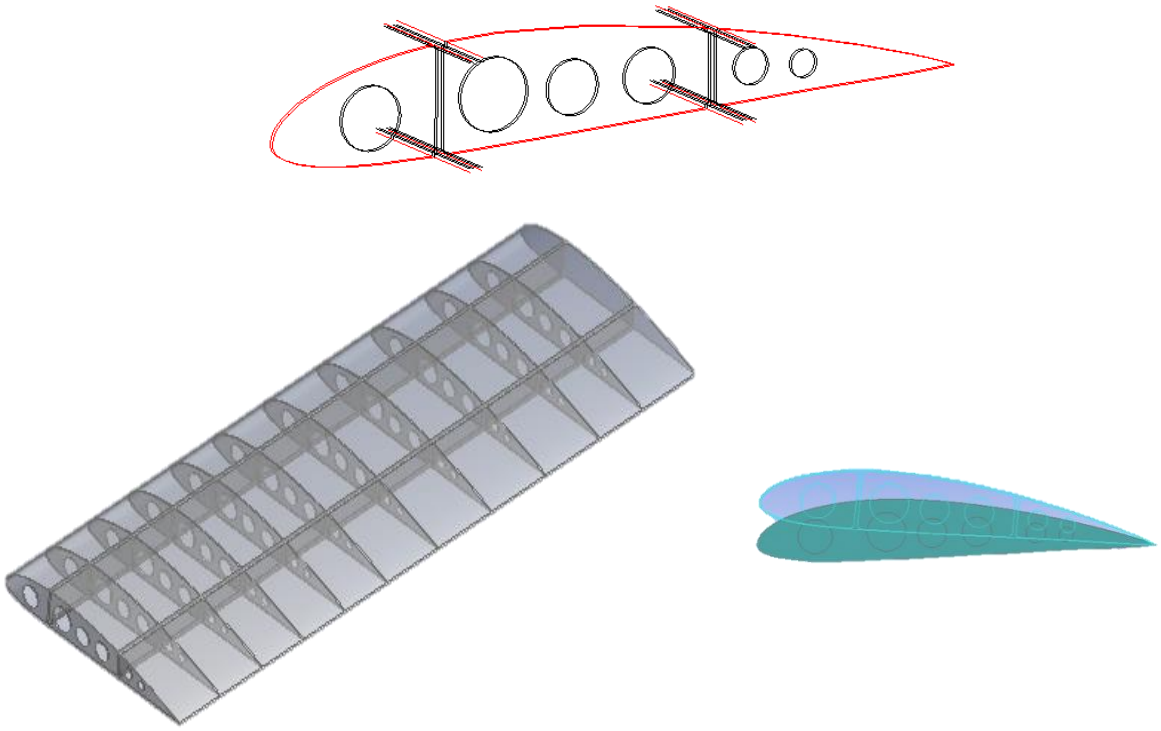

FIGURE 27. CAD model of the reference wing structure for study

5.3. MESHING

Precise and exact control over the spatial domain is essential during the FSI algorithm. Hence, fluid domain has been spatially discretized by means of hybrid unstructured grids. To ensure high-accuracy results on the Fluid-Structure Interface, finer mesh is required close to the aircraft wing by means of sizing and proximity. The application of inflation and refinement actions on the wing proximity was performed with the aim of robust boundary layer thickness throughout the whole algorithm.

Figure 28 shows a cross-sectional view of the triangle mesh in the model. Note that as mentioned above, the mesh is greatly refined in the vicinity walls of the wing surface. The generated mesh had a total of 138531 nodes and 735585 elements. The bias factor has been used to provide high

mesh density around the airfoil for greater contour quality and better flow visualization. This spatial domain has been controlled by several iterations where mesh ratios were analyzed. The resolution and density of the mesh are greater in regions where superior computational accuracy is needed, such as the near wall region of the airfoil for boundary layer purposes.

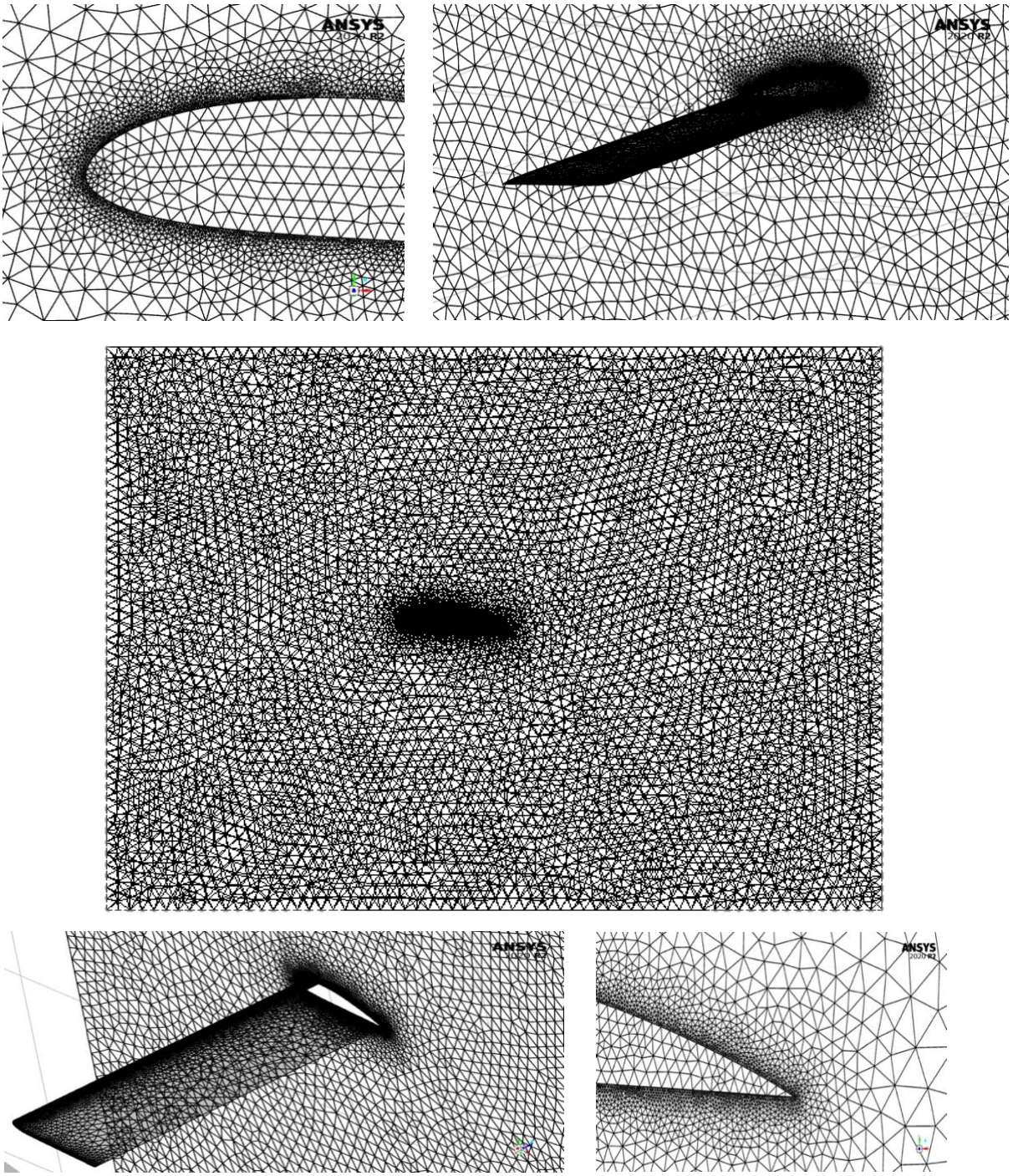

FIGURE 28. FSI Unstructured Mesh Greatly Refine at Wing Vicinity

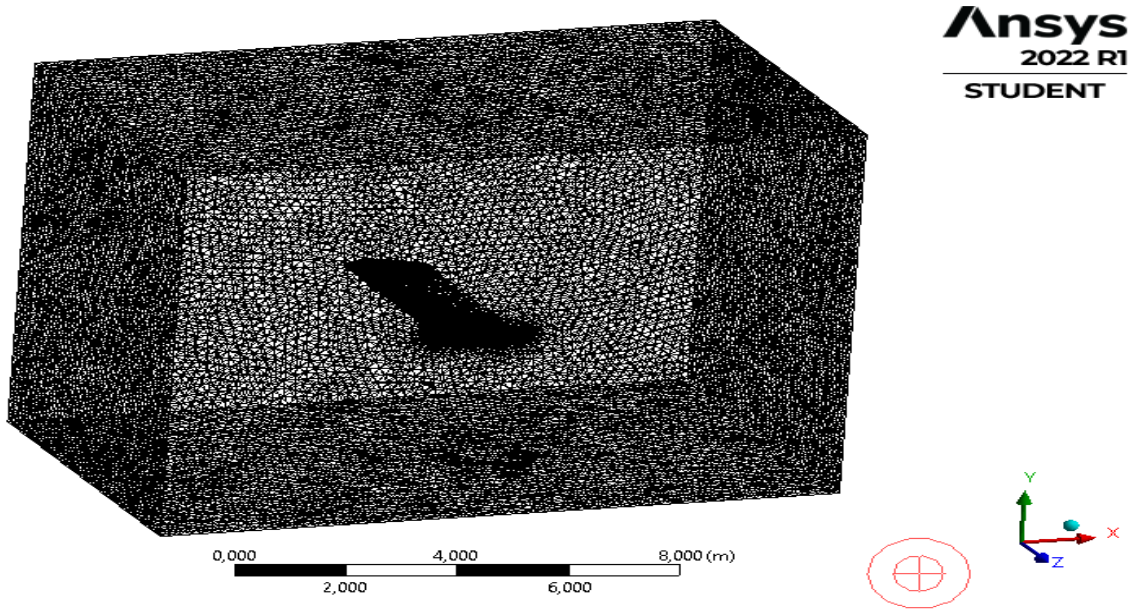

FIGURE 29. Rectangular Fluid Domain for Fluid-Structure Interface Application

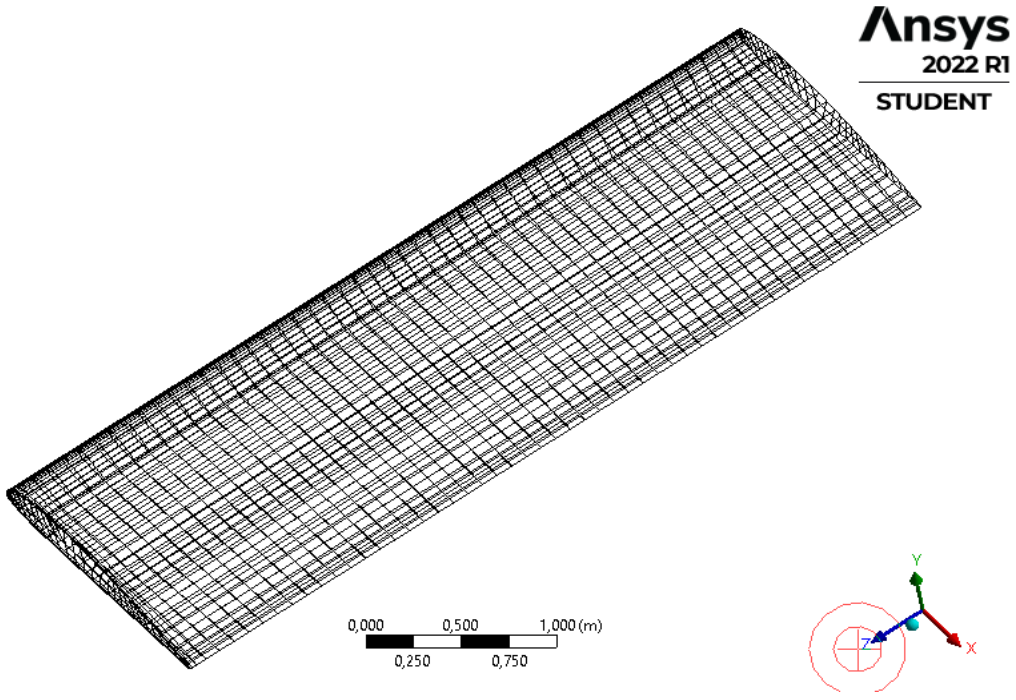

FIGURE 30. "Hershey Bar" Rectangular Wing as Structural Mesh for Fluid-Structure Interface Application

5.4. DYNAMIC MESH

Dynamic mesh capability was used to simulate wing structure motion. It was the biggest challenge of this Final Year project as it involves a combination of layering and remeshing linear boundary motion. System coupling was set for every timestep in which the dynamic mesh and the correlated boundary conditions were adjusted to wing surface vibrations according to flutter response. Upper and lower wing surfaces were intertwined with structural and fluid models to obtain aerodynamic load and wing deflection for every iteration.

5.5. TURBULENT MODEL

Three different turbulent models were studied for this Final Year Project. Validation of each one was carried out before processing with the computational simulations. Those aerodynamic models were chosen to validate with steady state data: Spalart Allmaras, K- Epsilon and SST Transition K-ω. Initially, the Spalart Allmaras model was analyzed obtain good approximations on lift and drag curves. Additional investigation limited by transient modeling of FSI lead to high sensitivity towards mesh sizing in the proximity of the wing surface. This method assumes constant viscosity. Thus, was the first one to be neglected. While SST Transition K- ω model introduces longer step time simulations, turbulent viscosity ratio and turbulent intensity can be modelled to tighten computational results. Turbulent intensity was firstly specified using ANSYS values of turbulent intensity from 5-8% and turbulent viscosity ratio of 5. Results indicated strong correlation in lift, drag, but large errors on mesh hybrid deflection. The turbulent viscosity intensity was set to 8% according to Literature Review. Furthermore, turbulent viscosity ratio was assumed to be 2 due to three-dimensional flow. Using explicitly K-epsilon turbulent model alone has no impact on Fluid Structure coupling method as not only boundary layer thickness is being coupled in the iteration, but also pressure distributions, torsional moment and wing deflection.

As the K-omega model is used for simulating flow in the viscous sublayer, and K-epsilon is ideal for simulating flow behavior in the vicinity of the boundary layer, a combination of both are needed for this complex interface. Therefore, SST hydrib turbulence model was selected as it provides two-fold system: turbulent kinetic energy and specific dissipation rate to predict

aeroelasticity phenomenon by means of computational analysis. This hybrid model combines k-omega and the k-epsilon solvers along with a blending function. The governing equations of the SST turbulent model are defined by means of k-epsilon eddy-viscosity and k-omega model:

$$\frac{\partial k}{\partial t} + U_j \frac{\partial k}{\partial x_j} + = P_k - \beta k\omega \frac{\partial}{\partial x_j}\left[(\upsilon + \sigma_k \upsilon_T)\frac{\partial k}{\partial x_j}\right] \quad (5.1)$$

$$\frac{\partial \omega}{\partial t} + U_j \frac{\partial \omega}{\partial x_j} + = \alpha S^2 - \beta \omega^2 + \frac{\partial}{\partial x_j}\left[(\upsilon + \sigma_\omega \upsilon_T)\frac{\partial \omega}{\partial x_j}\right] + 2(1 - F_1)\,\sigma_{\omega^2}\frac{1}{\omega}\frac{\partial k}{\partial x_i}\frac{\partial \omega}{\partial x_i} \quad (5.2)$$

5.6. BOUNDARY CONDITIONS

The surfaces bordering the fluid domain fall into the solid walls representing the Fluid Domain of the aircraft wing. Fluid-Structure Interface Surfaces are connected by declaring interface solutions on the CFD solver.

INLET

At inlet boundary condition we apply what FLUENT terms a VELOCITY INLET boundary condition. Here, V_{in}= 100 m/s. Moreover, inlet temperature is neglected.

OUTLET

FLUENT's PRESSURE OUTLET boundary condition is applied. This requires that a value for the gauge static pressure be provided. For p_{out}, a gauge pressure of 0 bar (absolute pressure is equal to atmospheric pressure), was specified.

$P_{abs} = P_g + P_{atm}$

SYSTEM COUPLING INTERFACE

Wing upper and lower surfaces were defined as FSI System Coupling areas where the governing equations of fluid and structural domain are solved simultaneously within panel method. In every node, these equations boundary condition is applied.

A. Solution Initialization

This coupled aeroelastic model used Finite-Volume discretization to convert the nonlinear partial-differential equations (PDEs) conservation of mass and momentum equations into a set of nonlinear algebraic equations. Equations of fluid and structure are solved sequentially, as opposed to being independently solved as a single matrix system. 5 different cases were analyzed depending on two main variables: steady or transient, and one-way or two-way coupling method.

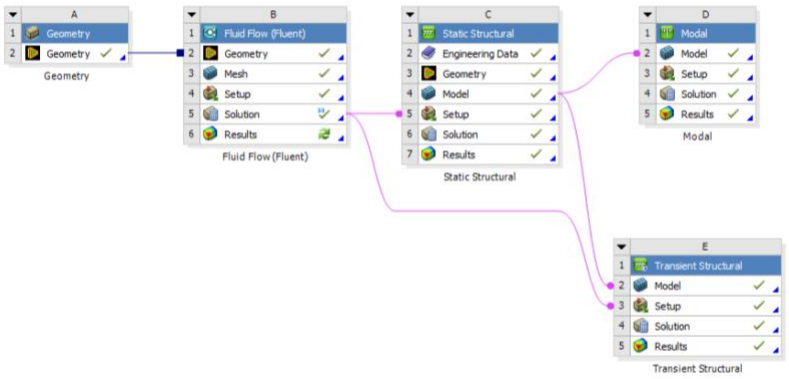

FIGURE 31. One-Way FSI Coupling Method

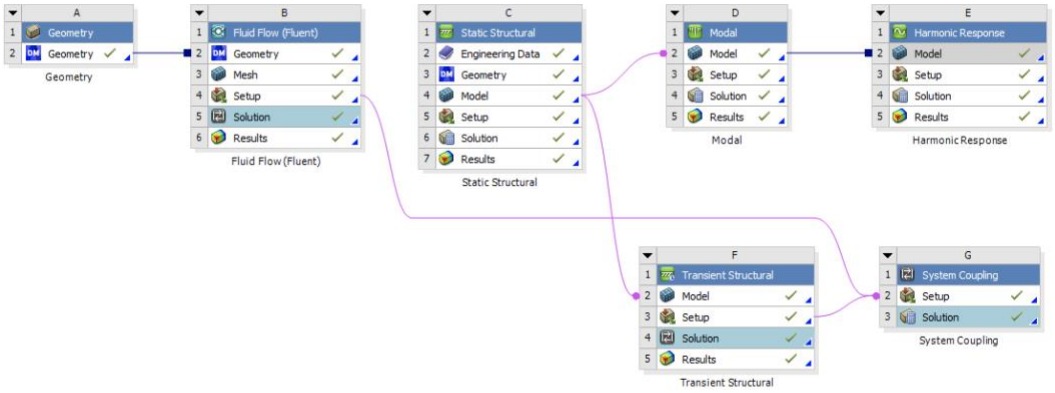

FIGURE 32. Two-Ways FSI Coupling Method

CHAPTER 6

"I have not failed. I've just found
10,000 ways that won't work."

Thomas A. Edison

Contents

6. AEROELASTIC NUMERICAL RESULTS

In the following section, FSI results by means of coupling Structural and Fluid Analysis with 2 different interfaces: one-way (linear) coupling and two-way (cycle iteration) are presented as pressure contours, displacements, shear and normal stresses, lift coefficients and phase and frequency response. **Section 6.1.** presents steady structural and fluid analysis simulations, regarding structural displacement and aerodynamic loads. **Section 6.2.** provides transient solutions based on unsteady aerodynamic loads and flutter instability. Lift Coefficient variation along flow-time is presented as it varies with time. Equivalent Von-Misses stresses and Shear Stresses for numerical results were obtained with two different programs: ANSYS and NASTRAN & PATRAN. In the case of NASTRAN & PATRAN model, a physical simplification of a flat plate was introduced as mesh quality was difficult to control in this software. Similarities in numerical results are observed comparing analytical derivation and ANSYS results. Finally, **TABLE 10** represents the damage size efficiency for different diameters. Results obtain both, analytically and numerically, indicate that aeroelastic coupling depends on critical flutter speed.

6.1. NON-COUPLED NUMERICAL RESULTS

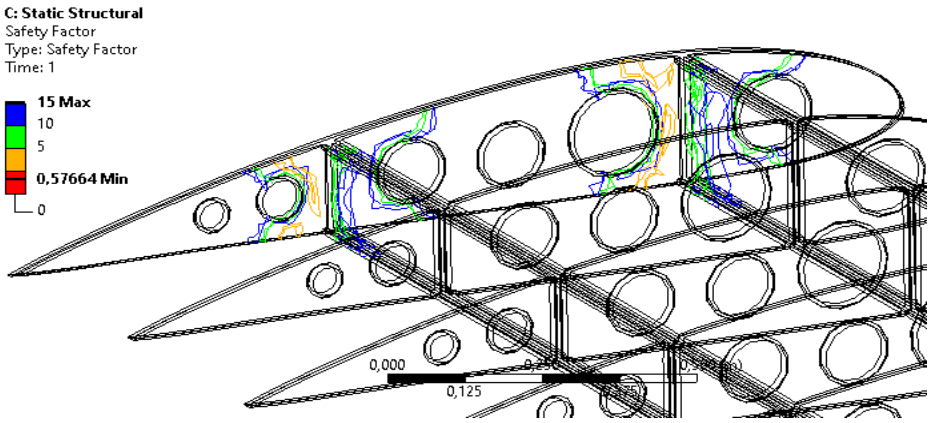

FIGURE 33. Non-Coupled Steady Structural Analysis of Safety Factor.

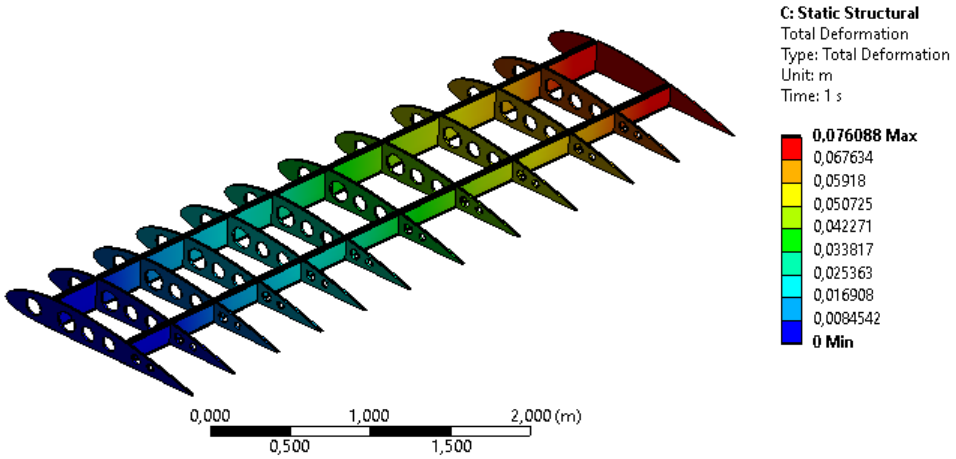

FIGURE 34. Non-Coupled Steady Structural Analysis of Internal Ribs Structure Displacement.

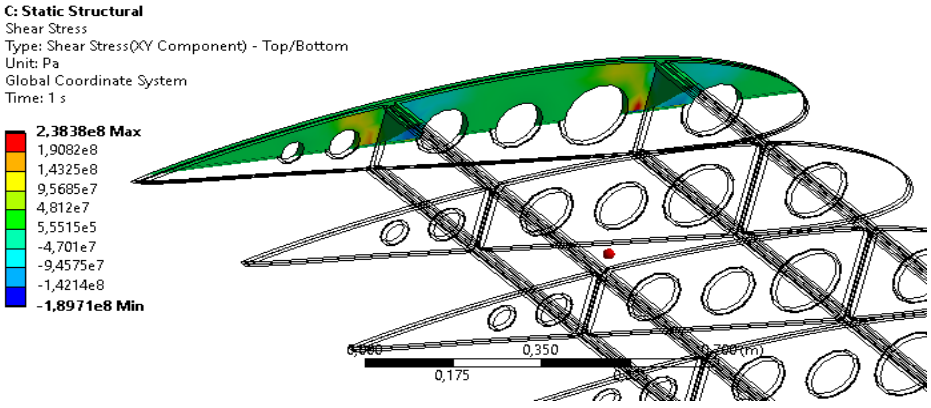

FIGURE 35. Non-Coupled Steady Structural Analysis of Shear Stress on Ribs.

Firstly, structural comments will be applied to previous results. Maximum deflection occurs at the wing tip, critical area under aeroelastic safety factor on rectangular wings, as it constitutes the first element where oscillation will start. Also, numerical results on Shear Stress suggests us that light weight structure based on internal holes are subject to high shear raisers. By analyzing rib circular surface, the ultimate tensile stress can be expressed as:

$$\sigma_{ult} = \frac{Pb}{t(b-d)}$$

Reducing weight by perforating wing ribs, results in higher tensile stresses.

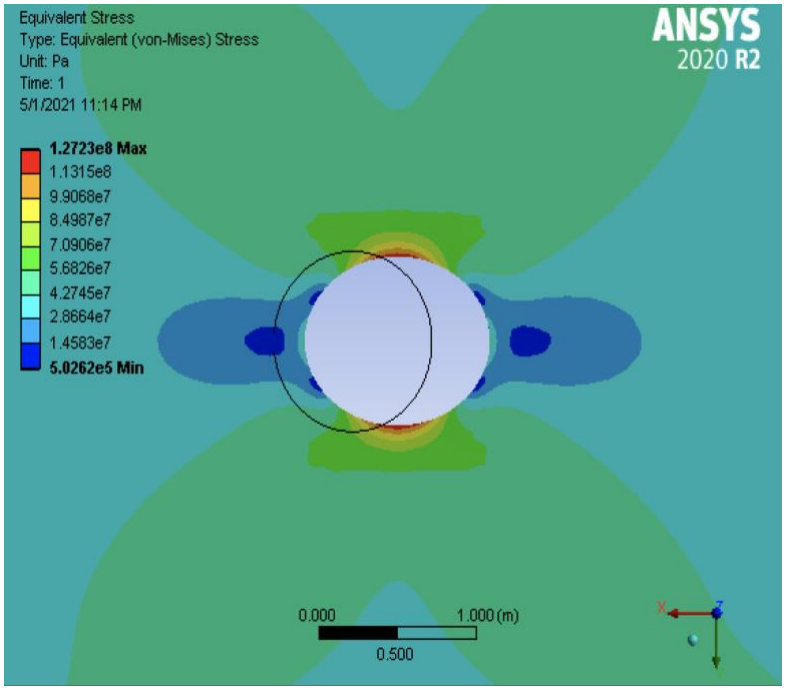

FIGURE 36. Stress Raiser On Wing Ribs Hole

Therefore, light sport aircrafts such as the one in study in this Final Year Project uses light structures to reduce inertia moment by paying a penalty in stress concentration. Stresses have a maximum sharp in the hole area and decreases with increasing the distance from the stressed zone. The higher the maximum stress, the higher the attenuation close to the circular area. Stress concentration factor is used to stablish a relation between the normal and tangential stresses.

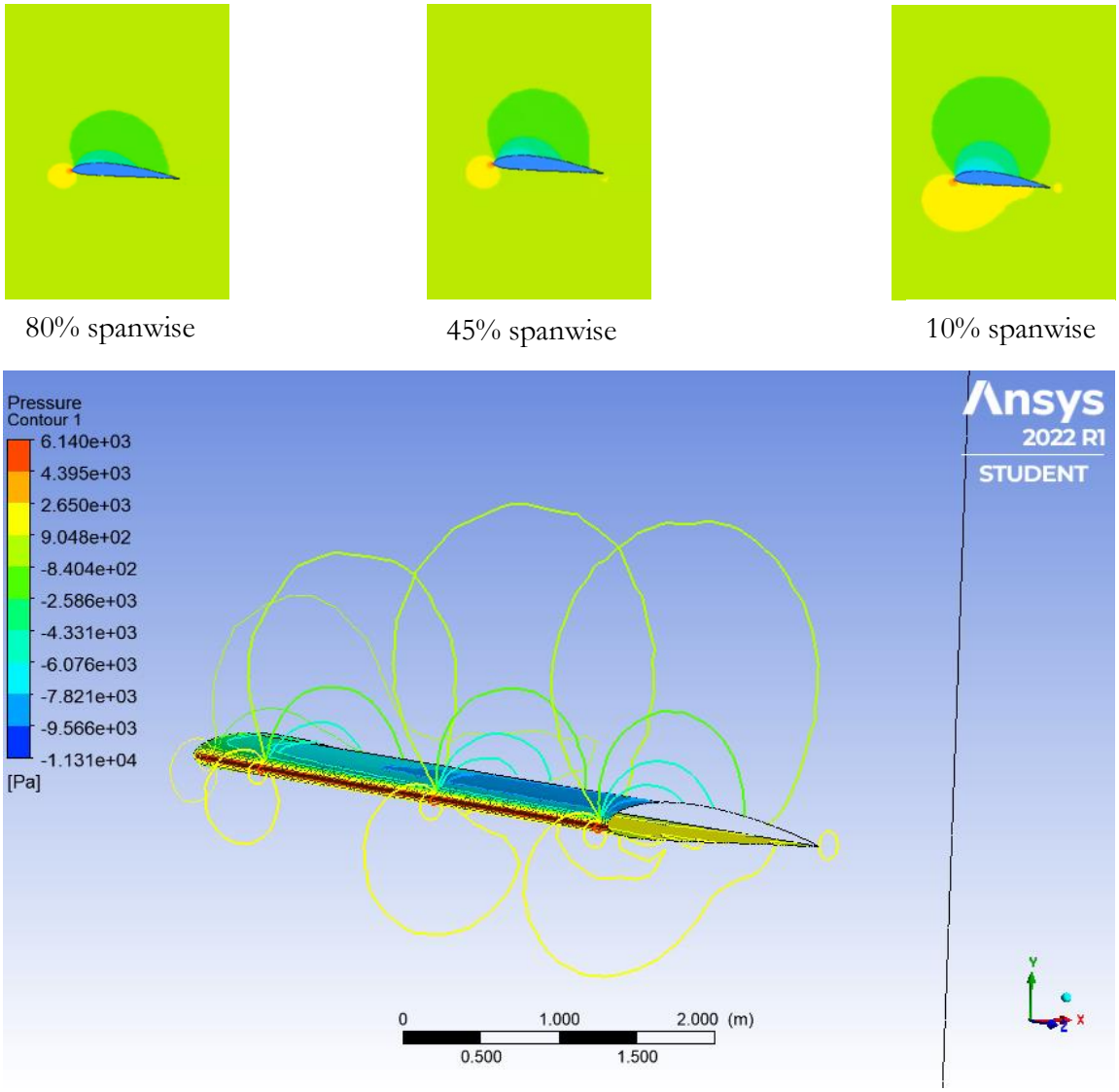

FIGURE 37. Pressure Distributions Spanwise Under Non-Coupled Steady Analysis

Pressure distributions are computed over the 3D aircraft wing showing accurate results. These contours provide us helpful information to understand how flutter will be imposed as a consequence of a self-induced vibration due to aerodynamic loads. Pressure in constantly changing along the wing span. As it gets closer to the wing tip, its contribution is reduced, leading to wing tip cortices. This phenomenon is due to pressure difference over the lower and upper surface. By means of this steady non-coupled analysis, physical phenomenon will be understood before moving to transient coupled analysis on an aircraft wing. Figure 37 provides pressure distribution in the XY Plane of symmetry as lift distribution. From this graph, pressure distribution over the wing is computed to link the one-way structural analysis.

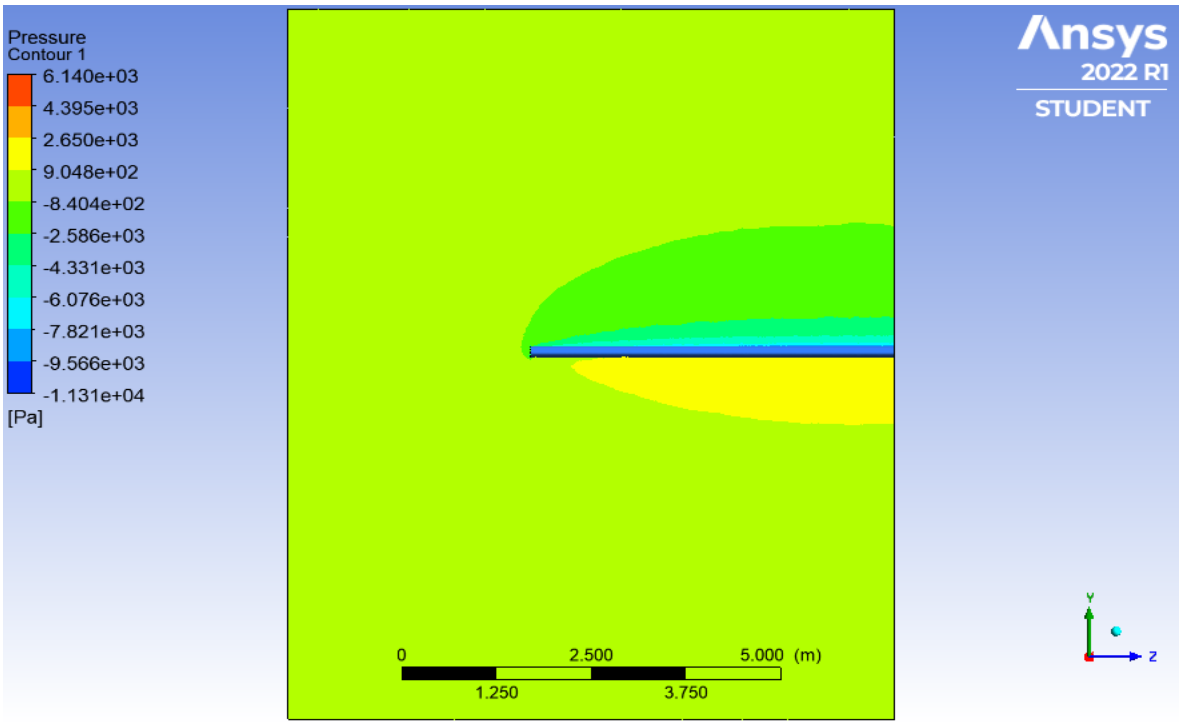

FIGURE 38. Lift Distribution Over Aircraft Wing

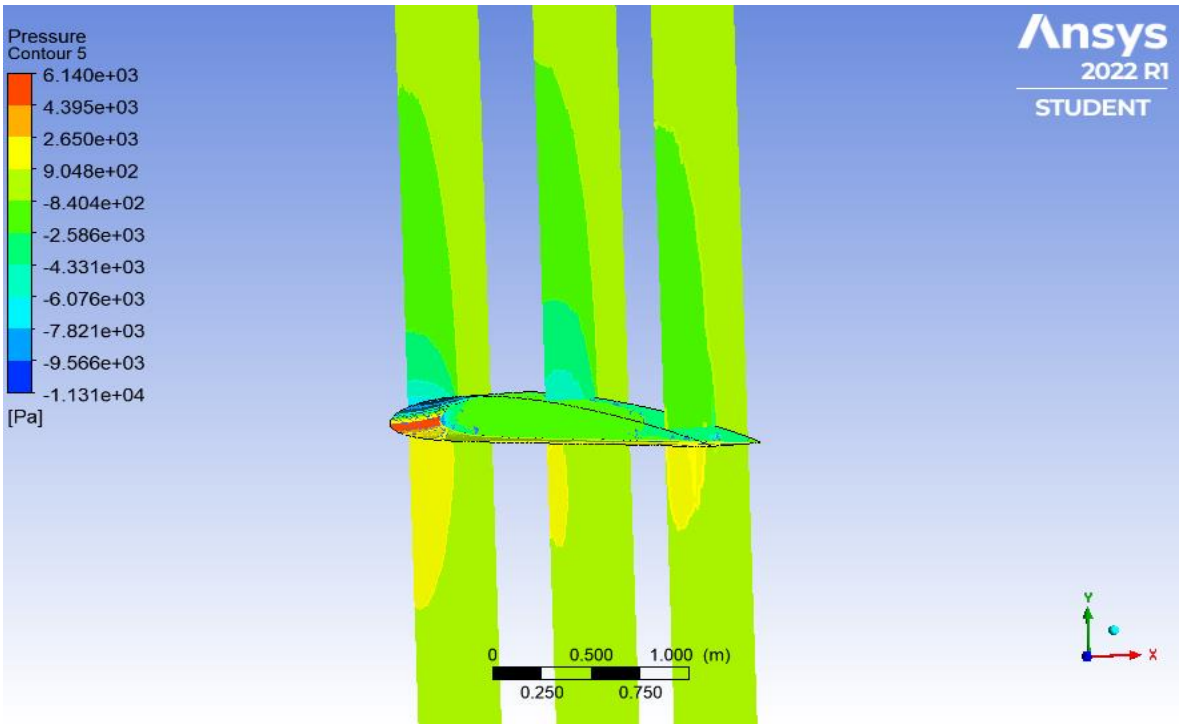

FIGURE 39. Lift Distribution Chordwise Over Aircraft Wing

6.2. COUPLED NUMERICAL RESULTS

In the following section, transient results will be presented by means of unsteady aerodynamics.

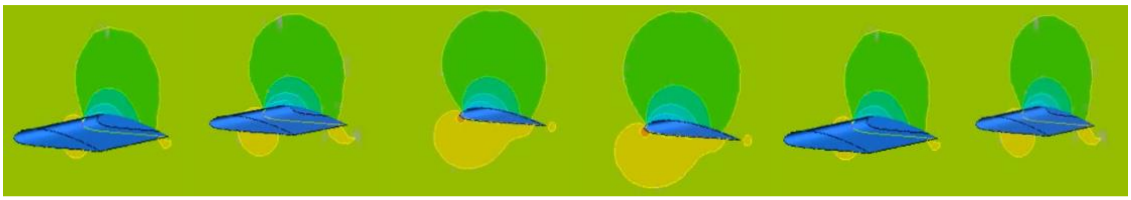

FIGURE 40. Oscillating 3D Wing Through Computational Flow-time

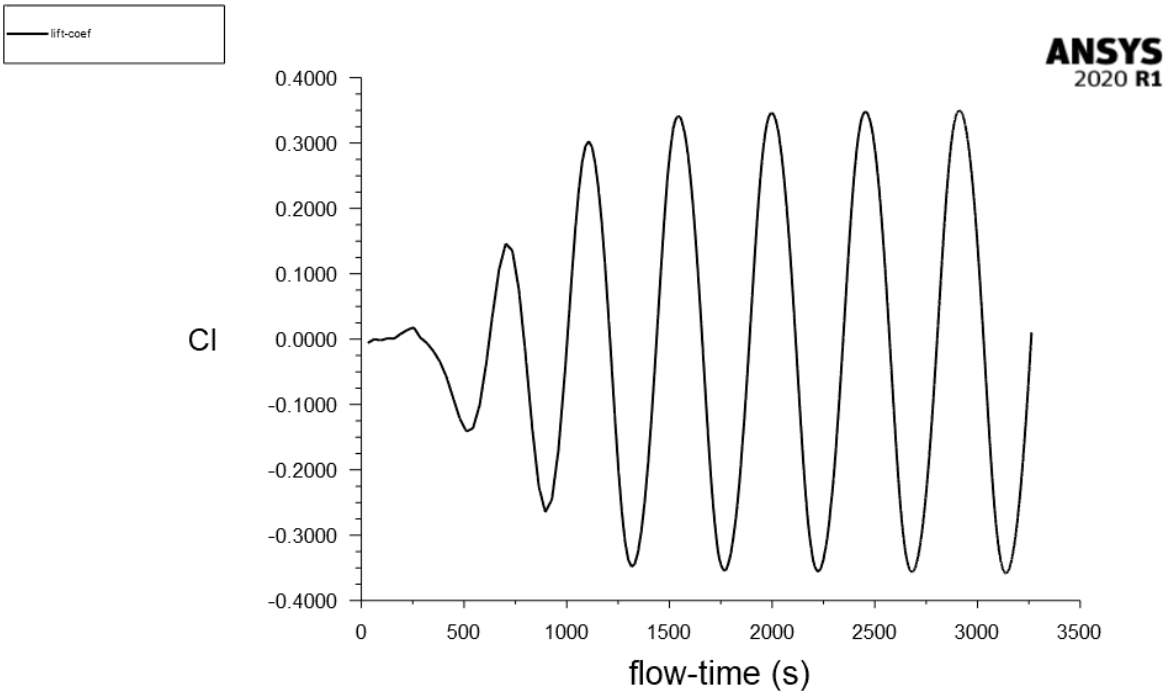

FIGURE 41. Unsteady Lift Coefficient Versus Computational Flow-Time

Airfoil pitching and plunging movements can be easily identify in the first sequence where pressure distributions induce an aerodynamic load over the aircraft wing. Depending on whether the aerodynamic force is lagging or leading the displacement, the incoming flow absorbs or feeds in energy from the aircraft wing, and the motion is damped or amplified, respectively. Hence, it is important to evaluate the critical airspeed limit for properly structural and aeroelastic design.

TABLE 4. Wing Tip Displacement for different Fluid-Structure Solvers

MODE	ANALYTICAL	NASTRAN & PATRAN	ANSYS One -Way FSI	ANSYS Two -Way FSI
1st bending	0.030	0.0196	0.03306	0.03298
1st chordwise bending	0.042	0.0216	0.04601	0.04578
Torsion & bending	-	-	0.04781	0.47190

Wing tips displacements have been analytically solved by applying Castigliano's Theorem. NASTRAN & PATRAN simplification of a flat plate over bending and torsional moments have been implemented to compare the numerical solutions from ANSYS coupled system. Numerical results agreement is based on solid-coupled interaction, while there is a decimal different on analytical results. Simplifications of the model and fluid behaviour are the main reason for that lack of similarity.

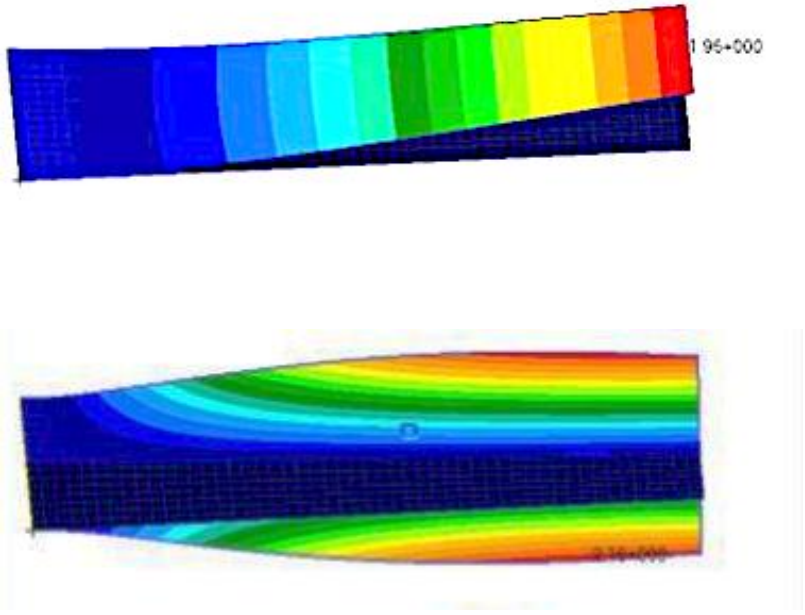

FIGURE 42. NASTRAN & PATRAN Model Simplification as Flat Plate.

1st Flap-wise

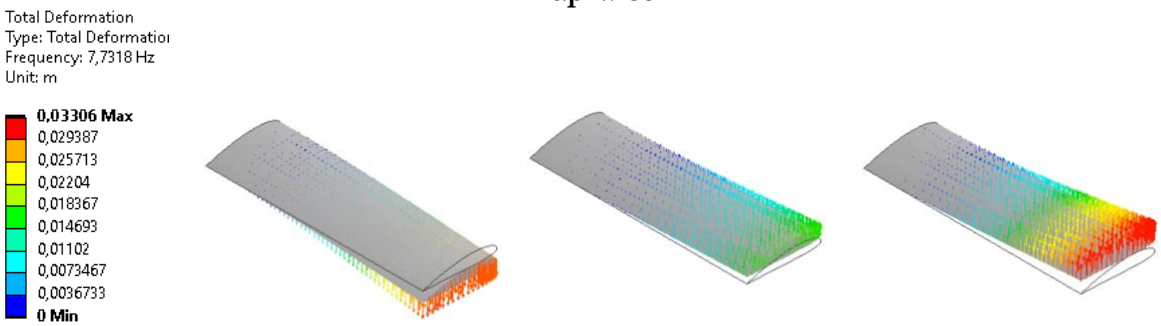

1st Edge-wise

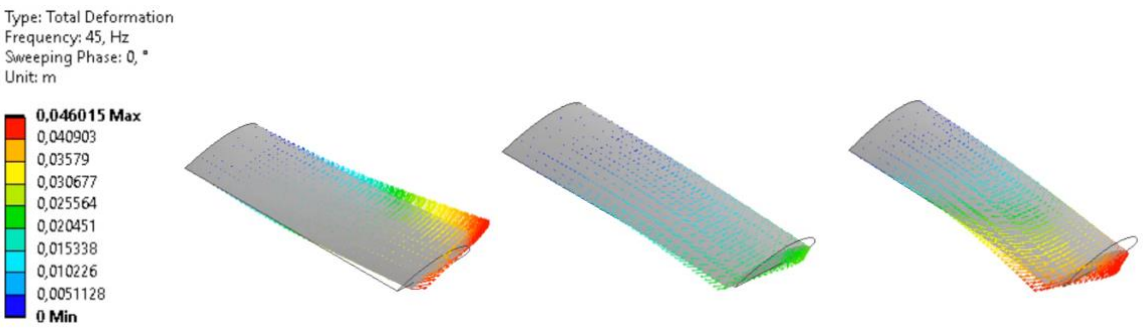

1st Torsional & Bending

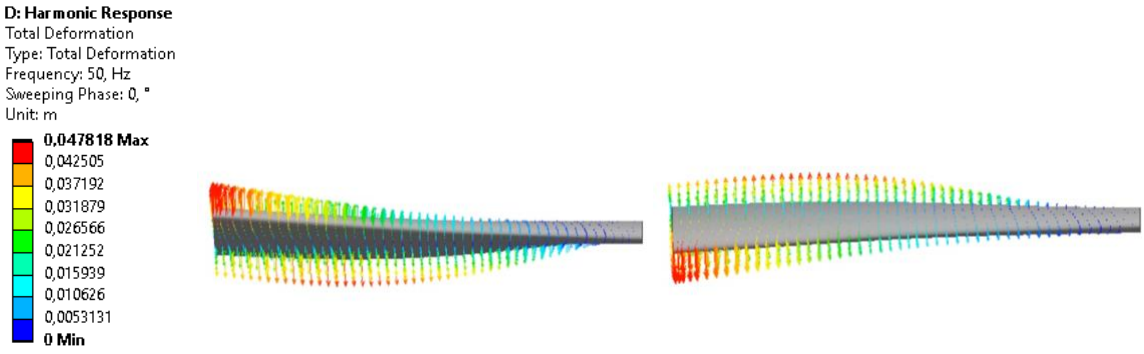

Shear and Normal Stresses are computed under coupling action at the given torsional & bending mode frequency, 50 Hz. Comparing these values with the ones obtained in the Steady Non-Coupled Analysis, it can be stated that aeroelastic has not only an effect on aerodynamics and elastic forces, but also on elastic forces that interacts together while coupling. Those assumptions lead us to redesign or tighten aircraft wing structural mass ratios. Aerospace engineers needs to tighten studies that model preliminary design phases, and thus, this is one of the aims of the Final Year Project, how to prevent an aeroelastic phenomenon by numerical methods.

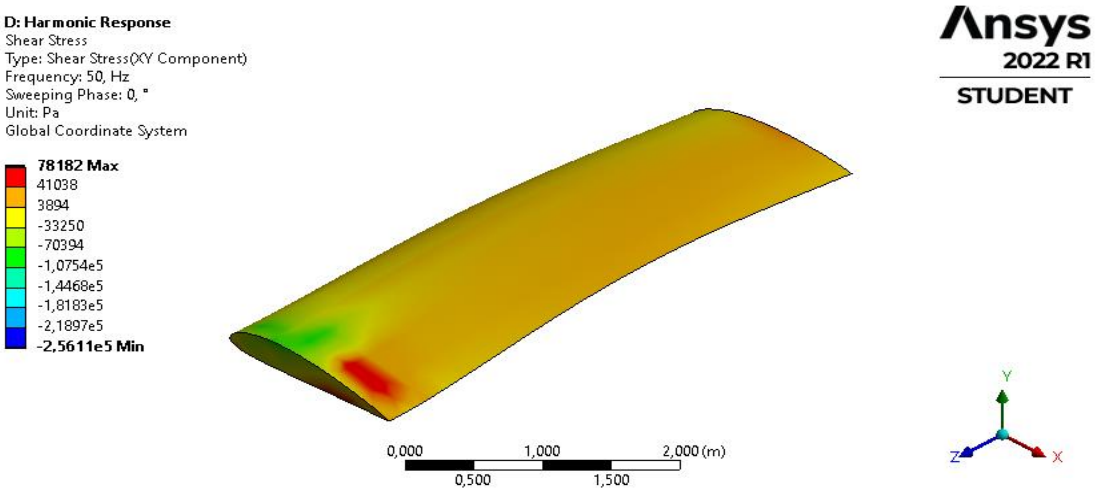

FIGURE 43. Shear Stresses Under Classical Coupling Mode

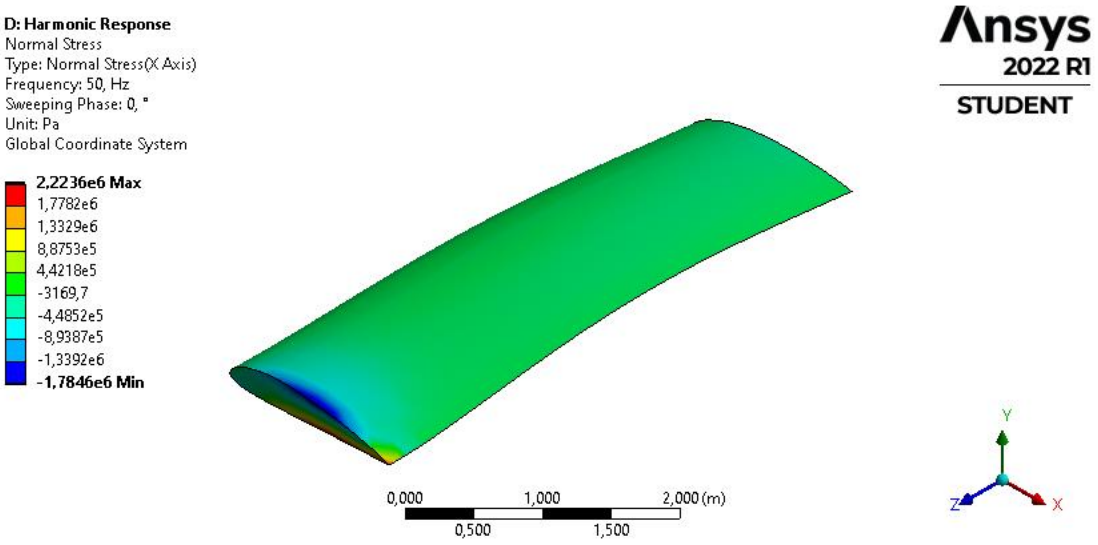

FIGURE 44. Normal Stresses Under Classical Coupling Mode

Pitching and plunging time stories for the aircraft wing tip displacements, in meters and rads, accordingly, have been measured using ANSYS point displacement function over a mesh node. This action allowed to determine pitching and plunging amplitude to formulate the aircraft movement as a function of time for the Critical Flutter Speed.

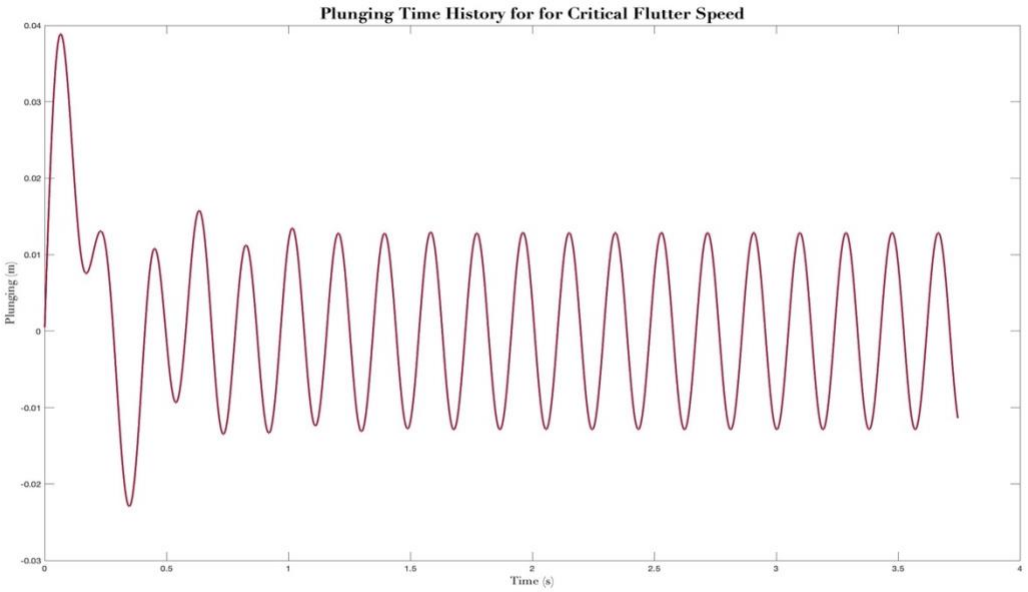

FIGURE 45. Plunging Time History for Critical Flutter Speed.

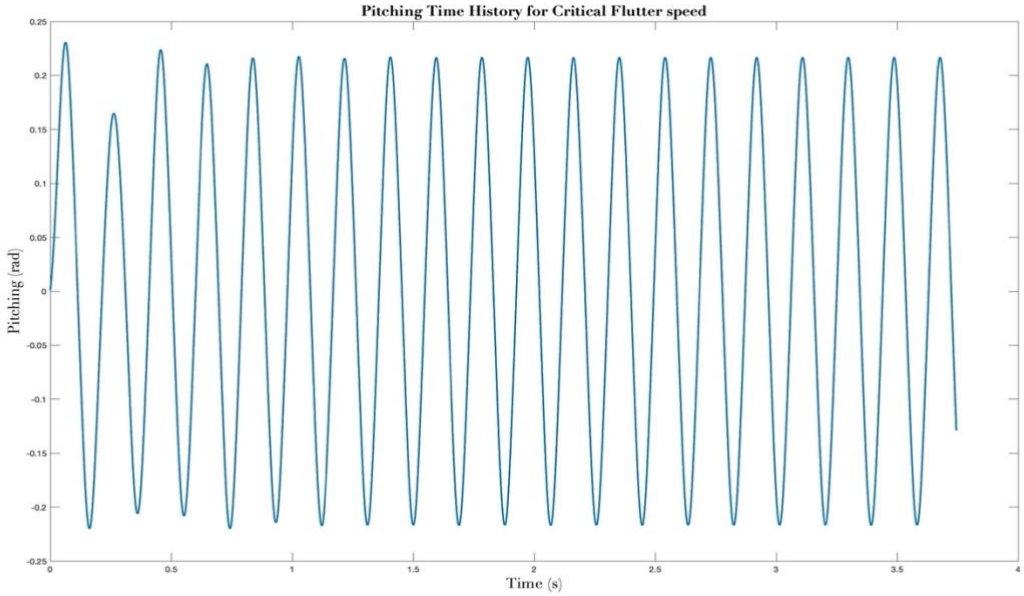

FIGURE 46. Pitching Time History for Critical Flutter Speed.

Once the aerodynamic and structural coupling results have been analyzed, it is considered to study the self-excited dynamic instability as a result of the interaction of inertial interaction. This oscillatory phenomenon, is characterized by the complexity to predict which the aerodynamic forces modify the natural mode-shapes and frequency, resulting in vibrations with increasing amplitude. Hence, lets the results speak for themselves.

Unsteady flow fluctuations, attributed to unsteady pressure field due to natural vibration motion, influences the flow field as it has been proved in the non-coupled static analysis. Nevertheless, pressure fluctuations are harmonic in time and also, they have the same frequency and a phase shift as the motion vector. Therefore, the only component that can amplify the mode of vibration and induce flutter is the imaginary component. Thus, phase will stablish whether our system is stable or not.

By analyzing unsteady pressure flow provided by Transient Two-Way Coupling FSI Analysis carried by Ansys at the critical flutter speed, we can observe how displacement motion and pressure components are not in phase.

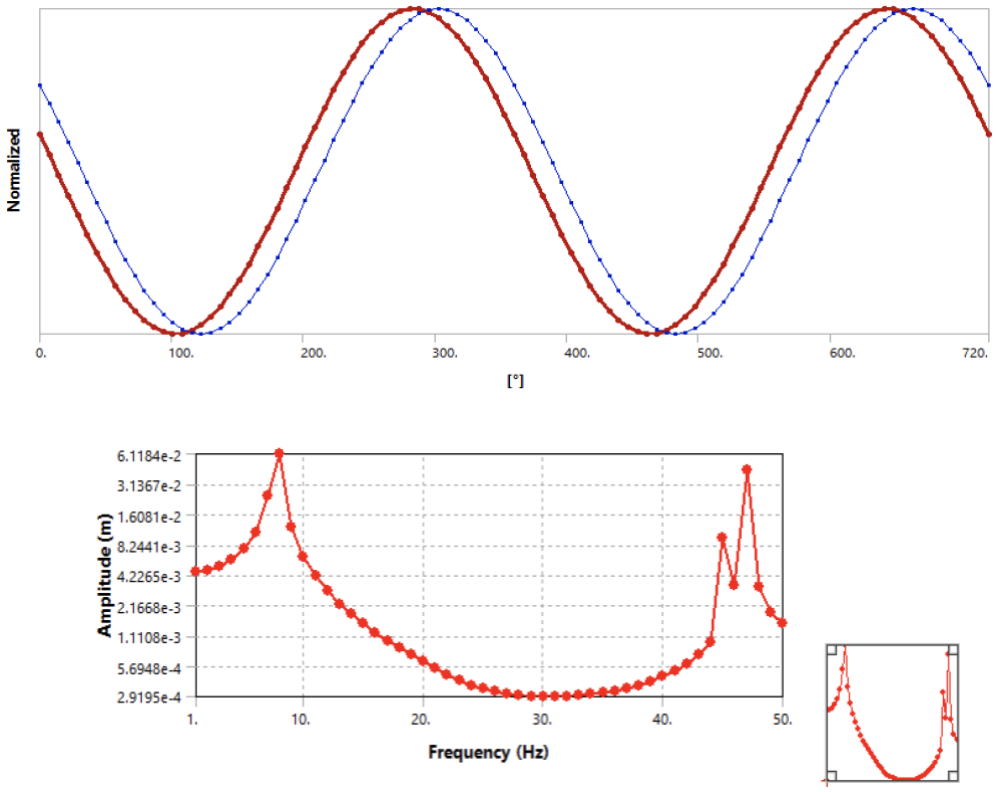

FIGURE 47. Displacement and Unsteady Pressure Field phase difference and the corresponding Critical Frequencies.

Therefore, as the pressure field is leading the displacement motion, the incoming flow absorbs energy from the aircraft wing, and the motion is amplified. Coupled bending-torsion motion has been obtained for the given Mach conditions. Hence, it is important to evaluate the critical airspeed limit for properly structural and aeroelastic design. The simplifications made during this Final year Project will limit the accuracy if the results but will provide an accurate tool to predict this instability.

Finally, there is a remaining question. What can we do as engineers to solve that problem? As we introduced, flutter occurs at the critical flutter speed, when the structure starts to oscillates with simple harmonic motion over time. This is a simple structural problem. The main reason that triggers purely structural natural modes to couple in an unfavorable manner due to the interaction of aerodynamic forces, depends on the mass ratio (the ratio of the aircraft wing mass to the mass of the surrounding fluid). Sometimes, increasing mass ratio introduces a penalty on weight, and thus on aircraft performance, fuel consumption, production costs and certification.

As it is simply an instability is due to the phase between the aerodynamic forces acting on the aircraft wing and the structural displacements, we can analyze different geometrical and design factors that will influence flutter coupling. Different solutions are proposed to prevent aeroelastic phenomenon to occur:

- Increasing the free stream velocity will increase the average Lift Coefficient. It means that the larger the free stream velocity, the larger the pressure coefficient. As lift is generated due to the presence of a suction side, the more negative the pressure, the biggest difference in pressure distribution resulting in greatest lift. This intuitive physical phenomenon has an enormous impact on aircraft structures when redesigning solutions needs to be studied. In Figure 48, the influence of the Mach number is analyzed.
- Spar Location will influence torsional stiffens and bending moment frequency. Also, the lift coefficient will be affected by spar locations spanwise.
- Sweep Angle reduces the effective velocity by increasing drag. As a projection angle is introduced, torsional-bending mode will be modified. That is why A400M forward configuration is said to be unstable in Flight Mechanics & Performance.
- Other structural factors such as skin Young Modulus or skin density needs to be considered in future work.

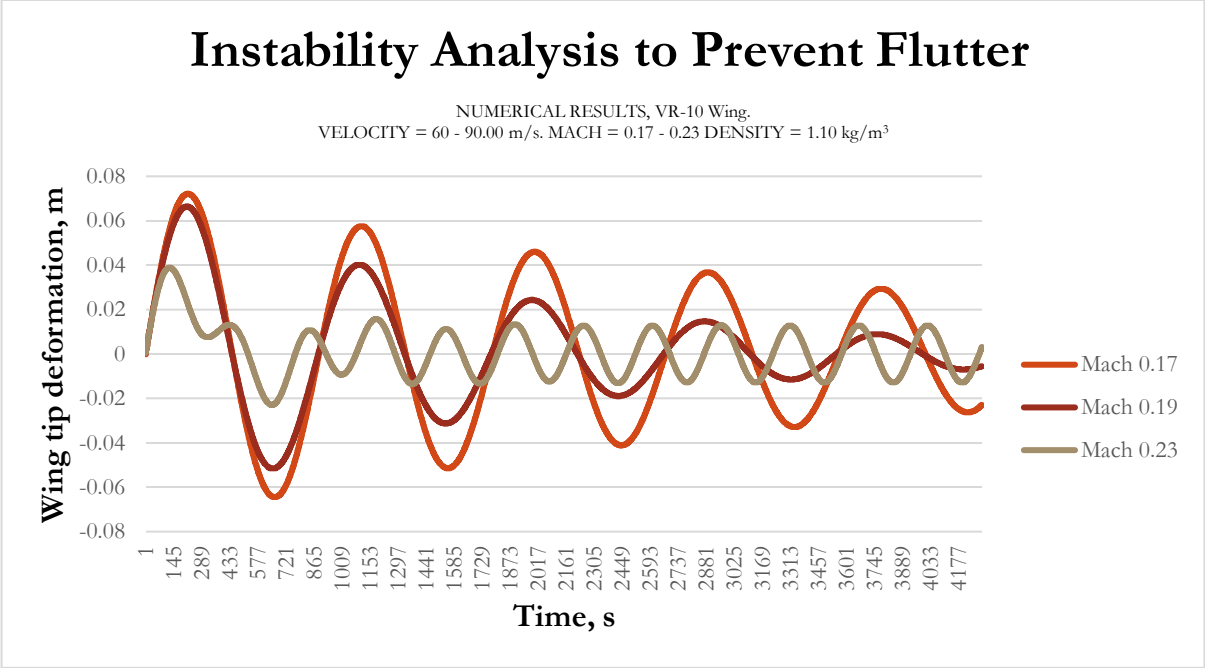

FIGURE 48. Instability Analysis to Prevent Flutter Phenomenon.

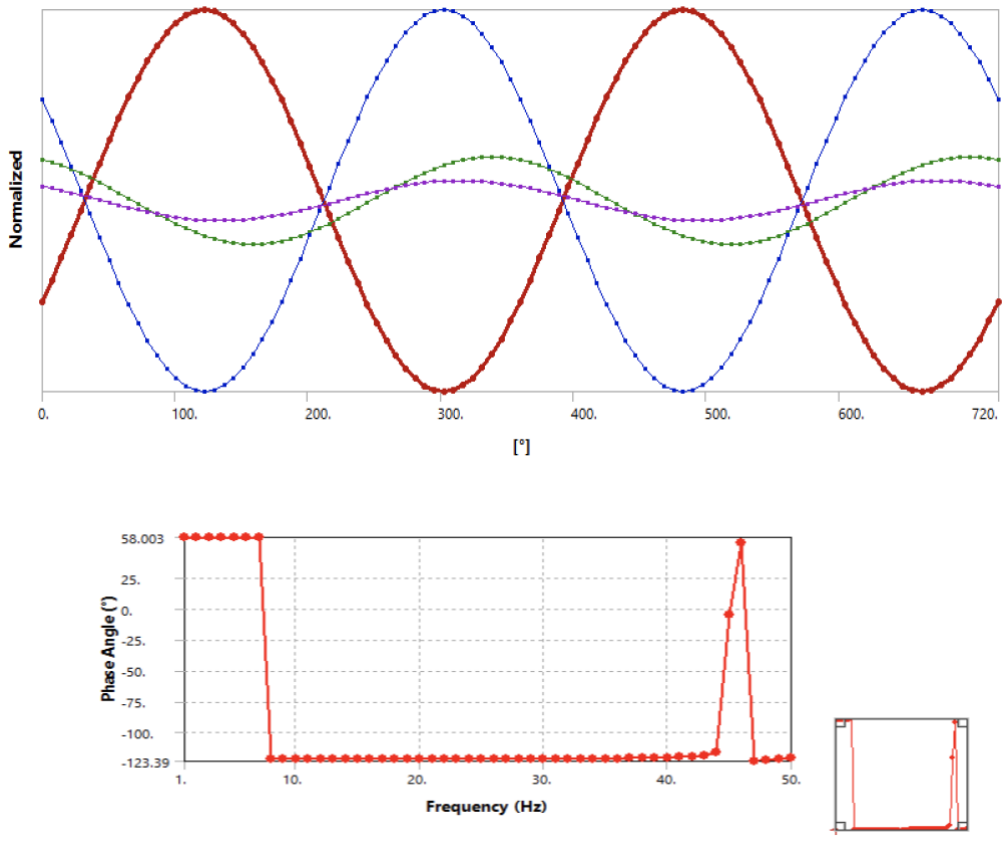

FIGURE 49. Corresponding Phase Difference in Which Displacement Lags Pressure Field And The System Is Stable

CHAPTER 7

"We are what we repeatedly do; excellence,
then, is not an act but a habit."

Aristotle

Contents

7. CONCLUSION

7.1. ACHIVEMENTS

Aeroelastic behaviour of a three-dimensional RV-10 aircraft wing by fully-coupled staggered Fluid-Structure Interaction has been achieved by high-accuracy numerical interaction of aerodynamic, elastic and inertial forces. Critical flutter speed, as unstable self-excited vibration, was associated with aerodynamic forces and structural flap and edge-wise modes. Classical coupling of torsional and bending moment was obtained at 120 m/s with a frequency of 50 Hz. K-P Method was defined to analytically stablish critical flutter speed and flutter limits. The obtain

results shows reasonable agreement for the first two coupling modes. Differences are observed increasing frequency spectrum.

The designed algorithm defined as ANSYS Fluid-Structure Interaction Framework, FSIF, correctly discretised both fluid and structural domains and obtained robust displacements as a function of unsteady pressure fields. FSI Methods were validated with one way and two-ways coupling methods. Two-ways coupling methods requires higher computational time but reduces lack of accuracy and dynamic mesh risks. Reynolds Averaged Navier-Stokes equation and Turbulence Transport equations governing the flow were integrated in the FSI solver according to the expected results. Steady analysis shows good agreement with published literature review on NACA2412 database.

Transient models obtained by applying SST K-omega turbulence method were improve after more than 367 total converging hours. Transient numerical post-processed results have been matched the phase difference and classical coupling motion of the first two modes. Those results indicate unstable flow for the selected Critical Flutter Speed. Higher frequencies values lead to incorrect aerodynamic values and no computational convergence as student license was used. Comparison between literature review on rectangular "Hershey bar" wings and numerical results shows accurate results. Moreover, experimental pressure distributions of an oscillating wing tested at European University Wind Tunnel facility are analysed aiming to provide accurate results. Despite the simplifications implemented in both the fluid and structural solvers, this framework has been proven to be powerful and potential tool to predict the aeroelastic performance of a wing in the early stages of aircraft design.

7.2. FUTURE WORK

Further work will include real test verification on labs, applying accelerometers to replicate this study in real life. Those tests have been already carried out at Wind Tunnel facilities on Universidad Europea de Madrid. Analytical results will be compared with computer-based solutions in order to provide insight into critical flutter speed and flutter aeroelastic phenomenon. Also, future research will be based on implementing geometrical modifications over RV-10 wing that modifies the results. Under this preliminary objective, a 3D wing model have been printed

at FAB LAB, Universidad Europea de Madrid, to perform aerodynamic measurement on the aircraft wing, regarding pressure distribution over the wing. These results will be compared with the steady state solutions in this Final Year Project.

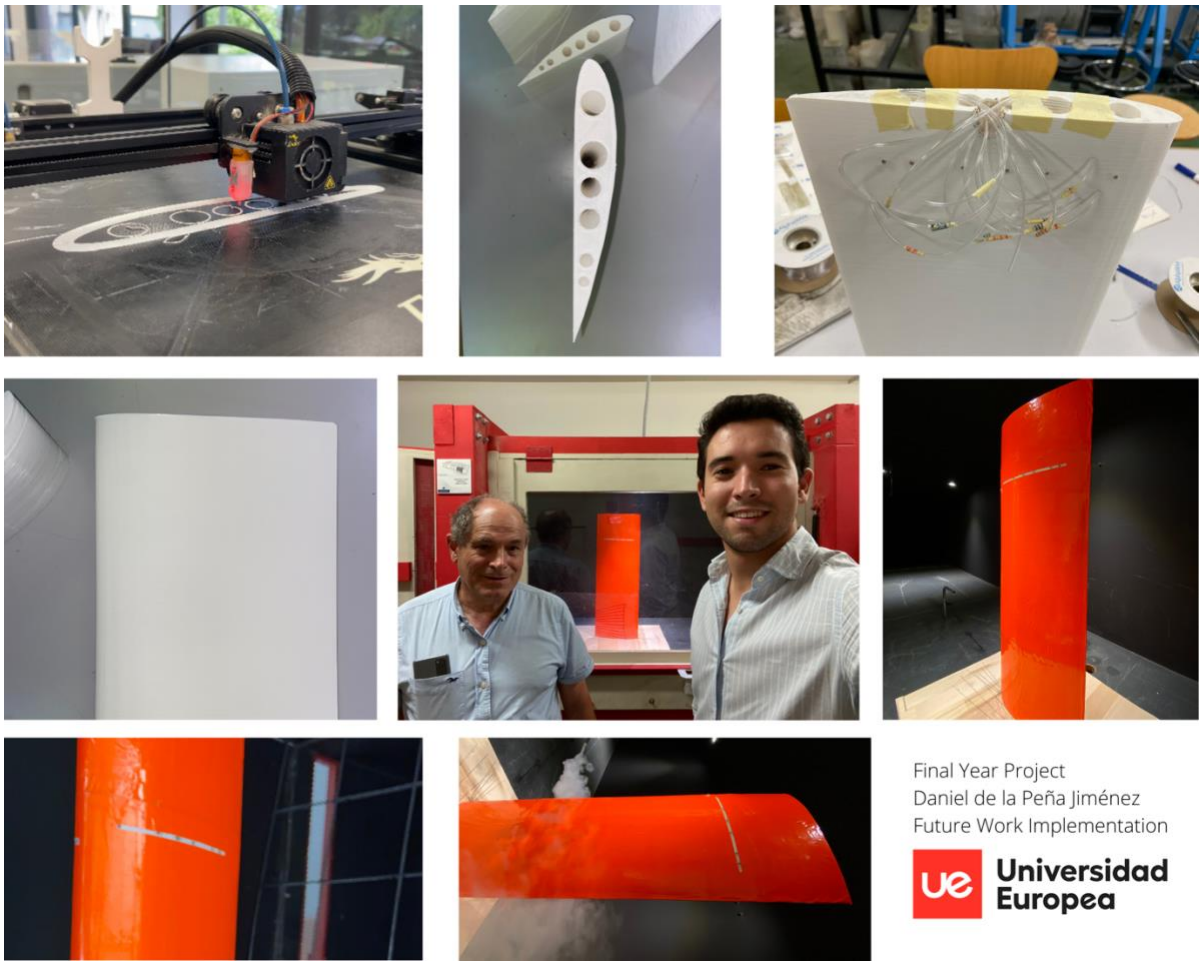

Following this project outline, the 3D printed model have been tested on flutter vibrations. Nevertheless, restrictions on the printed model and maximum Mach number on the Wind Tunnel facility limit the accuracy of the results. These tests will be implemented to observe structural behaviour and vibrations on the wing tips.

Last, but not least, as aerospace engineers I feel proud to finish this Bachelor's Degree with such an amazing field as aeroelasticity. The knowledge acquired at Universidad Europea de Madrid were essential to track a mathematical method intertwined with numerical simulations on unsteady aerodynamics, non-linear structural problems, incompressible fluid-mechanics and static and dynamic aeroelasticity.

I'm greatly happy with the Project Based Methodology and I will pursue my Master Graduate Program on Aircraft Engineering at UEM next year. Keep hungry, keep foolish!

Per Aspera Ad Astra.

REFERENCES

[1.] De la Peña Jiménez, D., (2021) "Futter stability analysis of an aircraft wing as a function of damping ratio", Embry Riddle Aeronautical University.

[2.] Kelly, G. S. (2021). *Fundamentals of Mechanical Vibrations* (2nd Ed). McGraw Hill.

[3.] A. R. Collar.(1992) *The first fifty years of aeroelasticity*. Aerospace, vol. 5, no. 2, pp. 12{20, Feb. 1978.

[4.] Herrin, D. W. (2007). *Vibro-Acoustic Design in Mechanical Systems*. Department of Mechanical Engineering.

[5.] De la Peña Jiménez, D., Golubev, V., (2021) "Numerical Studies of Controlled Viscous Limit-Cycle Oscillations in Modified Glauert Airfoil", Embry Riddle Aeronautical University.

[6.] T. H. G. Megson, *Aircraft Structures for Engineering Students*, 4th ed., ser. Elsevier Aerospace. Engineering Series. Oxford: Butterworth-Heinemann, 2007.

[7.] Brown University. (n.d.). *Introduction to Dynamic Aeroelasticity*. School of Engineering. Brown University. https://www.brown.edu/Departments/Engineering/Courses/En4/Notes/vibrations_forced/vibrations_forced.htm

[8.] Dowel, E. H., & Sisto, F. (1978). *A modern course in Aeroelasticity*. Sisto, F.

[9.] Jöcker, M. (2002). *Numerical Investigation of the Aerodynamic Vibration Excitation of High-Pressure Turbine Rotors* (Doctoral Thesis). https://www.diva-portal.org/smash/get/diva2:9213/FULLTEXT01.pdf

[10.] Stasolla, V. (2019). *Numerical analysis of aerodynamic damping in a transonic compressor*. Master Thesis. https://www.diva-portal.org/smash/get/diva2:1373074/FULLTEXT01.pdf

[11.] *Flutter Analysis*. (2012). RPMTurbo. http://www.rpmturbo.com/flutter/index.html

[12.] Prasad, C., & Alamdari, M. M. (2019, April). *New Approaches to Inverse Structural Modification Theory Using Random Projections*. Springer Publishing. https://link.springer.com/chapter/10.1007/978-3-030-12684-1_13

[13.] *Forced vibrations of damped single degree of freedom systems: damped spring mass system*. (n.d.). University at Alberta. https://engcourses-uofa.ca/books/vibrations-and-sound/forced-vibrations-of-damped-single-degree-of-freedom-systems/damped-spring-mass-system/

[14.] Meirovich., L. (2001). *Elements of vibration analysis*. Mc Graw Hill. https://kgut.ac.ir/useruploads/1523432144334wuh.pdf

[15.] Roseau., M. (n.d.). *Vibrations in Mechanical Systems*. Springer-Verlag.

[16.] Den Hartog, J. P. (n.d.). *Mechanical Vibrations*. Pérlelo. https://www.perlego.com/book/110952/mechanical-vibrations-pdf

[17.] Saffman., P. G. (n.d.). *Vortex Dynamics*. Cambridge. https://moodle2.units.it/pluginfile.php/95815/mod_resource/content/1/Vortex_Dynamics.pdf

[18.] Bisplinghoff and Ashley. (1996). *Principles of Aeroelasticity*. https://pikewallis.no/wp-content/plugins/formcraft/file-upload/server/content/files/1606ffb556c606---bunafelete.pdf

[19.] Hirsch. Willey. (1994). *Numerical Computation of Internal and External Flows* (Vol. 1. & 2). https://soaneemrana.org/onewebmedia/NUMERICAL%20COMPUTATION%20OF%20INTERNAL%20&%20EXTERNAL%20FLOWS%20BY%20C.%20HIRSEH%20%28VOL.-2%29.pdf

[20.] Pope. (2000). *Turbulent Flows*. Cambridge University. ftp://161.24.15.247/MOURA/AA-286/Bibliografia/Pope%20-%20Turbulent%20flows.pdf

[21.] Lincse. (n.d.). High-Order Methods for Computational Physics. License.

[22.] Ferziger et all. (2003). *Computational methods for fluid dynamics* (3rd Edition). https://www.academia.edu/627635/Computational_methods_for_fluid_dynamics

[23.] Wilcox. (2006). *Turbulence Modeling for CFD*. DCW. https://cfd.spbstu.ru/agarbaruk/doc/2006_Wilcox_Turbulence-modeling-for-CFD.pdf

[24.] J. Katz and A. Plotkin, Low-Speed Aerodynamics, 2nd ed., ser. Cambridge Aerospace Series, M. J.

[25.] Vega Coso, A. (2016) *Impact of the Unsteady Aerodynamics of Oscillating Airfoils on the Flutter Characteristics of Turbomachines*. Tesis doctoral. Almudena Vega Coso. Madrid, 2016.

[26.] G. SenGupta, J. Castro, and T. Kim. *Computational methods in aeroelasticity*. AIAA Short Courses, Honolulu, HI, April 2007.

[27.] R. Udrescu. *Effects of oscillating shock waves on the dynamics of fluttering panels*. 19th AIAA Applied Aerodynamics Conference, June 2001, doi:10.2514/6.2001-1669.

[28.] J. Katz and A. Plotkin. *Low-Speed Aerodynamics*. Cambridge University Press, New York, 2nd edition, 2001. ISBN: 9780521662192.

[29.] A. S. Cardeira. *Aeroelastic analysis of aircraft wings*. Instituto Superior Técnico (IST), December 2014. MSc dissertation.

[30.] J. M. R. D. C. Baltazar. *On the modelling of the potential flow about wings and marine propellers using a boundary element method*. Instituto Superior Técnico (IST), 2008. PhD dissertation.

[31.] J. N. Reddy. *An Introduction To The Finite Element Method*. McGraw-Hill Series in Mechanical Engineering. McGraw-Hill, 3rd edition, 2006. ISBN: 0072466855.

[32.] R. D. Cook, D. S. Malkus, M. E. Plesha, and R. J. Witt. *Concepts and Applications of Finite Element Analysis*. John Wiley & Sons. Inc, 4th edition, 2002. ISBN: 0471356050.

[33.] M. J. Patil, D. H. Hodges, and C. E. S. Cesnik. *Nonlinear aeroelasticity and flight dynamics of high-altitude long-endurance aircraft*. Journal of Aircraft, 38(1):88–94, 2001. DOI: 10.2514/2.2738.

[34.] C. Farhat and M. Lesoinne. *Two efficient staggered algorithms for the serial and parallel solution of three–dimensional nonlinear transient aeroelastic problems*. Computer Methods in Applied Mechanics and Engineering, 182(3-4):499–515, 2000.

[35.] M. J. Patil and D. H. Hodges. *On the importance of aerodynamic and structural geometrical nonlinearities in aeroelastic behavior of high-aspect-ratio wings*. Journal of Fluid and Structures, 19(7):905–915, August 2004. DOI: 10.1016/j.jfluidstructs.2004.04.012.

[36.] Spada, C.; Afonso, F.; Lau, F.; Suleman, A. *Nonlinear aeroelastic scaling of high aspect-ratio wings*. Aerosp. Sci. Technol. 2017, 63, 363–371, doi:10.1016/j.ast.2017.01.010.

[37.] Boeing, Visited in March 2022.

[38.] El Paso de Sevilla, Visited in January 2022. https://www.elpasadodesevilla.com/2013/03/hispano-de-aviacion.html

[39.] Airbus, Visited in September 2021, https://www.airbus.com/en/innovation/disruptive-concepts/biomimicry/albatrossone

[40.] NASA, Visited in June 2022, NASA. (1995, December). A historical overview of flight flutter testing. NASA. https://ntrs.nasa.gov/citations/19960004074

[41.] *Aerospace Engineer Blog*. (2012). Aerospace Engineer Blog. https://aerospaceengineeringblog.com/aeroelasticity-composites-and-the-grumman-x-29/

[42.] *ANSYS Mechanical APDL Modeling and Meshing Guide*, ANSYS, Inc., Canonsburg, PA, November 2010, release 13.0.

[43.] NASA. Aeroelastic Modeling of Elastically Shaped Aircraft Concept via Wing Shaping Control for Drag Reduction. https://ntrs.nasa.gov/api/citations/20170005442/downloads/20170005442.pdf

[44.] Belvis, R. D. (1990). Aeroelasticity. *Flow-Induced Vibrations*.

[45.] Hirsch, C. (2001). *Numerical Computation of Internal & External Flows*. Engineering 360. https://www.scirp.org/(S(lz5mqp453edsnp55rrgjct55.))/reference/referencespapers.aspx?referenceid=2748759

[46.] Brazilevs et al. (n.d.). *Computational fluid-structure interaction*. ResearchGate. https://www.researchgate.net/publication/41175239_Computational_fluid-structure_interaction_methods_and_application_to_cerebral_aneurysms_Biomech_Model_Mechanobiol_9481-498

[47.] dos Santos Almeida, J. D. (n.d.). *Structural Dynamics for Aeroelastic Analysis*. Politecnico Lisboa. https://www.academia.edu/32590442/Structural_Dynamics_for_Aeroelastic_Analysis_Examination_Committee

[48.] Aerodynamics & Aeroelasticity. Class Notes. Universidad Europea de Madrid. Degree in Aerospace Engineering of Aircraft. Dr. Martínez Lucci.

[49.] Fluid- Mechanics I & II. Class notes. Universidad Europea de Madrid. Degree in Aerospace Engineering of Aircraft. Dr. Martínez Lucci.

ANNEX I: FSI ALGORITHYMS

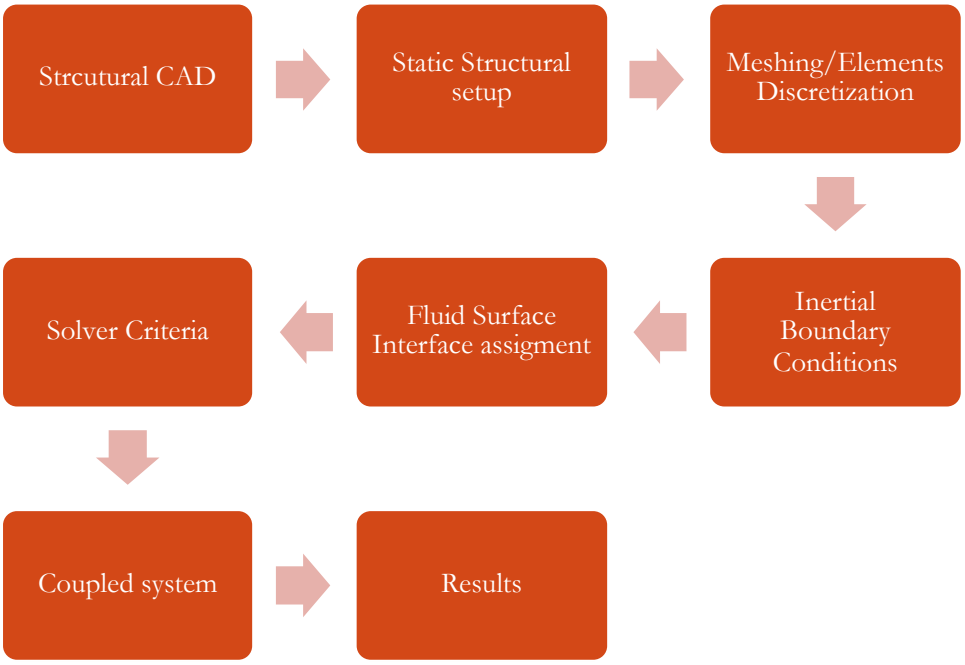

FIGURE X. STRUCTURAL ANALYSIS METHOD BASED ON FSI MODEL

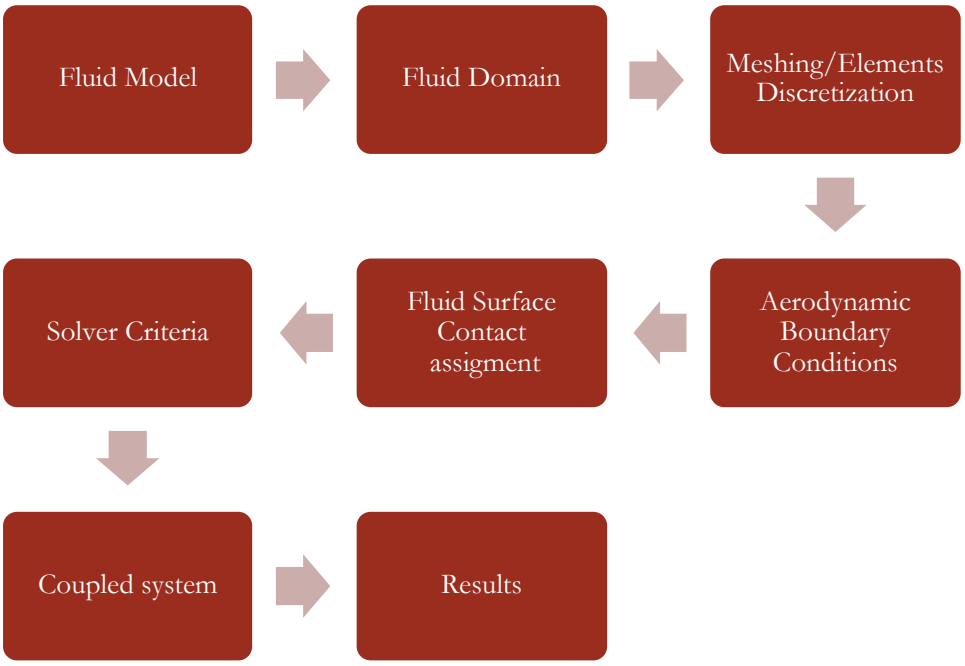

FIGURE X. FLUID DYNAMIC ANALYSIS METHOD BASED ON FSI MODEL

ANNEX II: RV-10 STRUCTURAL LAYOUT

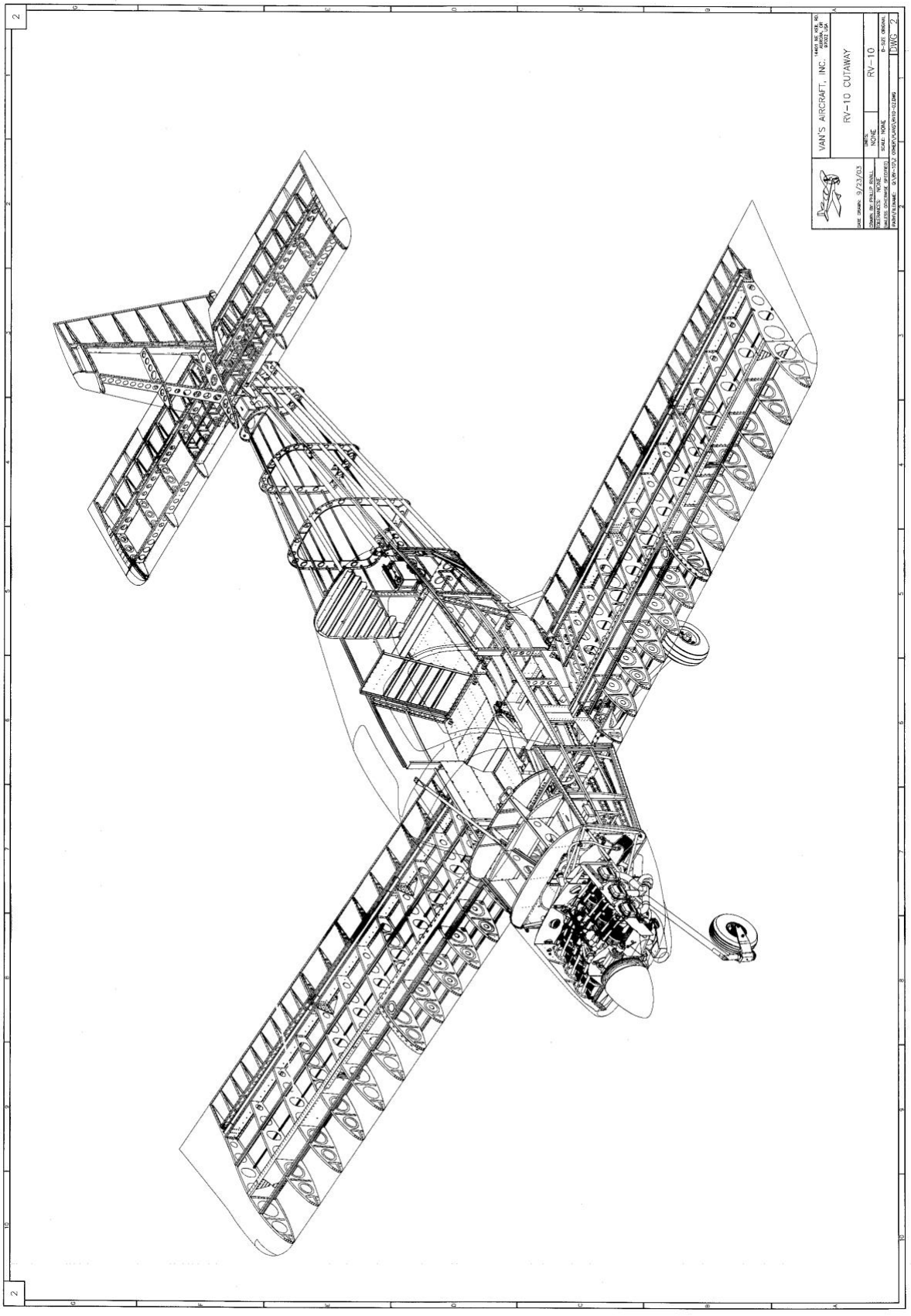

ANNEX III: RV-10 WING-FUSELAGE ATTACHMENT

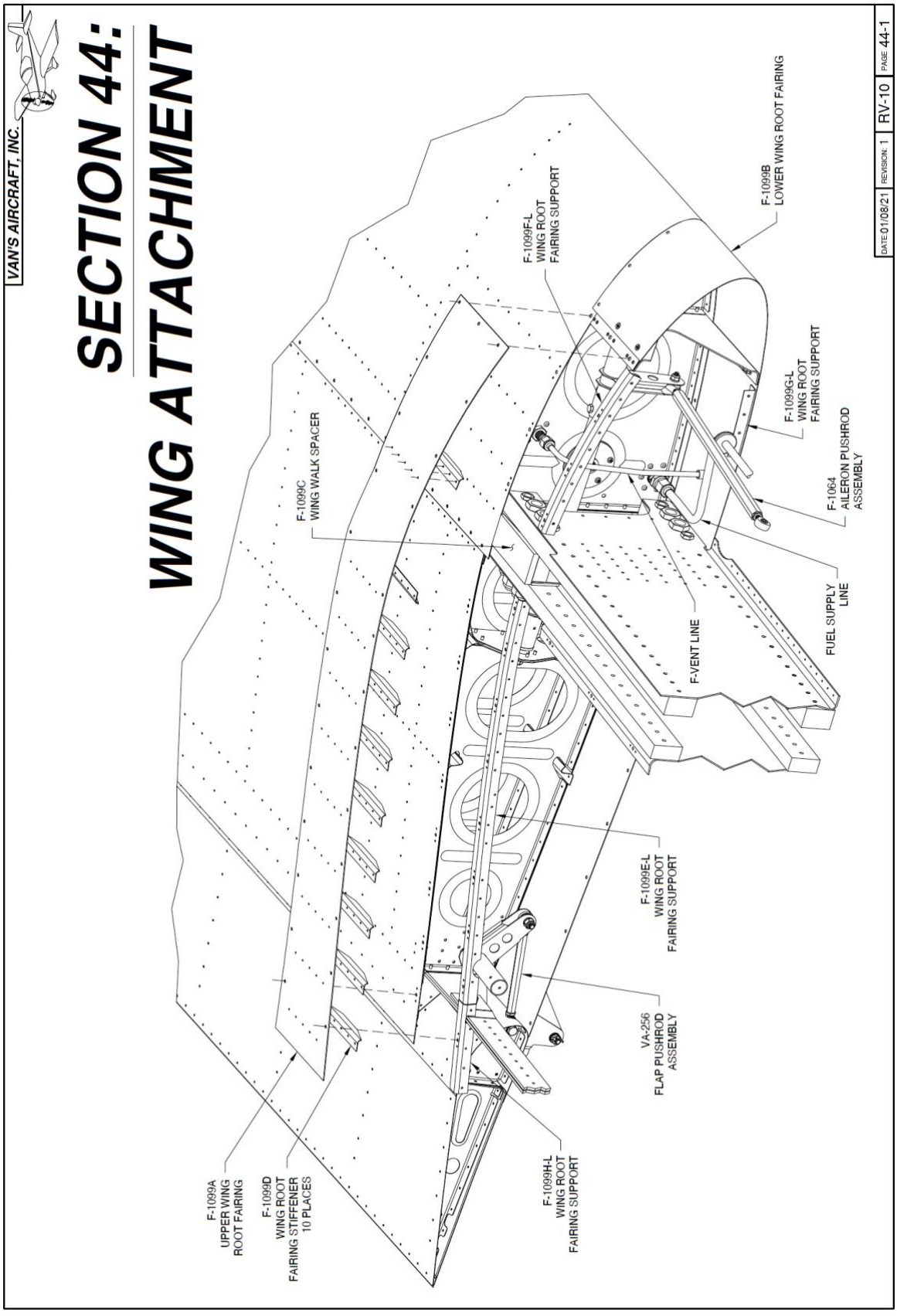

ANNEX IV: P-K METHOD

%This MATLAB CODE is property of Daniel de la Peña Jiménez, in partial

%fulfillment of the requirement of the award of the degree of

% BACHELOR'S DEGREE ON AEROSPACE ENGINEERING

%This code solves Binary Aeroelastic model by solving eigenvalue solution %at critical flutter speed.

Once the velocity is set, you can find %frequency and amplitude in V-g plot.

In order to proceed, I have divided the following code into:

% 1. Specify wing geometrical and elastic parameters.

% 2. Set inertia and structural stiffness matrices.

% 3. Calculate Vf.

%

%==

% CONFIDENTIAL -2021/22 - Universidad Europea de Madrid- CONFIDENTIAL

%==

```
% Initialize variables
clear; clf

s = 4.8;
c = 1.6;
m = 100;
kappa_freq = 5;
theta_freq = 10;  % pitch freq in Hz
xcm = 0.5*c;      % position of centre of mass from nose
xf = 0.48*c;      % position of flexural axis from nose
e = xf/c - 0.25;  % eccentricity between flexural axis and aero
velstart = 0;
velend = 200;
velinc =0.1;

a = 2*pi; % 2D lift curve slope
rho = 1.225; % air densit
Mthetadot = -1.2; % unsteady aero damping term
M = (m*c^2 - 2*m*c*xcm)/(2*xcm); % leading edge mass term
damping_Y_N = 1;
if damping_Y_N == 1

z1 = 1.7; % critical damping at first frequency
z2 = 0; % critical damping at second frequency
w1 = 2*2*pi; % first frequency
w2 = 14*2*pi; % second frequency
```

```
alpha = 2*w1*w2*(-z2*w1 + z1*w2)/ (w1*w1*w2*w2);
beta = 2*(z2*w2-z1*w1) / (w2*w2 - w1*w1);
end

% Set up system matrices
a11=(m*s^3*c)/3 + M*s^3/3; % I kappa
a22= m*s*(c^3/3 - c*c*xf + xf*xf*c) + M*(xf^2*s); % I theta
a12 = m*s*s/2*(c*c/2 - c*xf) - M*xf*s^2/2; %I kappa theta
a21 = a12;
A=[a11,a12;a21,a22];
% Structural stiffness matrix
k1 = (kappa_freq*pi*2)^2*a11; % k kappa heave stiffness
k2 = (theta_freq*pi*2)^2*a22; % k theta pitch stiffness
E = [k1 0; 0 k2];
icount = 0;
for V = velstart:velinc:velend % loop for different velocities
    icount = icount +1;
   if damping_Y_N == 0; % damping matrices
C = [0,0; 0,0]; % =0 if damping not included
else % =1 if damping included
C = rho*V*[c*s^3*a/6,0;-c^2*s^2*e*a/4,-c^3*s*Mthetadot/8] +alpha*A + beta*E;
% Aero and structural damping
end
K = (rho*V^2*[0,c*s^2*a/4; 0,-c^2*s*e*a/2])+[k1,0; 0,k2]; % aero / structural
stiffness
Mat = [[0,0; 0,0],eye(2); -A\K,-A\C]; % set up 1st order eigenvalue solution
matrix
lambda = eig(Mat); % eigenvalue solution
% Natural frequencies and damping ratios
for jj = 1:4
im(jj) = imag(lambda(jj));
re(jj) = real(lambda(jj));
freq(jj,icount) = sqrt(re(jj)^2+im(jj)^2);
damp(jj,icount) = -100*re(jj)/freq(jj,icount);
freq(jj,icount) = freq(jj,icount)/(2*pi); % convert frequency to hertz
end
Vel(icount) = V;
end
% Plot frequencies and dampings vs speed
figure(1)
subplot(2,1,1); plot(Vel,freq,'k');
vaxis = axis; xlim = ([0 vaxis(2)]);
grid
title(' STABILITY ANALYSIS', 'Interpreter','latex','Fontsize',18);
subtitle('Author: Daniel de la Peña Jiménez','Color','blue','Fontsize',14);
ylabel('Freq (Hz)','Interpreter','latex','rotation',90, 'Fontsize',18);
xlabel ('Air Speed (m/s)','Interpreter','latex','rotation',0, 'Fontsize',18);
grid
subplot(2,1,2);
plot(Vel,damp,'k')
xlim = ([0 vaxis(2)]); axis([xlim ylim]);
ylabel('Damping Ratio (%)','Interpreter','latex', 'Fontsize',18);
xlabel ('Air Speed (m/s)','Interpreter','latex','rotation',0, 'Fontsize',18);
grid
```

ANNEX V: XFLR5 AIRFOIL DATABASE

FIGURE X. NACA 65-415.

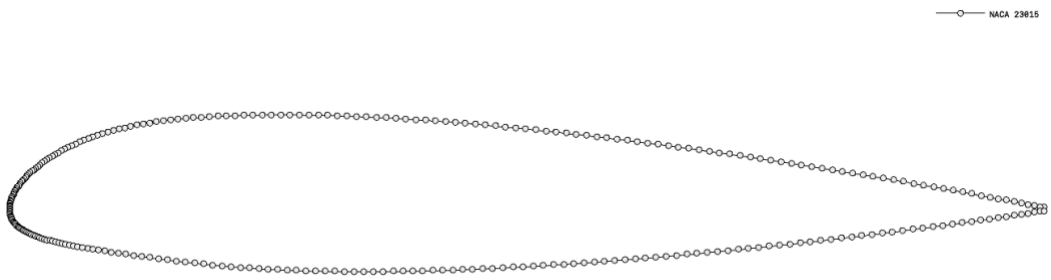

FIGURE X. NACA 23015.

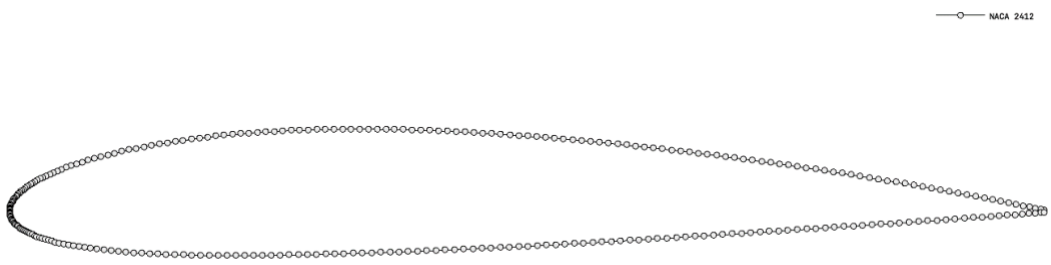

FIGURE X. NACA 2412.

FIGURE X. NFL-0115.

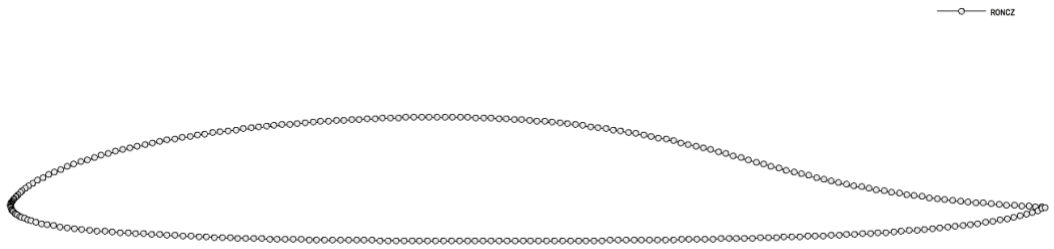

FIGURE X. RONCZ AIRFOIL.

FIGURE X. SH1 AIRFOIL.

FIGURE X. NACA 66-210.

FLUTTER STABILITY ANALYSIS OF AN AIRCRAFT WING AS A FUNCTION OF THE AEROELASTIC DAMPING RATIO

Daniel de la Peña Jiménez, ERAU[1]; PhD. Almudena Vega Coso, UEM[2]
[1]Undergraduate Researcher, Embry-Riddle. [2]Associate Professor, Faculty of Aerospace Engineering, Universidad Europea

Abstract

This report provides insight into flutter stability analysis as a function of damping ratio. Flutter, an **unstable self-excited vibration** in which the structure extracts energy from the air stream and often results in catastrophic structural failure, is analyzed as dynamic instability, which may eventually result in stall or **buffeting conditions** or classical bending and torsion coupling actions. The characteristic equation of motion is analyzed in order to study stability and its relationship with the **damping ratios** on an aircraft wing. Analytical results of different mode shapes and time-dependent boundary conditions are provided in this independent research study, under the guidance of PhD. A. Vega Coso.

Those results indicate stability dependence on damping ratio as it is basically a free vibration problem. Further research is focused on considering and proving detailed results on experimental data and evaluating aeroelasticity as an essential topic on aircraft design.

Introduction

Aeroelasticity phenomenon is a combination of physical phenomena which include iteration between inertia, elastic and aerodynamic forces. It has a high impact on stability and control, -and thus, on flight mechanics-, structural vibrations and static aeroelasticity.

According to [4], **flutter** is considered one of the most important of all the aeroelastic phenomena and is the most difficult to predict. It is an unstable self-excited vibration in which the structure **extracts energy from the air stream** and often results in catastrophic structural failure [5].

This phenomena, understood as a dynamic instability, is a self-excited vibration phenomena, due to the structure own vibration motion and it does not need of any external excitation to occurs, on the contrary to what happens to forced response[1]. Furthermore, **classical bending and torsion coupling** actions occurs when the aerodynamic forces associated with motion in two modes of vibration cause the modes to couple in an unfavorable manner.

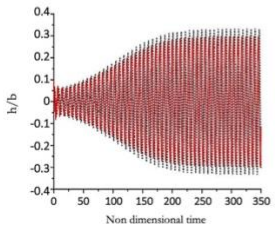

Figure 1. Limit Cycle Oscillation

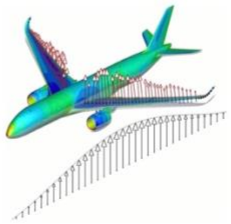

Figure 2. Gust simulation on an aircraft.

Free vibrations

Free vibrations can be defined as a system in which **no external force** is causing motion, and that the motion is primarily the result of initial conditions, such as an initial displacement of the mass element of the system from an equilibrium position and/or an initial velocity. Thus, by physically representing a **SDOF** free vibration as a damped spring-mass system, we can obtain the differential equation for damped motion of an aircraft wing:

$$m\ddot{x} + c\dot{x} + kx = 0 \qquad \lambda = -\zeta\omega_n \pm \omega_n\sqrt{\zeta^2 - 1}$$

where **m** and **k** are the mass and stiffness matrices, respectively; **c**, is the damping force, and **x** is the n-dimensional column vector of generalized coordinates. The **damping ratio**(ζ) and the **undamped natural frequency**(ω_n) can be expressed:

$$\zeta = \frac{c}{2\sqrt{mk}} = \frac{c}{c_{cr}} \qquad \omega_n = \sqrt{\frac{k}{m}}$$

Results

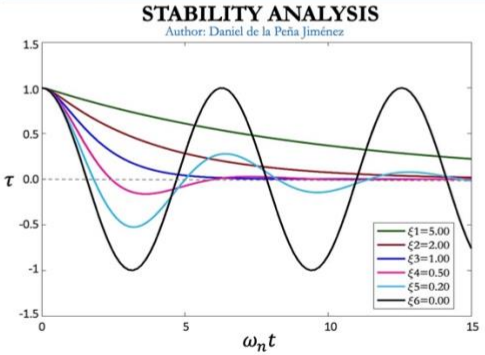

Figure 3. Stability analysis as a function of the damping ratio.

Table 1. Response classification.

Scenarios	DR	Description
OVERDAMPED RESPONSE	$\zeta > 1$	$X(t) = C_1 e^{(-\zeta\omega_n + \omega_n\sqrt{\zeta^2-1})t} + C_2 e^{(-\zeta\omega_n - \omega_n\sqrt{\zeta^2-1})t}$
CRITICALLY DAMPED RESPONSE	$\zeta = 1$	$X(t) = X_0 e^{(-\zeta\omega_n)t} + \omega_n X_0 t e^{(-\zeta\omega_n)t}$
UNDERDAMPED RESPONSE	$0 < \zeta < 1$	$X(t) = Ae^{(-\zeta\omega_n)t}[\sin(\omega_d t + \phi)]$
FLUTTER RESPONSE	$\zeta < 0$	Self-excitation instability

Discussion

Overdamped response results in both real roots for the characteristic equation being real and negative. This has a physical impact on the system, as the restoring force is high enough to avoid the system to oscillate. Therefore, a free force overdamped harmonic oscillator **tends to equilibrium.**

Critically damped response behaves similarly with a **faster response on the decay** with no possible oscillation. As overdamped systems, the solutions to the characteristic equations are real and negative, reaching the steady-state value the fastest without being underdamped.

Underdamped response is obtained when the damping ratio is ranged from zero to one. The response of the system is a **sinusoid function** in which energy varies while being dissipated. Reducing the damping ratio results in an oscillation in the form of $\sin(\omega_{dt} - \varphi)$, although the amplitude is constantly decreasing up to **equilibrium state** along the time.

Further discussion on **resonance** on an aircraft wing undergoing an external aerodynamic nature excitation due to atmospheric turbulence or gust is achieved by mathematically representing this phenomenon due to an **external harmonic force**.

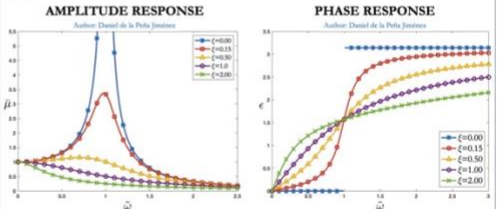

Figure 4. Normalized amplitude and phase vs normalized frequency.

It is found that the **normalized amplitude** strongly depends on the damping ratio (ζ) as the frequency for which the maximum amplitude is obtained shifts away from the **natural frequency** when the damping ratio increases. Also, this excitation frequency increases as **phase** increases from 0 to π. At $\pi/2$, the natural frequency is equal to the **excitation frequency** of the gust.

Conclusions

Stability dependence on damping ratio is achieved by integrating a free vibration problem and the equations of motion. The damping ratio coefficient can be modified by applying the following design solutions:

- Adjust the stiffness of the aircraft wing structure.
- Change geometrical wing parameters.
- Distribute mass for damping ratio stability.

References:
1. Vega Coso, A. (2016) Impact of the Unsteady Aerodynamics of Oscillating Airfoils on the Flutter Characteristics of Turbomachines. Tesis doctoral. Almudena Vega Coso. Madrid, 2016.
2. Kielb, R. (2012, August). CFD for turbomachinery unsteady flows - An aeroelastic design perspective. American Institute of Aeronautics and Astronautics. https://arc.aiaa.org/doi/10.2514/6.2001-429
3. Corral, R., Gallardo, J. M., and Marrel, C., 2009. "A conceptual flutter analysis of a packet of vanes using a mass-spring model". J. Turbomach, 131, April, pp. 021016–1–7.
4. Dowel, E. H., & Sisto, F. (1978). "A modern course in Aeroelasticity."
5. Meirovich., L. (2001). Elements of vibration analysis. Mc Graw Hill. https://kgut.ac.ir/useruploads/15234321443343wuh.pdf

Contact:
Daniel de la Peña Jiménez
delapeD1@my.erau.edu | +1 (386) 316-2870
Embry Riddle Aeronautical University
Universidad Europea de Madrid